Order Number 9205501

Evolution of the Witwatersrand basin: Evidence from the quartzites

Ritger, Scott D., Ph.D.

University of Cincinnati, 1991

U·M·I
300 N. Zeeb Rd.
Ann Arbor, MI 48106

EVOLUTION OF THE WITWATERSRAND BASIN: EVIDENCE FROM THE QUARTZITES

A Dissertation submitted to the

Division of Graduate Studies and Research
of the University of Cincinnati

in partial fulfillment of the
requirements for the degree of

DOCTOR OF PHILOSOPHY

in the Department of Geology
of the College of Arts and Sciences

1990

by

Scott D. Ritger

B.A., Carleton College, 1983

M.S., Lehigh University, 1985

Committee Chair: Dr. J. Barry Maynard

UNIVERSITY OF CINCINNATI

June 5 1991

I hereby recommend that the thesis prepared under my supervision by Scott D. Ritger

entitled Evolution of the Witwatersrand Basin: Evidence from the Quartzites

be accepted as fulfilling this part of the requirements for the degree of Doctor of Philosophy

Approved by:

Abstract

In this dissertation I present a tectonic, geochemical, and thermal history for the Witwatersrand basin, located on the Archean Kaapvaal craton, South Africa. The foreland basin tectonic setting of the Central Rand Group controls both the chemical and the thermal evolution of the basin, and unifies the basin evolution model presented here.

I interpret the early tectonic history of the basin, recorded by the bi-modal Dominion volcanics and the predominantly fine-grained clastic sediments of the West Rand Group, to be one of crustal thinning and subsequent thermal subsidence in an incipient rift setting. The transition to a foreland basin coincides approximately with the onset of Central Rand sedimentation--Central Rand Group sediments are predominantly sandstones and conglomerates, they have been syndepositionally folded and faulted, and unconformities are common.

Formation-bounding unconformities in the Central Rand represent major depositional hiatuses during which CO_2-charged meteoric water infiltrated and leached the unlithified sediments, strongly controlling the chemical and petrographic evolution of the Central Rand Group. Petrographically, the result of meteoric leaching is an almost complete absence of feldspar in the Central Rand Group. Geochemically, the leaching is manifest in two ways: (1) a consistent intraformational trend towards upwards

enrichment in Al and upwards depletion in Ca, Na, Fe and Mg (Sutton et al., 1990), and (2) the presence of intensely altered paleosols beneath several "reefs" (mineralized basal conglomerates) in the Central Rand Group. These paleosols are Fe-depleted, presumably reflecting their formation in a low-oxygen atmosphere.

The major role that I assign to syndepositional alteration contradicts recent work by Palmer et al. (1989) and Phillips (1988), who favor metamorphic (hydrothermal) alteration as an explanation of the Central Rand Group's exceptionally aluminous composition. In fact, the preservation of syndepositional alteration profiles beneath unconformities suggests that metamorphism was essentially isochemical and therefore not capable of introducing gold to the basin, as Phillips and Myers (1989) proposed.

Combining the foreland basin tectonic setting and the results of one dimensional thermal modelling demonstrates that Witwatersrand metamorphism was probably a result of burial beneath the Ventersdorp and Transvaal Supergroups.

Acknowledgements

I would like to thank my committee members, Dr. Barry Maynard, Dr. Holly Huyck, and Dr. Craig Dietsch, for their careful readings of this dissertation and their many suggestions and comments. More importantly, I thank each of them for their friendship and support during my years at the University of Cincinnati.

I also wish to thank Dr. Sally Sutton of the University of Texas at Austin for analytical help (both XRF and microprobe analyses) and for numerous discussions of Witwatersrand geochemistry.

In South Africa, many thanks to Dr. Charles Kingsley of Anglo-American Prospecting Services, who coordinated from start to finish a visit that was productive, informative, and very enjoyable. This project could not have been brought to completion without Charles' considerable help. Also in South Africa, I would like to thank Keith Kenyon and Clyve Feather for all of their help and hospitality during my visits to Anglo-American's research laboratory in Johannesburg.

Table of Contents

List of Tables

List of Figures

Preamble

The Witwatersrand basin of South Africa has received the attention of geologists primarily because it is tremendously enriched in gold. Almost half of all the gold recovered worldwide through all of history has come from the Witwatersrand--a total of 42 million kilograms of gold recovered in only 105 years of Witwatersrand mining. As might be expected, most research on the Witwatersrand basin has been directed towards understanding the origin of the gold. Following early (and often acrimonious) debate between the "placerists" and the "hydrothermalists", from the 1960's to the present there has been widespread acceptance of the "modified placer" model of gold mineralization. According to the modified placer model, Witwatersrand gold was initially detrital in origin, but was later remobilized by metamorphism. The modified placer theory explains features of the gold that are apparently detrital (concentration in basal conglomerates, association with other heavy minerals, and occurence as rounded, deformed particles) and features that are apparently hydrothermal (delicately crystalline morphologies, uniform fineness, and the absence of nuggets).

Working within the framework of the modified placer model, which suggests the source of the gold is outside the basin, I initially chose to undertake a provenance study using the volumetrically dominant, but economically insignificant greenschist facies meta-sandstones. Many previous provenance studies have used the conglomerates, and unfortunately, have had remarkably little success. Recognizing that sandstone-based provenance studies have been successful in a variety of basins worldwide for a number of years, I hoped that a sandstone-based study might prove more successful in the Witwatersrand basin than had the conglomerate-based studies.

However, two developments altered the provenance-directed course of my research. First, my initial petrographic study of 110 Witwatersrand sandstone samples indicated an almost total absence of feldspars and rock fragments, the two common components of sandstones that typically yield the most provenance information (in contrast to quartz, which is generally not useful in determining provenance). Instead of the common three component system (quartz-feldspar-rock fragments) that is widely applied in provenance studies, the Witwatersrand sandstones presented an unusual two component system of quartz grains and sericite matrix. Not only was this assemblage of little use in determining provenance, but it also raised questions of origin of the sericite matrix. Was the sericite matrix originally rock fragments, or feldspars, or a mud matrix? When did the conversion from precursor grain to sericite occur? Recognizing a major matrix component made it clear that a traditional provenance study was untenable for the sandstones of the Witwatersrand basin. Instead, my initial petrographic study prompted a study of the alteration history of the Witwatersrand meta-sandstones.

The second development that influenced the direction of my research was a renewal of interest in the hydrothermal model of gold mineralization by Phillips and others (Phillips, 1987 and 1988; Phillips et al., 1987; Palmer et al., 1989; Phillips and Myers, 1989). The revival of the hydrothermal model was, like my work, based on studies of the unmineralized sandstones and shales of the basin. Recognizing an unusually aluminous bulk chemistry in selected stratigraphic horizons and a pervasive greenschist facies metamorphism in the basin, Phillips and others hypothesized a metasomatic event in which hydrothermal fluids removed alkalis and residually concentrated aluminum by exploiting lithologic contacts, faults, and shear zones (Phillips, 1987 and 1988; Palmer et al., 1989). They then expanded the scope of the metasomatic event beyond the aluminosilicates and into the realm of gold mineralization. Noting that several features of Witwatersrand gold are difficult to explain by the placer model of mineralization, Phillips and Myers (1989) explicitly argued that the Witwatersrand gold is of hydrothermal origin.

The work of Phillips and colleagues focussed attention on the alteration history of the Witwatersrand basin and therefore reinforced my decision to move away from a traditional provenance study and instead to examine aspects of the chemical evolution of the sediments in the Witwatersrand basin. Specifically, is the abundance of sericite matrix in the sandstones and the generally aluminous bulk chemistry a product of hydrothermal alteration, as proposed by Phillips, or is it the product of earlier chemical alterations, during either weathering or diagenesis? The question is clearly relevant to models of mineralization. In simplest terms, the hydrothermal model, as presented by Phillips, is based on and requires major metasomatism. The modified placer model, on the other hand, calls for only minor metasomatism.

On a much broader scale, beyond the mineralization of the basin, an investigation of weathering in the Witwatersrand basin is of great interest because the basin is extremely old, almost 3,000 Ma. Interest in Archean weathering stems from several observations that suggest the Archean atmosphere had less O_2 but more CO_2 than today's. Among the most important of these observations are the presence of easily oxidized detrital minerals (uraninite and pyrite) in fluvial sediments, the absence of redbeds in the Archean, the proliferation of banded iron formations at approximately 2,000 Ma, and the presence of water-lain deposits in spite of a sun 20-30% less radiant than today's (which implies significant greenhouse warming). Because weathering profiles record the interaction between the Earth and atmosphere, they can provide additional, and more direct, evidence for the presence (or absence) of atmospheric differences between the Archean and the present. For example, Holland has constrained O_2 levels in the Archean and Proterozoic atmosphere using the behavior of iron in soils (see, for example, Holland, 1984; Holland et al., 1989; Holland and Beukes, 1990). I use a very similar line of reasoning in my examination of Witwatersrand paleosols.

To investigate the role of weathering and diagenesis versus metasomatism in the Witwatersrand, I relied heavily upon integrated geochemical and stratigraphic data. The specific techniques and principles involved are discussed in chapters 5 and 6. First, however, by way of introduction to the basin and to provide essential background information to the discussion of chemical alterations, I discuss the age, tectonics, metamorphic history and petrography of the basin. Portions of the discussion that follows are from the extensive Witwatersrand literature; other portions are the result of my own work on approximately 300 thin sections, polished sections, doubly polished sections, and whole rock samples since 1987 at the University of Cincinnati.

Chapter 1. Introduction

Geography and History

The Witwatersrand basin lies entirely within the Republic of South Africa (figure 1), in the northern part of the country known as the high veld--a flat and nearly treeless expanse of land. There is little surface expression of the Witwatersrand because the basin is overlain by essentially undisturbed, flat-lying volcanics and sediments of the Ventersdorp, Transvaal, and Karoo systems. Beneath this volcano-sedimentary cover, Witwatersrand sediments are nearly horizontal over most of the basin. Only along the margins and around the Vredefort dome have Witwatersrand strata been structurally disturbed into dipping beds, the more resistant of which form subdued ridges that stand above the veld. One of these ridges, the "white water ridge" ("Witwatersrand" in Afrikaans) in the vicinity of modern Johannesburg marks the original discovery site of Witwatersrand gold. A thin quartz pebble conglomerate that crops out along the ridge was sampled in 1886 by George Walker and George Harrison. When the conglomerate, later to be named the Main Reef Leader, left a tail of gold in Harrison's pan, the rush began. Claims were bought and sold, stamp mills were brought in, mines opened, the town of Johannesburg was laid out, and prospecting intensified. Prospectors discovered similar Witwatersrand strata cropping

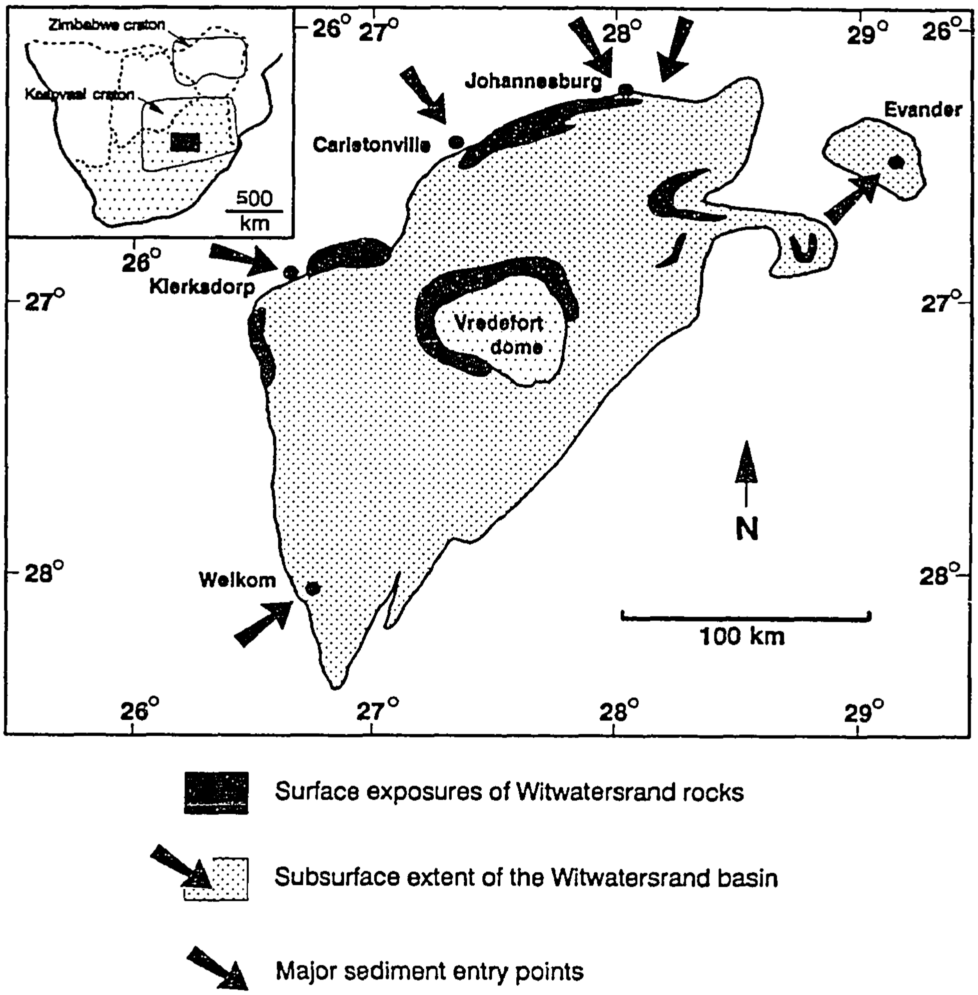

Figure 1. Geologic setting (inset) and location map of the Witwatersrand basin. The basin is situated on the Kaapvaal craton. To the north is the Limpopo mobile belt, which marks the suture between the Kaapvaal and Zimbabwe cratons. Also shown on the figure are the six major entry points to the basin. A fluvial fan is present at each entry point, and each fan is a major goldfield.

out east of Johannesburg (the "East Rand") and as far west as Klerksdorp (figure 1). Surface drilling in the vicinity of Johannesburg proved the continuation of the south-dipping Main Reef Leader to a depth of 730 m, where gold grades were still economic, to the surprise of many who held that the Witwatersrand deposits were only "surficial". Thus, within the first 10 years of exploitation the huge extent of the deposits was more or less known.

As a consequence of the Boer war, World war I, the depression, and South Africa's adherence to the gold standard, the first half century of mining was sporadic, particularly in the goldfields farther removed from Johannesburg. However, in the 1930's, 1940's and 1950's, mining activity increased in response to a variety of developments: South Africa went off the gold standard, geophysical exploration techniques improved, mining companies consolidated, and uranium became a mineable commodity. The geographic limits of the basin were extended as well. In 1946, the opening of the first mine at Welkom stretched the basin 100 km to the south into the Orange Free State, and in 1958 the easterly limit of the basin was expanded 60 km when mining began at Evander. Today, the massive and stable Witwatersrand mining industry has extracted more than 42 million kilograms of gold. Production is expected to continue at the rate of at least 600,000 kilograms gold per year into the next century (South African Chamber of Mines, 1988).

Geologic setting

The Witwatersrand basin forms part of the Kaapvaal craton, an Archean age granite/greenstone complex (figure 1). To the north, the Kaapvaal craton is bounded by the Limpopo mobile belt, which is composed of high grade gneisses and metamorphosed sediments and anorthosites (Windley, 1977). The Limpopo belt separates the Kaapvaal from the Archean Zimbabwe craton. Radiometric ages from the Kaapvaal craton are variable, probably reflecting several episodes of granite emplacement (Cahen et al., 1984). The oldest dates from the craton are 3,555 $\pm$ 111 Ma from a granitic gneiss in Swaziland (Barton et al., 1980) and 3,540 $\pm$ 30 Ma for basal greenstone volcanics of the Onverwacht group at Barberton (Hamilton et al., 1979).

The Archean supracrustal sequence on the Kaapvaal craton consists of the Dominion Group, the Witwatersrand Supergroup, and the Ventersdorp Supergroup (figure 2). The Dominion Group lies directly on the Archean granitic crust of the Kaapvaal craton. At the base of the Dominion Group is the Rhenosterspruit Formation, a thin (< 60 m) conglomeratic sandstone (Tankard et al., 1982). Overlying the Rhenosterspruit is the much thicker Rhenosterhoek Formation, which consists of roughly 1,100 m of basaltic andesite (Crow and Condie, 1987). Flows are dominant, with lesser tuffs and breccias. The uppermost formation of the Dominion Group is the Syferfontein, which consists of dacitic to rhyolitic

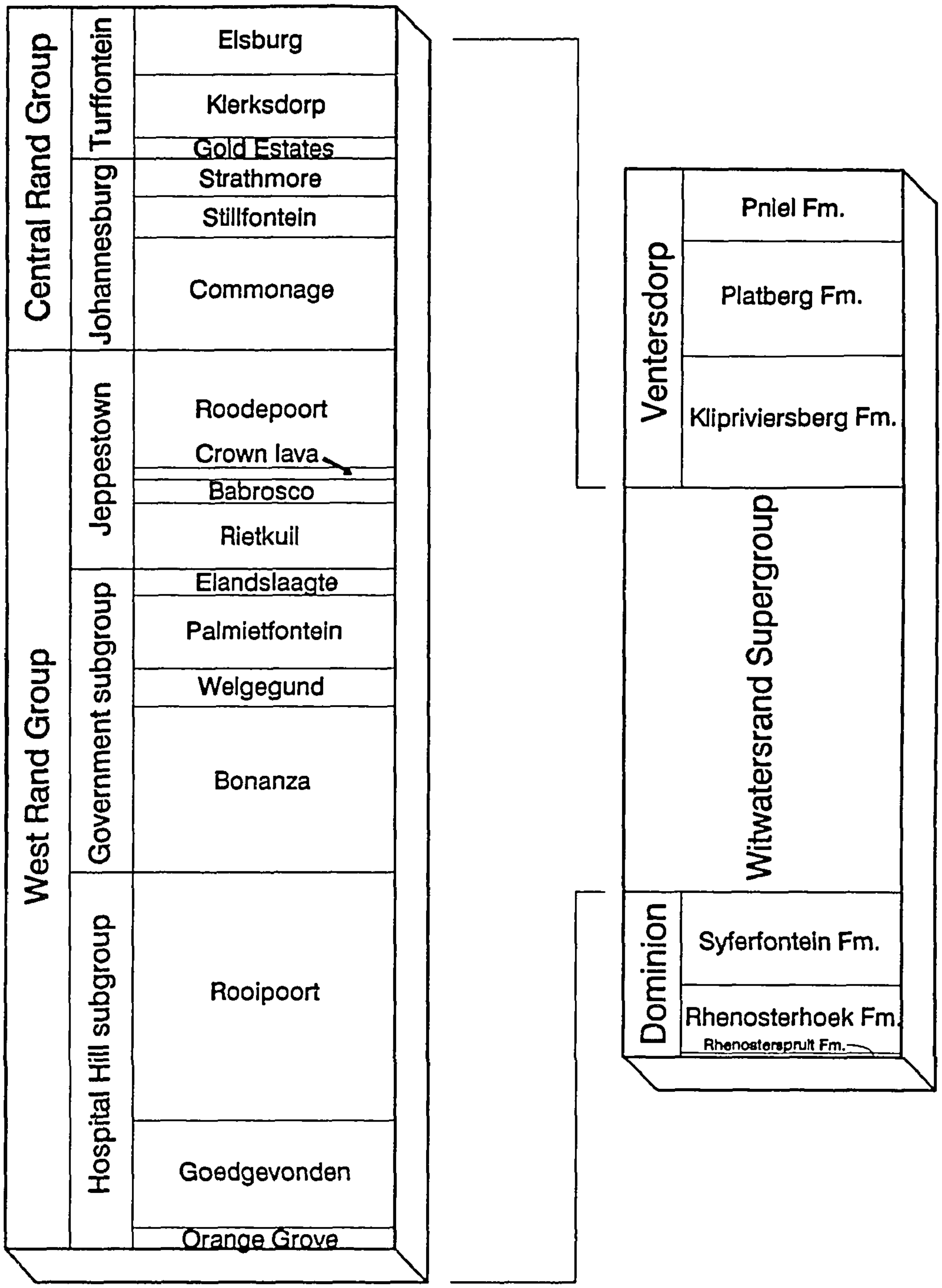

Figure 2. The generalized stratigraphic column for the Dominion Group, Witwatersrand Supergroup and Ventersdorp Supergroup in the vicintiy of the Klerksdorp goldfield. From SACS (1980) and Antrobus et al. (1986).

tuffs and breccias. The maximum thickness of the Syferfontein formation is 1,550 m (Tankard et al., 1982).

The areal extent of Dominion rocks is not firmly established. Scattered outcrops occur along the northern and western margin of the Witwatersrand basin, and also around the Vredefort dome (figure 1 of Watchorn, 1981), but there is no evidence that the Dominion group is present beneath the eastern half of the basin. Reimer (1987) estimated the total areal extent of the Dominion group to be about 16,000 km^2, implying that less than half of the Witwatersrand is underlain by the Dominion.

Mineralization in the Dominion Group is limited to conglomerates of the Rhenosterspruit Formation, where it takes the form of apparently paleo-placer concentrations of gold and uranium. Uranium is much more important than gold in the Dominion. Only 25,000 kg of gold were extracted from the Dominion mines from 1936 to 1961, when production shut down. Over the same period, roughly 2,000,000 kg of uranium were recovered (Antrobus et al., 1986).

The Witwatersrand Supergroup, which is composed of a series of shales, sandstones and conglomerates, overlies the Dominion volcanics uncomformably, and has been subdivided into the older West Rand Group and the younger Central Rand Group (figure 2). Sediments of the West Rand Group, which has a maximum thickness of 7,500 m (Tankard et al., 1982) consist of equal parts of sandstone and shale, and are divided, from bottom to top, into the Hospital Hill, Government and Jeppestown Subgroups. Primarily on the basis of bimodal-bipolar paleocurrents, hummocky cross-stratification, basin-wide fining up sequences, and chemically deposited sediments, the Hospital Hill and Jeppestown Subgroups are interpreted to have been deposited in a shallow marine or inland sea environment. The Government Subgroup, which contains fining-up sequences and unimodal paleocurrents, was probably deposited in fluvial lobes or fan deltas (Tankard et al., 1982).

The Central Rand Group is significantly coarser grained than the West Rand: quartz arenites, subgreywackes, subarkoses, and quartz pebble conglomerates are the dominant rock types. Two subgroups, the Johannesburg and Turffontein, are recognized. The boundary between the two is the Booysen's shale, a basin-wide fining up sequence that probably resulted from rapid subsidence (Tankard et al., 1982). Total thickness of the Central Rand Group in the type areas is just over 3,000 m, with the Turffontein being the slightly thicker of the two formations (Pretorius, 1976).

Six major entry points to the basin have been recognized (figure 1). At each entry point a large fluvial fan formed. Gradients on these fans were approximately 1:20, accounting for the coarse nature of the sediments (Pretorius, 1976). The fans coalesce at their extreme distal ends, and some reworking of fine grained sediments becomes evident. The unimodal orientation of these reworked deposits and the general asymmetry of the fans suggest that the distal regions either were deposited under the influence of longshore currents (Pretorius, 1976) or were reworked in an axial river system running parallel to the basin margin (Wheelock, 1987). The proximal fan deposits, on the other hand, are clearly alluvial or fluvial. Braided channels, gravel bars, unimodal downslope paleocurrents, trough and planar cross beds, and scour surfaces are recognized (Minter, 1979; Tankard et al., 1982).

Gold production in the Witwatersrand basin is predominantly from the Central Rand Group. Geographically, six main gold fields correspond to the six alluvial fans built up at the sedimentary entry points to the basin (figure 1). Generally, the high-grade ore is found in the more proximal fan deposits, whereas the lower grade ore is found in the distal fan deposits. Within each goldfield, economic concentrations of gold and uranium occur in quartz pebble/pyrite conglomerates, or "reefs", that lie immediately above regional unconformities. The reefs are usually less than one meter thick, and the gold itself is commonly limited to a thin interval (usually the base) of the reef. At the smallest scale, gold is usually associated either with pyrite, which commonly constitutes as much as 10% of the reef, or with carbon, which occurs either in thin (1-2 cm max.) seams, generally at the base of the reef, or dispersed as small particles of "fly-speck" carbon within the reef.

The Ventersdorp Supergroup is a 5 km thick sequence of subaerially erupted volcanic rocks with a minor sedimentary component. Three groups are recognized--the Klipriviersberg, the Platberg and the Pniel (Winter, 1976). The Klipriviersberg, which conformably overlies Central Rand sediments over the entire basin, is composed of as much as 2 km of thick mafic lavas, some of them komatiitic (Crow and Condie, 1988). The numerous thick flows were apparently erupted in rapid succession, because there are no sediments or paleosols between flows. The composition, areal extent, and continuity of flows suggests an analogy between the Klipriviersberg Group and more recent continental flood basalts.

A hiatus in volcanism, a period of normal faulting, and the deposition of sediments mark the transition from the Klipriviersberg Group to the 1,800 m thick Platberg Group (SACS, 1980). Above its basal clastic sediments, the Platberg is dominantly volcanic, with intermediate to felsic rocks prevalent. The Pniel Group, at the top of the Ventersdorp, consists of the clastic sediments of the 400 m thick Bothaville Formation and the overlying intermediate volcanics of the 700 m thick Allanridge Formation (SACS, 1980).

Age

Radiometric ages to constrain the age of sedimentation in the Witwatersrand basin have been obtained from the underlying Dominion volcanics, the overlying Ventersdorp volcanics, and from volcanics and sediments within the basin. Whole rock ages from all of these sources are suspect, because they may be partially reset or because they may have inherited older xenocrysts. The most reliable of these ages indicate that the Witwatersrand is extremely old, in excess of 2,500 Ma. This Archean age is surprising considering the lack of Witwatersrand deformation--Witwatersrand sediments are virtually undisturbed structurally and the effects of metamorphism are apparent only in thin section, in contrast to the highly deformed, metamorphosed gneissic terranes and greenstone belts that are typical of the Archean (Windley, 1977).

Ion microprobe U-Pb ages from single zircons have confirmed the great age of the basin. Armstrong et al. (1990) analyzed zircons from the basement and from the Dominion and Ventersdorp volcanics. The basement granitoid they analyzed yielded a single zircon $^{207}Pb/^{206}Pb$ age of 3,120 $\pm$ 5 Ma. The Dominion Group's Syferfontein Formation, which immediately underlies the Witwatersrand, yielded a single zircon $^{207}Pb/^{206}Pb$ age of 3,074 $\pm$ 6 Ma. An upper age limit for Witwatersrand Supergroup sedimentation comes from the overlying Ventersdorp volcanics. Zircons from two formations of the Ventersdorp (the Makwassie quartz porphyry and the Klipriviersburg basalts) yielded single zircon $^{207}Pb/^{206}Pb$ ages of 2,709 $\pm$ 4 Ma and 2,714 $\pm$ 8 Ma, respectively. These two ages, which are not statistically different from one another, indicate first, that Ventersdorp volcanism proceeded rapidly, and second, that deposition of Witwatersrand sediments was complete by about 2,720 Ma at the latest.

In addition to the ages obtained from the underlying Dominion Group and the overlying Ventersdorp Supergroup, single zircon ages have been collected from volcanic and sedimentary units of the Witwatersrand Supergroup. Barton et al. (1989) analyzed zircons from the Orange Grove quartzite, at the base of the Witwatersrand section, and found one population of circa 3,300 Ma zircons and another, smaller population of circa 3,000 Ma zircons. The younger zircons establish that Witwatersrand sedimentation did not begin before 3,000 Ma. Armstrong et al. (1990) analyzed zircons from a 40 kg sample of the Crown lava, which lies near the top of the West Rand (figure 2), with little success. However, zircons from a second sample have been analyzed, yielding an age of approximately 2,900 Ma (Minter, pers. comm., 1990). Robb et al. (1990) analyzed a number of single detrital zircon grains from various stratigraphic levels within the Witwatersrand. Although the ages of detrital zircons can tell us only about the crystallization history of source rocks, and therefore give only the maximum age of deposition, the results of Robb et al. (1990) are consistent with Witwatersrand sedimentation between 3,000 and 2,700 Ma. The $^{207}Pb/^{206}Pb$ ages of detrital zircons range from 3,305 Ma to 2,894 Ma, with a geometric mean of 3,073 Ma. Significantly, 45% of the zircon ages fall within 30 m.y. of the geometric mean, implying a major crust-forming event at about 3,073 $\pm$ 30 Ma. This event corresponds approximately with the Pb/Pb age (3,074 $\pm$ 6 Ma) of the immediately underlying Dominion volcanics. A possible scenario, then, is one in which at about 3,070 Ma there is a major crust-forming episode in the Witwatersrand source area that is accompanied by Dominion volcanism, followed by Witwatersrand sedimentation between 3,000 Ma and 2,700 Ma. To develop this scenario further, and to integrate the radiometric data with structural and sedimentological data, a tectonic reconstruction of the Witwatersrand basin is necessary.

Chapter 2. Tectonic evolution of the Witwatersrand basin

Understanding the tectonic evolution of the Witwatersrand basin is valuable for several reasons. First, with respect to the mineralization, knowledge of the tectonic setting may provide a direct link to the source of the gold. The modified placer model does not ultimately address the question of the source of the gold. If the gold is a placer deposit, what were the source rocks, where were they during deposition, and where are they now?

Second, did the basin's tectonic evolution control mineralization on a large scale? For example, a foreland basin typically cannibalizes earlier-deposited sediments, thus recycling and possibly concentrating placer gold. A steep-sided, fault-bounded basin may show great variations in sediment supply, depending on when and where the faults are active. An uncomplicated thermally subsiding basin with minimal faulting and transport will simply unroof the source area.

Third, what can the tectonic evolution of the Witwatersrand basin tell us about the evolution of continental crust through geologic time? The Witwatersrand is one of the oldest and best preserved basins on Earth. As such, it provides an opportunity to compare Archean basin development to more recent basins and to consider crustal development during the transition from Archean style tectonics (small, mobile plates) to Proterozoic style tectonics (large, stable plates).

Early views on the evolution of the Witwatersrand basin were shaped largely by the work of Pretorius (1975, 1976, 1981), who has referred to the basin at various times as a half-graben, a yoked basin, or simply an asymmetric, fault-bounded basin. More recently the basin has been modeled as a thermally subsiding continental rift (McKenzie et al., 1980; Nisbet, 1984) or as a foreland basin on the craton side of an Andean-type margin (Burke et al., 1986; Winter, 1987). These models have been largely speculative--perhaps necessarily so, considering the paucity of rock outcrop available for study. Whatever the hinterland of the Witwatersrand basin may have been, a combination of erosion, younger sedimentary cover and massive intrusion (the Bushveld) has left very little material for study.

Data for a reconstruction of the Witwatersrand basin must therefore come from within the basin, with only minor contributions from other areas of the Kaapvaal craton. In chapter 1 I summarized the geologic setting, stratigraphy, and radiometric ages relevant to the basin. I will here provide some additional data that are pertinent to understanding the basin evolution--basin geometry, total thicknesses of sediments, and folding and faulting of the strata. Following this, I will discuss various models of basin evolution.

Basin geometry and sediment thickness

Reported thicknesses for the Witwatersrand basin vary, depending on where total sediment thickness is measured and what units are included as part of the basin. Witwatersrand Supergroup strata alone attain a maximum thickness of about 7,500 m (figure 2). To this is generally added the 2,500 m thickness of the Dominion Group, because the Dominion lies entirely within the geographically defined basin (if we define the basin as the areal extent of Witwatersrand Supergroup sediments). I do not include the Ventersdorp as basin fill because it extends hundreds of kilometers beyond the geographic Witwatersrand basin. Thus, the maximum thickness of the basin fill is about 10,000 m.

In map view, the basin is elliptical (figure 1), and approximately 350 km along the northeast-southwest axis by about 200 km in breadth. The length may be much greater, but younger cover obscures both the northeast and southwest limits of the basin. As figure 1 reveals, Witwatersrand sediments are exposed only in isolated areas, primarily along the northwest margin of the basin. The basin is asymmetric, with steeper dips on the northwest side and shallower dips on the southeast. Paleocurrent analyses also indicate a marked asymmetry--virtually all of the sediment in the basin was delivered from source areas to the north and west (figure 2 of Robb and Meyer, 1990). By extrapolating isopachs, Pretorius (1976) has postulated that the original extent of the basin to the northwest was greatest during West Rand sedimentation. As deposition progressed, the northwest margin migrated southeastward (figure 3), while the southeast margin remained relatively stable. The effects of the migrating basin margin are observed in the Central Rand sediments, where unconformities of the type illustrated in figure 4 are common. The presence of ripped up mud clasts (Minter, 1976), ubiquitous channelling and erosion of the footwall, and analogy with modern fan processes all suggest that the units involved were unlithified. This sequence of uplift, erosion, and redeposition is considered by the placerists to have been important in concentrating the gold.

Folding and faulting

Many of the goldfields contain evidence of minor folding. The folds that are observed commonly influence sedimentation patterns, and so were active during deposition of Witwatersrand sediments. At the east end of the basin, the East Rand goldfield contains small en echelon folds. Payshoots are aligned with these folds, suggesting the folding was active during Central Rand sedimentation (Antrobus and Whiteside, 1964; Stanistreet et al., 1985). In the nearby northeast corner of the basin, the Bird lava thickens over synforms and thins over antiforms--clear evidence of active folding during Johannesburg (Central

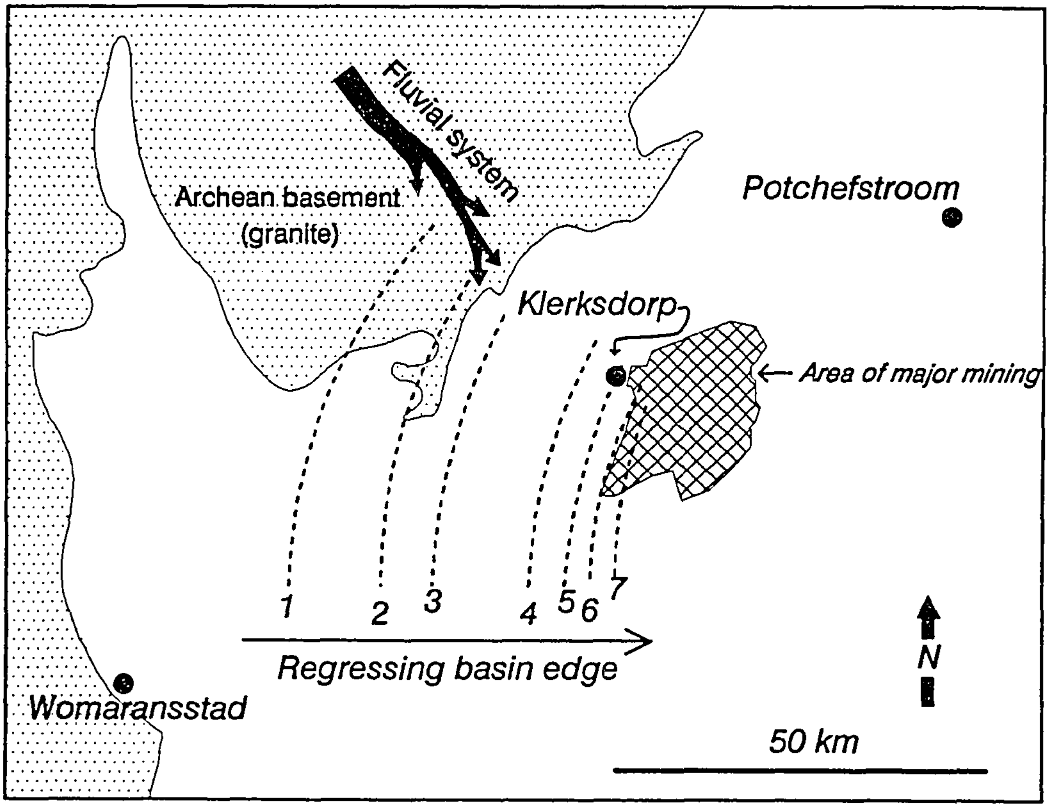

Figure 3. Migration of the basin margin at the Klerksdorp goldfield. The numbered dashed lines indicate the position of the basin margin during deposition of the Dominion (#1), Government (#2), Jeppestown (#3), Main (#4), Livingstone (#5), Vaal (#6) and Kimberley (#7) reefs. From Pretorius (1975).

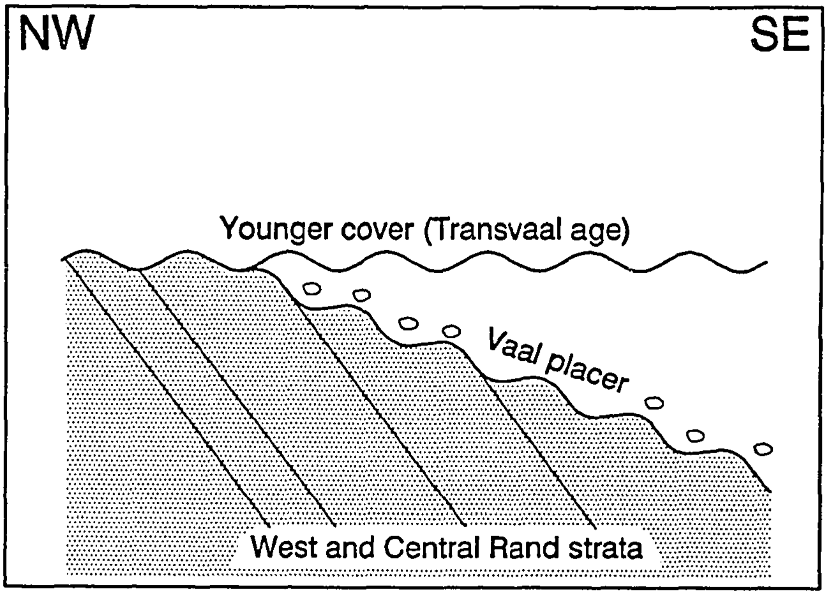

Northwestern basin margin

Figure 4. Schematic representation of a typical angular uncomformity along the NW margin of the basin that demonstrates two episodes of uplift and erosion during basin evolution. First, the Vaal reef is deposited on top of uplifted and eroded older Witwatersrand units (the shaded units). Younger cover (the Black reef of Transvaal age) is then deposited on top of the uplifted and eroded Vaal reef. From Burke et al. (1986).

Rand) sedimentation. From the far west of the basin, Minter et al. (1986; figure 32) described a fold that was active during deposition of the uppermost Turffontein sediments. The folding produced a local truncation of the Van den Heeversrust Member by the overlying Uitkyk Boulder Member. Except for the area disturbed by folding, these two members are conformable. A final example comes from the Klerksdorp goldfield, where three stratigraphic units (the Mapaiskraal Member, the Gold Estates Formation, and the Klerksdorp Formation) show clear evidence of deposition, then folding, and then peneplanation (figures 17, 18, and 21 of Antrobus et al., 1986). The folds are paired anticlines and synclines, with fold axes parallel to the basin margin (figure 5).

These examples provide clear evidence of folding synchronous with sedimentation. Any model of basin evolution must therefore account for both the sedimentation patterns and the syn-sedimentary deformation.

The most abundant faults in the basin, and those that have been most thoroughly mapped (because they offset the reefs), are faults that postdate Witwatersrand sedimentation. The majority of these faults parallel the depositional axis of the basin, are relatively steep, and have normal displacements of $\leq$5,000 m, but generally 1,000-2,000 m, resulting in a system of horsts and grabens (Pretorius, 1976). These major faults are contemporaneous with Ventersdorp deposition (figure 6). In figure 6,

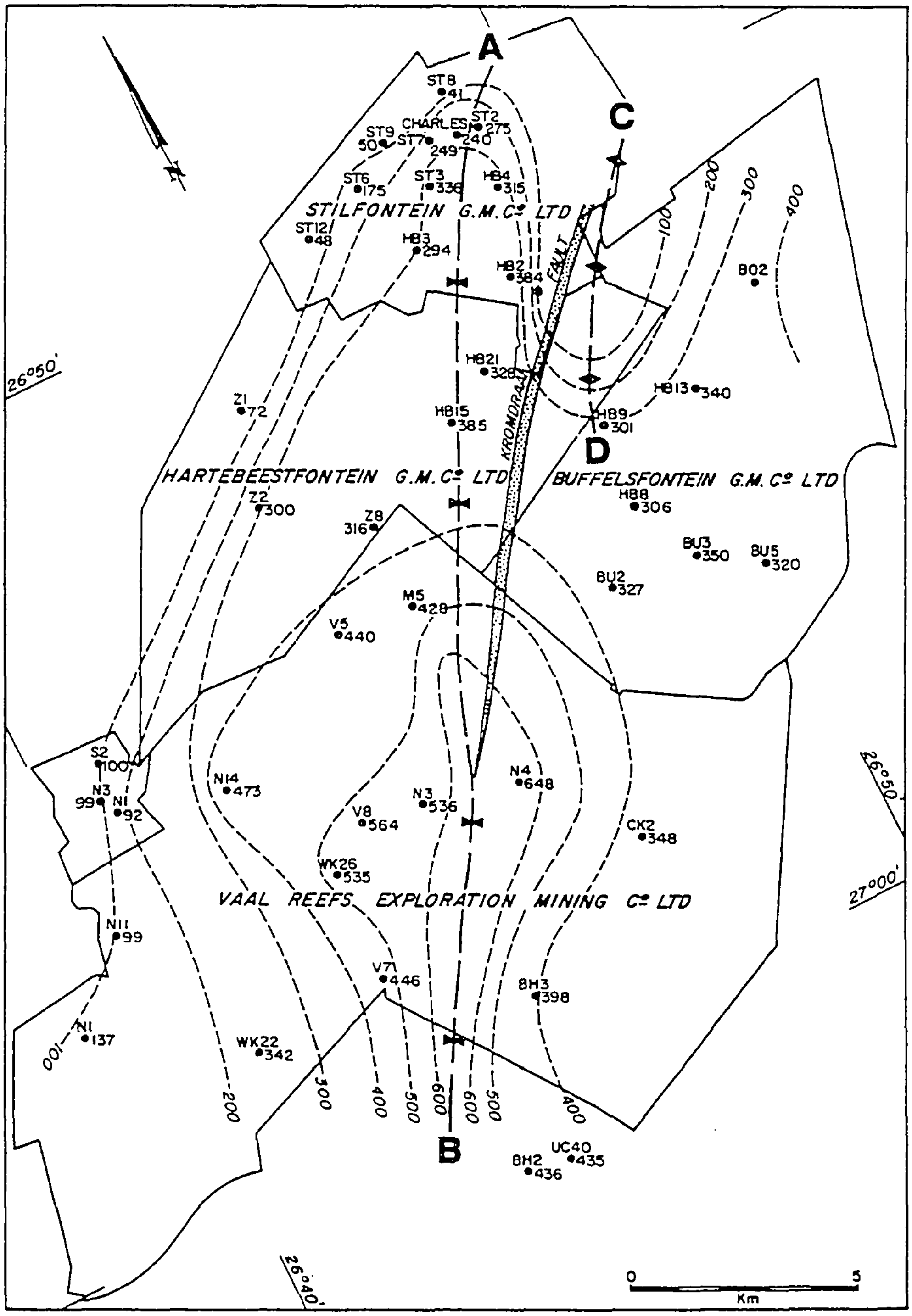

Figure 5. From the Klerksdorp goldfield, isopachs of the Klerksdorp formation that indicate the sediments were gently folded and then planed off by erosion prior to deposition of the overlying Elsburg formation. The fold axes (syncline A-B and anticline C-D) are aligned NE-SW, parallel to the basin margin. From Antrobus et al. (1986).

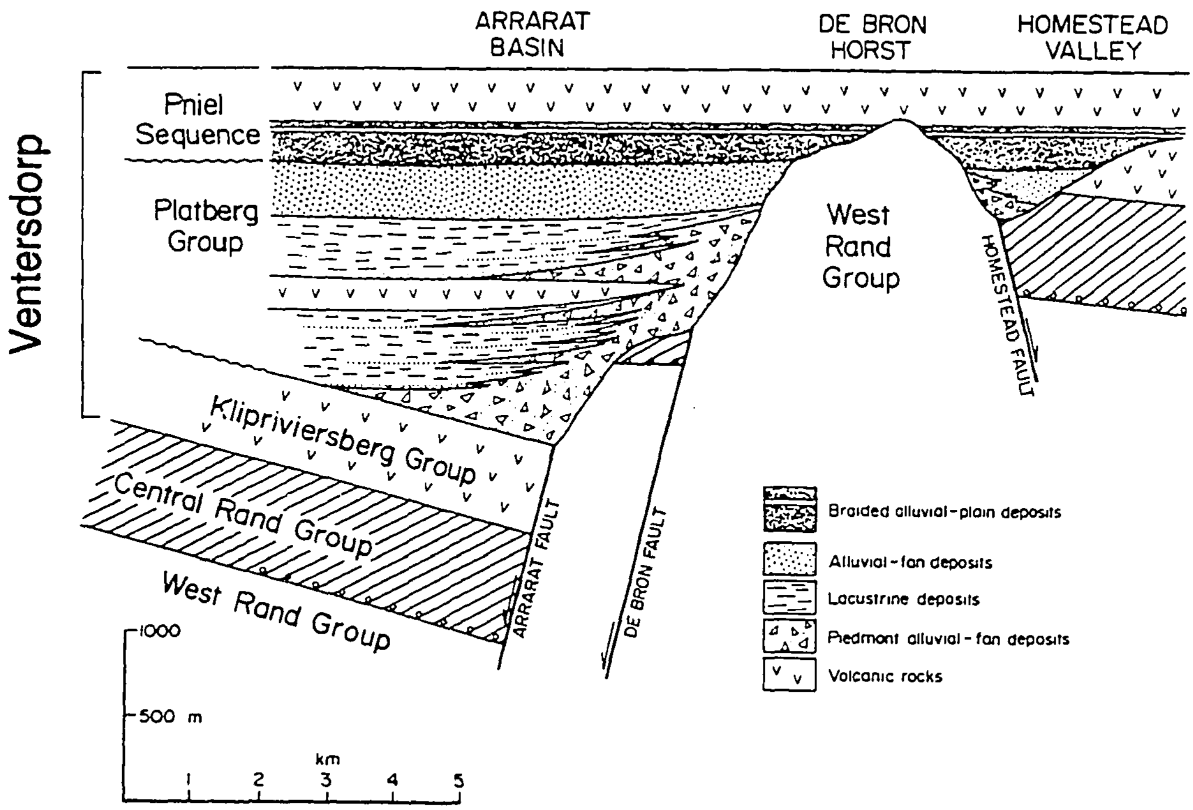

Figure 6. Faulting associated with Ventersdorp volcanism and sedimentation. See text for detailed explanation. From Tankard et al. (1982).

Witwatersrand sediments and basal Ventersdorp lavas (the Klipriviersberg) are offset by the faults; the middle Ventersdorp rocks (Platberg Group) form a wedge off the fault block (indicating contemporaneous activity) and the upper Ventersdorp rocks (Pniel sequence) lie undisturbed over the faulted region. There are also numerous smaller, post-Witwatersrand faults throughout the basin. Stannistreet et al. (1985) have demonstrated the interrelationship of the majority of these late faults and their origin during a Ventersdorp rifting event.

Faults that are synchronous with Witwatersrand sedimentation are also present, although such faults are found only very near the basin margin. Winter (1987) described two thrust faults that displace the Basal reef in the Welkom goldfield, and indicated that one of these faults terminated prior to deposition of the uppermost Witwatersrand sediments. A similar scenario is described by Els and Beukes (1987) in their study of the Middlevei placer at the Carletonville goldfield. Normal faults that offset the lowermost conglomerate by 50 cm do not offset the upper conglomerates, which are 1-2 m higher in the section. Further down in the stratigraphic section, Burke et al. (1986) referred to a report of Cluver (1957) wherein faults were described as disrupting West Rand sediments but not Central Rand sediments. Finally, both Pretorius (1976) and Burke et al. (1986) postulated a fault-bounded northwest margin to the basin. Because the dip of the Witwatersrand sediments along this margin changes from approximately 20° at the surface to near vertical at depth, the fault must have been active during deposition (Burke et al., 1986). The sense of displacement on this basin-bounding fault is disputed. Pretorius considered normal displacement most likely; Burke et al. interpreted reverse faulting.

That reports of intrabasinal, syndepositional faults are few and of a rather cursory nature should not be interpreted as evidence that such faults are scarce. The scant documentation may instead reflect either an inability to recognize early faults through the many later faults or a simple lack of interest. The post-Witwatersrand faults have attracted considerable attention because they offset gold-bearing horizons. Early, pre-Central Rand faults that do not offset the important gold reefs may have been overlooked or ignored.

Application of tectonic models

Cratonic sedimentary sequences are generally thin and laterally extensive. Thick, discrete cratonic basins, such as the Witwatersrand, imply major crustal disturbances. The disturbances that have been invoked to explain the Witwatersrand basin are many: rifting, rifting followed by thermal contraction, granite diapirism, interference folding, high angle faulting, and structural loading in the hinterland leading to foreland subsidence are among the more commonly cited ideas. Particular types and sequences of sedimentologic, volcanic, and tectonic activity are implicit in each model. For example, continental rifting, when well developed as it would have to be to account for the size and depth of the Witwatersrand basin, is characterized by abundant normal faulting and prodigious, usually chemically bimodal, volcanism. Such faulting and volcanism is present below and above the Witwatersrand Supergroup (the Dominion Group and the Ventersrsdorp Supergroup), but not within the Witwatersrand sequence.

Granite diapirism and interference folding (Pretorius, 1981), as applied to the basin, are quite similar. In both, gently uplifted regions of Archean basement provide positive areas from which sediment is eroded and deposited into an adjacent basin. Topographic relief is ascribed to diapir emplacement in the former, and to the intersection of northwest- and northeast-trending folds in the latter (producing domes where anticlines intersect and basins where synclines intersect). The chief difficulty with these models is their inability to explain the great thicknesses observed in the basin and the rapid lateral variations in thickness. Doming and folding of the craton more typically produce low relief, laterally extensive deposits (Miall, 1984, p. 442). Also, the apparently fault-bounded northwest margin (Pretorius, 1976 and Burke et al., 1986) and the presence of the basal Dominion volcanics argue against these essentially non-tectonic models.

The models which remain (rifting plus thermal subsidence, foreland basin, and high angle faulting) more closely fit the actual geologic record of the Witwatersrand basin. Of these, the classic interpretation of Pretorius (1975) is most frequently invoked. Various terms have been applied to his ideas--intermontane basin, yoked basin, half graben--but Pretorius (1975) suggested that the Basin and Range province of the U.S. provides an analog. However, the Basin and Range is an extensional regime and is probably better classified as incipient rifting, which will be discussed below. A better comparison may be to the Tertiary basins developed adjacent to western U.S. Laramide uplifts (e.g., the Powder River, Bighorn and Wind River basins). These Laramide uplifts and basins developed in a compressional tectonic setting as a result of drag between the North American craton and the shallow-dipping, subducting Farallon plate (Kaufman, 1982). The basins, which I will refer to as "intermontane," are similar to the Witwatersrand on several counts. Intermontane basins are bounded by steep reverse faults; a similar steep boundary fault may define the northwest margin of the Witwatersrand basin (Pretorius, 1976). Their overall dimensions are similar, as are their shapes--elliptical, but not exceedingly elongate. Alluvial or fluvial fans debouching from the border uplifts are the dominant mode of sedimentation in intermontane basins, as is the case for the Central Rand. Finally, sediment accumulation rates in the basins are similar. A maximum of 300 m.y. was available for Witwatersrand sedimentation, during which a total of 10,000 m of sediment accumulated in the basin. If sedimentation was continuous over the full 300 m.y., then the sediment accumulation rate was roughly 0.033 m/1000 years. This is, of course, a minimum estimate. If the basin was inactive for a time either after Dominion volcanism or before Ventersdorp volcanism, the accumulation rate would have been greater. Comparison with the data of Schwab (1976) indicates that a minimum accumulation rate of 0.033 m/1000 years is compatible with rates determined for other intermontane basins (figure 7).

There are, however, some critical differences between Laramide intermontane basins and the Witwatersrand basin. Fault-bounded intermontane basins do not achieve the same thickness as the Witwatersrand basin. A compilation of six such basins (basins 58-63 of Schwab, 1976) reveals a maximum thickness of 4,000 m and an average of 2,800 m versus the 10,000 m of the Witwatersrand. Also, West Rand deposition was dominantly subaqueous, whereas cratonic successor basins, forming adjacent to basement uplifts, are well above sea level and thus inundation by sea water is not likely. In terms of regional extent, more recent successor basins do not form as isolated basins. They form in areas where underlying tectonic stresses are compressional, with the result that multiple basins form in a region. The Witwatersrand, by contrast, is apparently an isolated basin.

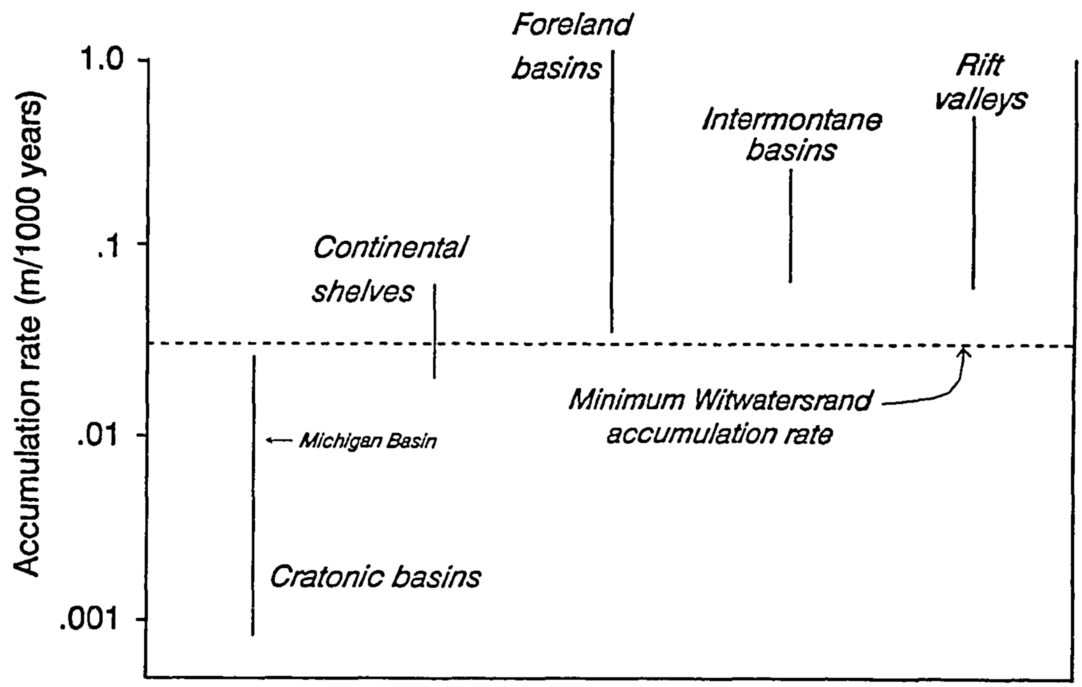

Figure 7. Sediment accumulation rates for various basin types, from Schwab (1976). The "successor" basins of Schwab are here referred to as "intermontane" basins because I include only those basins associated with western U.S. Laramide uplifts (basins 58-63 of Schwab). The solid horizontal line indicates the <u>minimum</u> accumulation rate for the Witwatersrand, assuming that sedimentation was continuous over the 300 million year interval between Dominion and Ventersdorp volcanism. More likely, sedimentation occurred over only a portion of the total time available, in which case the accumulation rate for the Witwatersrand would be higher.

Finally, it is not clear how the basal Dominion volcanics can be fit into the successor basin model. Basins resulting from compressional basement uplifts such as the Bighorn and Powder River are distinctly non-volcanic.

Basin formation by a process of thermal decay was first proposed by McKenzie (1978). The idea caught on rapidly, and several workers have attempted to extend such thermal models back into the Precambrian (McKenzie et al., 1980; Bickle and Eriksson, 1982; Nisbet, 1984). The Witwatersrand, with its underlying and overlying volcanics to provide time control, and its well-documented stratigraphy, has proved one of the better basins for such work. Thermal basin development is two-phased, with an initial stretching and rifting phase followed by a thermally subsiding phase. The rift phase may be associated with sediments, volcanics, or both. Because of the extension and associated fault displacements, sediments are generally coarse-grained and are characterized by rapid thickening and thinning in the fault-bounded structural highs and lows. The volcanics in rifts are generally bimodal (basalts and rhyolites). The lithospheric thinning of this initial stage results in a passive upwelling of hot asthenosphere, creating an elevated geothermal gradient (McKenzie, 1978). As this anomaly cools, the thermal contraction leads to prolonged, slow subsidence. The sediments associated with this later phase of basin evolution are therefore finer-grained, and their deposition is uninterrupted by either faults or intrabasinal volcanics.

The model provides a reasonable interpretation of the early stages in the Witwatersrand. The Dominion volcanics are ascribed to the initial stretching/rifting event. The bimodal composition of the volcanics (Crow and Condie, 1987) is consistent with the model. Following the initial rifting phase, the model predicts slow, prolonged subsidence. The West Rand sediments, which contain 50 percent shale, fulfill this prediction reasonably well. However, with the record of Central Rand sediments, the model begins to break down. Rather than revealing a continuum of ever finer, low relief sedimentation, the Central Rand presents conditions of higher energy and greater relief. The sand:shale ratio increases from 1:1 in the West Rand to 12.6:1 in the Central Rand (Pretorius, 1976). There is also an increase in quartz pebble conglomerates, again an indicator of high energy sedimentation. In addition to the changing character of the sediments, there are geometric and structural relationships in the Central Rand that are not amenable to simple subsidence. Evidence of syndepositional folding appears (figure 5) and the basin margin begins to shift southeastward (figure 3). The basin-wide appearance of a thick shale (the Booysen's shale) in the Strathmore Formation (figure 2) indicates a major episode of rapid subsidence. Syndepositional faults occur. None of these observations can be explained by steady thermal subsidence. Finally, the applicability of thermal subsidence to the entire Witwatersrand sequence can be assessed using sediment accumulation rates. Figure 7 includes a field for cratonic basins, one of which is the Michigan basin. The Michigan basin is one of the basins to which McKenzie (1978) originally, and successfully, applied the thermal subsidence model. Yet it is clear from figure 7 that sediment accumulation rates in the Michigan basin, an ideal thermally subsiding basin, are significantly lower than the minimum calculated rate for the Witwatersrand.

The most recent entries into the field of Witwatersrand basin models are those of Burke et al. (1986) and Winter (1987), who both suggested a foreland basin. The principles that underly a foreland basin model are quite simple (figure 8): loading of the lithosphere will lead to isostatic compensation (subsidence). Subsidence at the point of loading will decrease the elevation of the anomalous load, but in addition, the semi-rigid nature of the lithosphere will also result in subsidence adjacent to the load. In this region of subsidence, the topographic low will be filled by sediments derived primarily from the load (the "hinterland"). Also important in foreland basins is the concept of a mobile hinterland and a migrating basin. The depositional locus is not static. The hinterland advances on the basin by thrusting, eventually re-incorporating earlier (proximal) deposits and recycling them into the basin (figure 9; Allen et al., 1986).

To evaluate the relevance of a foreland basin model to the Witwatersrand, two important lines of evidence must be

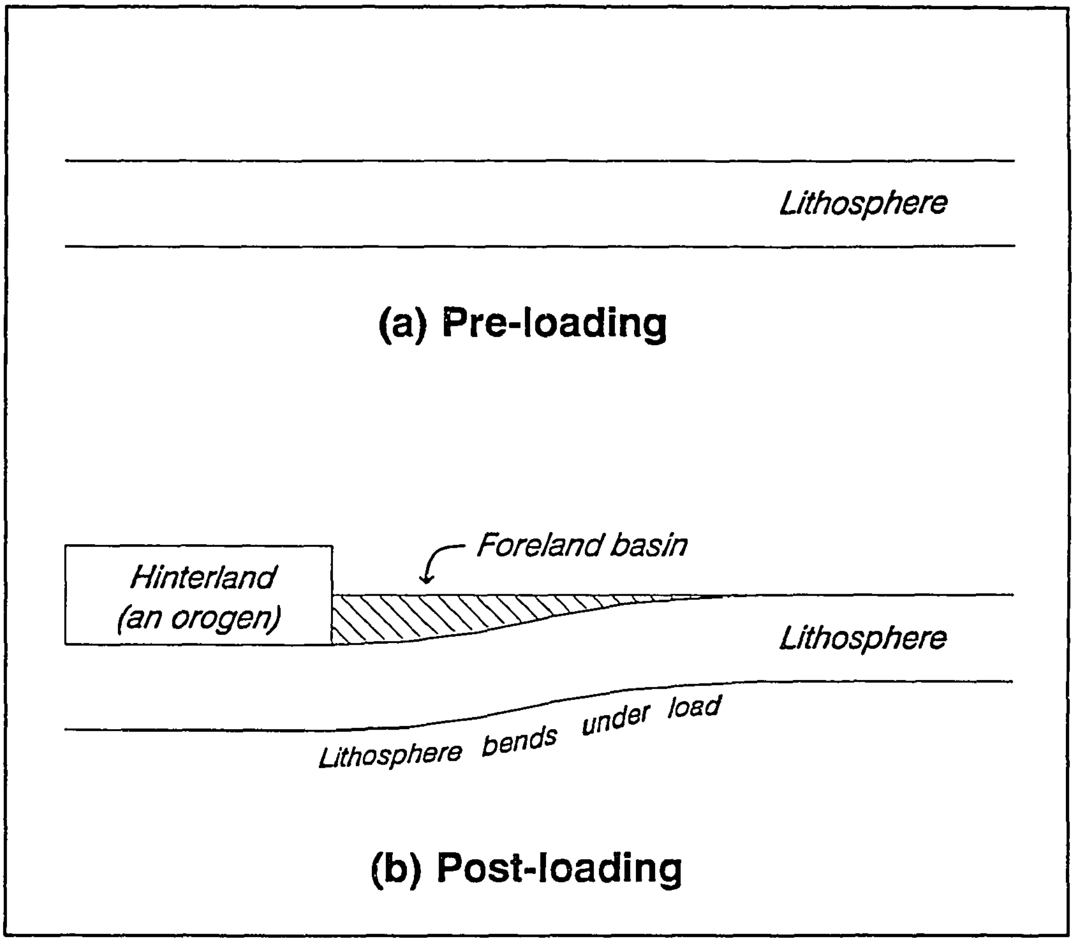

Figure 8. A simple model of foreland basin development. Loading of the crust results in a depression, which is then filled by the eroding hinterland.

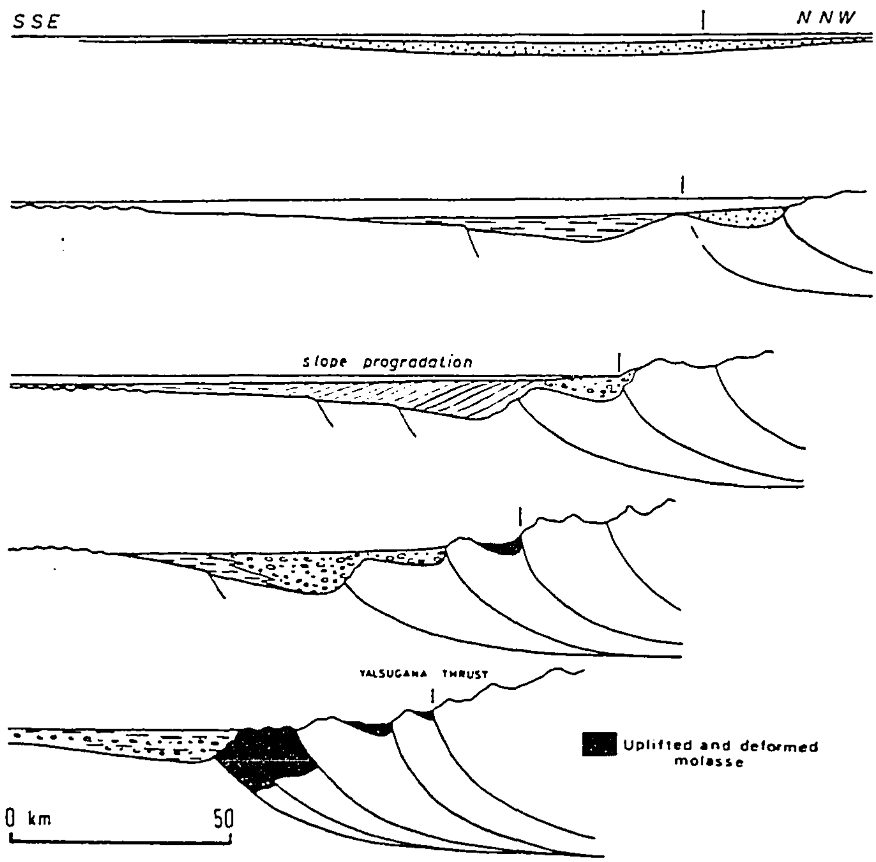

Figure 9. Typical development of a foreland basin. Early, proximal sediments are commonly thrust up at the basin edge and redeposited as the basin migrates from the hinterland (at right) toward the craton (at left). This example is from the Venetian basin, Italy. From Massari et al. (1986).

pursued. First, we must consider the structure and sedimentology of the basin itself: are they compatible with what is known of more recent foreland basins? Second, we must consider the hinterland: what is the evidence for an elevated structural front to the northwest of the Witwatersrand basin?

To address the first question, it is useful to divide the Witwatersrand basin fill into lower (Dominion and West Rand) and upper (Central Rand) segments. The Dominion volcanics and the lowermost West Rand sediments are not easily interpreted in the context of a foreland basin. The volcanics could conceivably be distal deposits of a developing magmatic arc in the hinterland, but the volcanics are not tuffs, they are flows. Also, the volcanics are not andesitic, but bimodal. The West Rand sediments contain a high proportion of shales and show evidence of sydepositional faulting. The shales are not difficult to reconcile with the early, distal stages of a foreland basin. Indeed, fine-grained, subaqueous sediments are typical of the "flysch" stage of development. However, syndepositional faulting of the distal facies is not characteristic of a foreland basin. Faulting, when present, occurs later in the basin evolution as the hinterland advances by propogation of thrust faults in the basin sediments. The earliest stages of foreland basin development should be an uncomplicated response to lithospheric loading--simple subsidence.

Upsection in the upper West Rand and Central Rand sediments, the sedimentologic and tectonic record is more consistent with the foreland basin model. On a very broad scale, foreland basins fill in two stages: An initial underfilled stage characterized by subaqueous, fine-grained, flysch type sediments, and a later, shallow water to fluvial, coarse grained, molasse stage (Miall, 1978; Allen et al., 1986; Covey, 1986). These two stages correlate with the Upper West Rand and the Central Rand sediments, respectively. Sediment dispersal in the molasse stage is controlled by the advancing thrusts from the hinterland. These structural highs are regularly breached along strike, resulting in alluvial fans along the basin margin (figure 10). The similarities between these foreland basin sediment dispersal patterns and the patterns that have been reconstructed for the Witwatersrand (figure 1) are striking. As the basin edge thrusts of a foreland basin advance, the basin margin and the basin depocenter also migrate cratonward. Pretorius (1976) has documented such a migration for the Witwatersrand, from the northwest toward the southeast (figure 3).

The thermal subsidence model was unable to explain the Booysen's shale, syndepositional folding, and the high sediment accumulation rate in the basin. These 3 features fit well with a foreland basin model. Sudden basin-wide subsidence of the type represented by the Booysen's shale is typical of foreland basins (Allen et al., 1986), resulting

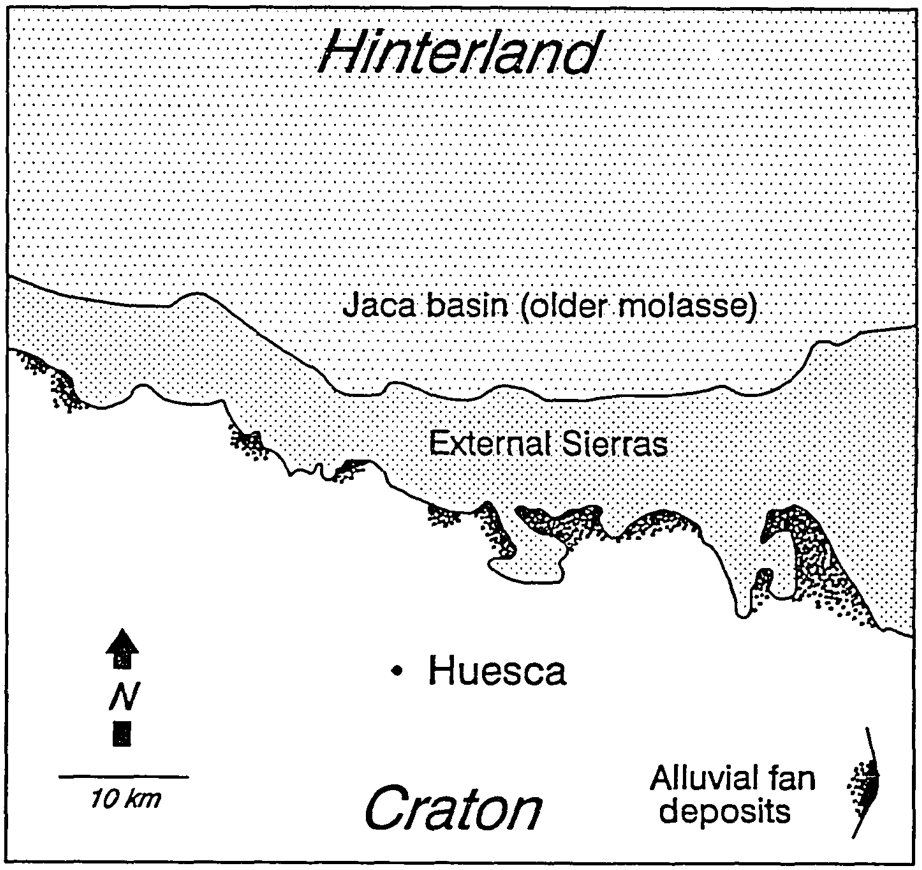

Figure 10. Miocene alluvial fan sedimentation at the edge of the Tertiary Ebro foreland basin in the Pyrenees of Spain. From Hirst and Nichols (1986).

from loading events in the hinterland (such as the renewed advance of a thrust sheet). Likewise, syndepositional folding is common, frequently preceding the breakout of a thrust fault. Finally, as figure 7 indicates, the calculated sediment accumulation rate for the Witwatersrand basin agrees with accumulation rates determined for foreland basins (Schwab, 1976).

I turn now to the question of a hinterland for the proposed foreland basin. Ventersdorp volcanism, Bushvelde intrusion, and 2,500 m.y. of erosion have conspired to make this a difficult topic, because the original hinterland is no longer present. There is, however, reason to believe that the region to the northwest of the basin was tectonically active in the Archean. The Limpopo mobile belt, which divides the Kaapvaal and Zimbabwe cratons and lies to the northwest of the basin, has been interpreted as the deeply eroded root of a collisional zone (Light, 1982; Burke et al., 1985). Metamorphic assemblages indicate > 30 km of burial (Light, 1982), which requires a considerable amount of crustal thickening. Peak metamorphism and granitization is dated at 2.7 to 2.6 Ga (Tankard et al., 1982), which is roughly contemporaneous with Witwatersrand sedimentation. Also, Burke et al. (1986) have proposed an Andean-type subduction margin preceding the peak of Limpopo activity. As observed today in South America, foreland basins commonly develop on the craton side of an Andean margin (Johnson et al., 1986).

The best fit model

As might be expected for a complex basin of great age that is largely covered by younger rocks, none of the idealized models have been able to satisfactorily explain all features of the basin. However, combining models into a composite history permits a satisfactory interpretation. Stretching and rifting provides the best explanation of the early basinal phases--the Dominion volcanics and the lowermost West Rand sediments, which are largely low energy and slightly faulted. The prolonged thermal subsidence that is predicted to follow initial stretching may have been present in the West Rand as well, but by the time Central Rand deposition was underway, the higher energy sediments, syndepositional folding and faulting, migrating basin margin and depocenter, and a sudden basinwide subsidence event (the Booysen's shale) indicate that thermal decay can no longer explain the basin subsidence. Rather, this structural and sedimentological record is better interpreted as resulting from a foreland basin developed in front of an advancing hinterland on the northwest side of the basin. The nature of thermal versus foreland basin subsidence curves make it extremely difficult to determine at what point in the Witwatersrand stratigraphy the transition in basin styles occurs. On depth vs. time graphs (figure 11), foreland basin subsidence curves are concave down (Allen et al., 1986; Cross, 1986); thermal decay curves are concave up (McKenzie,

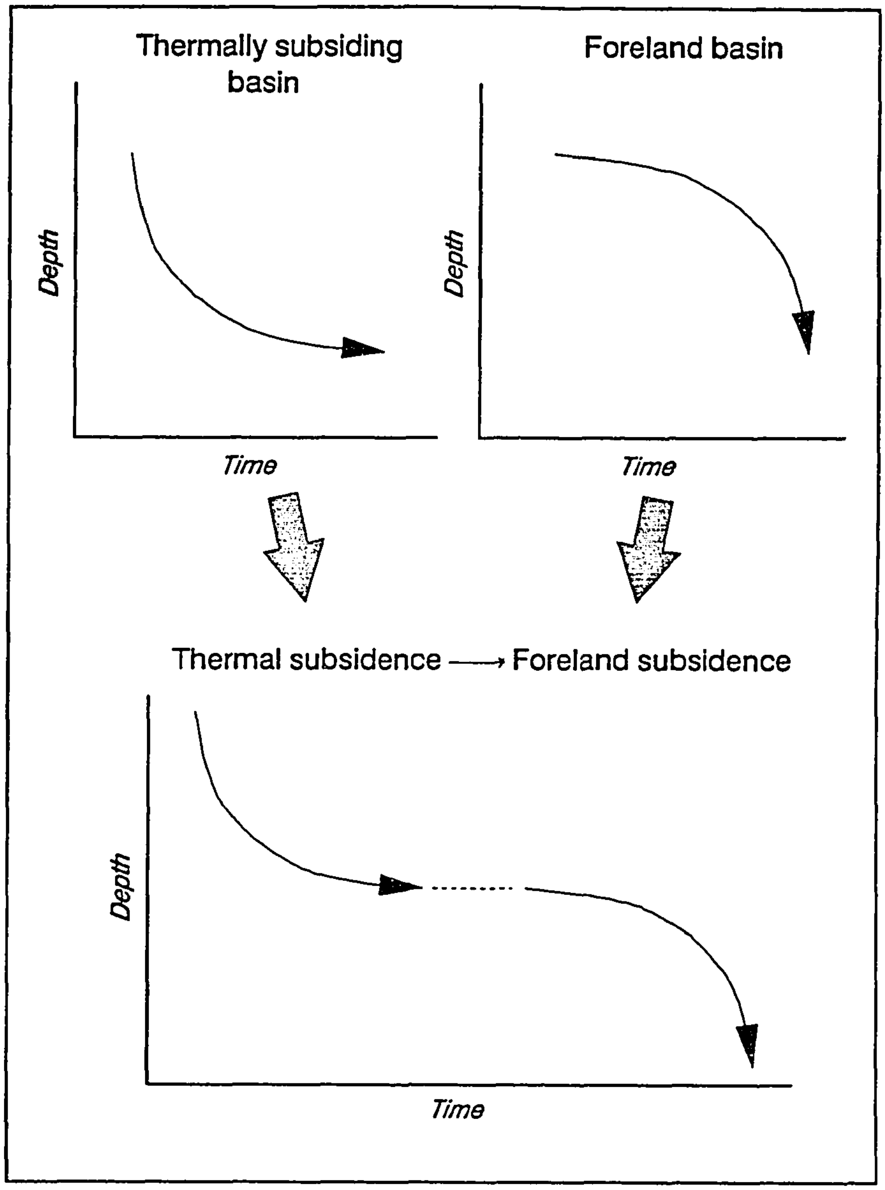

Figure 11. Idealized subsidence curves for a rift/thermal decay basin and a foreland basin. Note that the final stages of a thermally contracting basin show slow subsidence (McKenzie, 1978), as do the early stages of a foreland basin (Allen et al., 1986; Cross, 1986). No abrupt rate change will occur when a foreland basin follows a thermally contracting basin.

1978). Thus, when thermal subsidence is followed by foreland basin subsidence, there will be no sudden change in subsidence rate: the two types of curves overlap smoothly.

Combining the two basin types in a temporal sequence also helps account for the great sediment thickness in the basin. Subsidence is great because it is a product of a sequence of (1) crustal thinning, (2) thermal contraction, and (3) structural and sediment loading.

The basin evolution proposed here is two-phased--an initial stretching/rifting event with some associated thermal subsidence, followed by a transition to a foreland basin. That there is no mention of Pretorius' "intermontane" basin does not imply that such models are not applicable. Actually, the distinction between a successor basin and a foreland basin may be one of scale. The structural style of foreland basins can vary widely, from something as complex as imbricated intrabasinal thrusts to relatively straightforward marginal thrusts (figure 12). Assuming a simpler style (figure 12a, for example), it is quite easy to see how a study restricted to local relationships, particularly along the thrust-bounded margin, would lead Pretorius (1976) to interpret a high-angle, fault-bounded basin.

Finally, the proposed basin evolution must be rooted in an underlying tectonic framework. Burke et al. (1986) have suggested that an Andean-type subduction margin formed to the northwest of the Witwatersrand basin at approximately

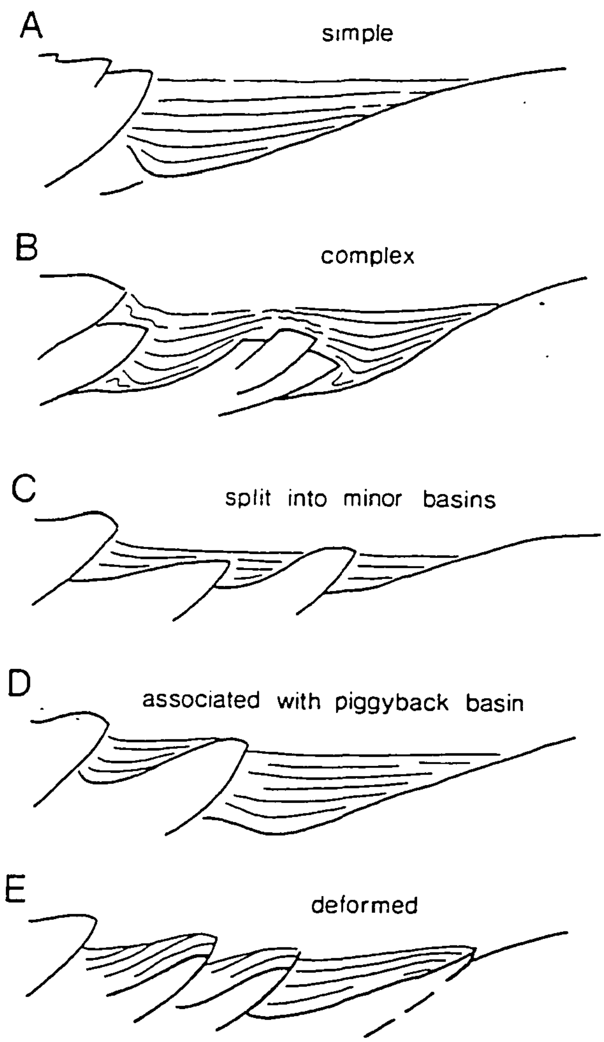

Figure 12. Variations in foreland basin styles. Profile A most closely resembles the Witwatersrand basin. From Ricci Lucchi (1986).

2.8 Ga. This subduction zone is considered the precursor to continental collision between the Kaapvaal and Zimbabwe cratons. Crow and Condie (1987) have recognized a subduction zone component (LILE enrichment and Ta-Nb depletion) in the Dominion volcanics, supporting the results of Burke et al. (1986). Based on these data, the early stretching and rifting phase of the Witwatersrand basin could have been a result of back arc extension. As subduction continued, the developing arc became a hinterland, driving the foreland basin stage of the Witwatersrand. It is also possible that the continental collision between the Kaapvaal and Zimbabwe cratons created a greatly thickened crust (the Limpopo belt) to drive foreland basin subsidence (Burke et al., 1986). Figure 13 summarizes the tectonic setting and basin evolution I propose for the Witwatersrand basin.

Figure 13. Tectonic reconstruction of the Kaapvaal and Zimbabwe cratons during evolution of the Witwatersrand basin. Stage 1: At about 3,070 Ma, the Dominion lavas are extruded in an incipient back-arc basin. Stage 2: Between about 3,000 Ma (the age of the youngest detrital zircons) and 2,900 Ma (the age of the Crown lava), continental subsidence as a consequence of (1) thermal contraction and (2) a developing hinterland (the magmatic arc) leads to deposition of the West Rand sediments. Stage 3: From about 2,900 Ma until sometime before 2,700 Ma (the age of the Ventersdorp volcanics) the arc continues to build, and thrust faults propogating from this hinterland reach the basin margin. The elevated structural front of the thrust faults provides the relief for deposition of the coarser grained Central Rand alluvial fans. Also, the thrust faults may have introduced second cycle sediments (in which gold is concentrated) by the uplift and erosion of older West Rand sediments. Extrusion of the Klipriviersberg lavas at about 2,700 Ma (not shown) brings clastic sedimentation in the Witwatersrand basin to a close.

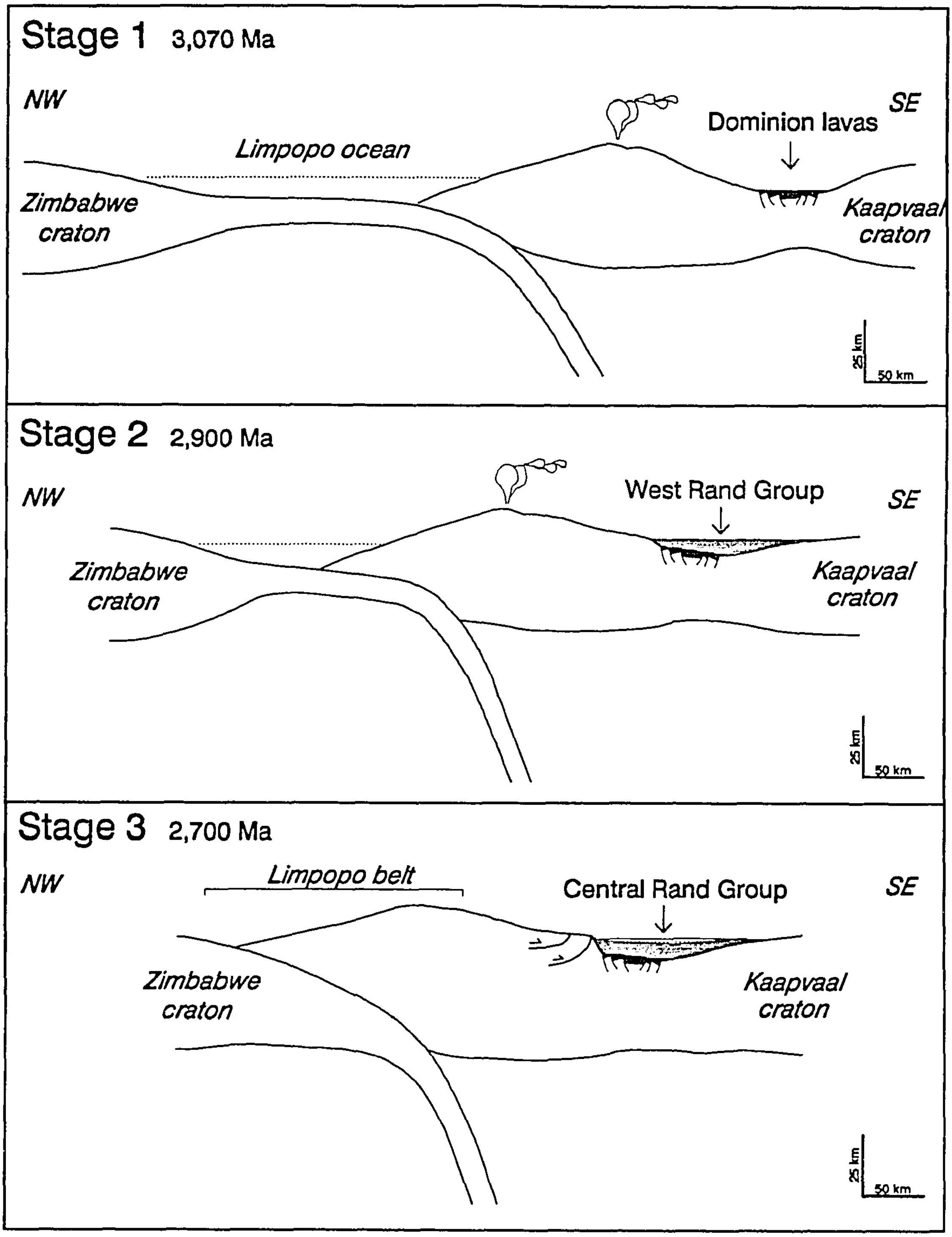

Stage 1 3,070 Ma
NW
SE
Dominion lavas
Limpopo ocean
Zimbabwe craton
Kaapvaal craton
25 km
50 km
Stage 2 2,900 Ma
NW
West Rand Group
SE
Zimbabwe craton
Kaapvaal craton
25 km
50 km
Stage 3 2,700 Ma
NW
Limpopo belt
Central Rand Group
SE
Zimbabwe craton
Kaapvaal craton
25 km
50 km

Chapter 3. The thermal evolution of the Witwatersrand basin

Very little has been written of the Witwatersrand basin's metamorphic history. This is primarily because gold mineralization in the basin is strongly controlled by sedimentary features, and the sedimentary features have not been visibly altered by metamorphism. From a mining perspective, therefore, there is little motivation for examining a metamorphic event (or events) that appears to have had no important economic effect. However, metamorphism becomes more important when one's focus shifts from recovering gold to understanding its origin, which requires that the gold be more closely examined physically and chemically.

The main result of a series of investigations into the origin of the gold has been the recognition that, on a very small scale (millimeters to centimeters), the gold in the Witwatersrand is not quite as closely tied to the sedimentology as it appears to be at outcrop scale. Instead, textural observations indicate that much of the gold has crystallized in place, and is therefore not a simple placer mineral. The "modified placer model", which combines the macroscopic association with sedimentary features and the microscopic observations of neo-formed grains, invokes metamorphism to remobilize and recrystallize original detrital gold, and is thus the first explicit recognition of a metamorphic imprint on the basin. Nevertheless, even with widespread acceptance of the modified placer model, the P, T, and t of metamorphism remain sketchy. Perhaps because the movement of gold is minor, and because there is no outcrop-scale evidence of metamorphism, there has been little incentive to work out the detailed thermal history of the basin.

Recently, however, Phillips et al. (1987) and Phillips and Myers (1989) revived the hydrothermal model of mineralization. Because their model calls on a fluid-rich metamorphism to mineralize the basin, it becomes important to define the physical and chemical conditions of metamorphism, and to determine whether these conditions were compatible with the widespread gold mineralization in the Witwatersrand. Phillips (1987, 1988) presents a partial assessment of the Witwatersrand metamorphism, reviewing the bulk chemical evidence for metamorphism and the approximate P-T conditions that are indicated by the metamorphic assemblage. However, Phillips stops short of fitting the proposed P-T conditions into a geologic model for the Witwatersrand. Because the conditions he proposes are rather unusual, a geologic model is needed. Also, an assessment of the metamorphism is potentially interesting from the perspective of the Witwatersrand as a well-preserved Archean cratonic basin. A 3 billion year-old basin might well be characterized by heat budgets different from those of younger basins. In particular, mantle heat fluxes and crustal heat generation by radioactive elements would have been greater in the Archean.

To address the thermal evolution of the Witwatersrand basin, I will first review the geological and petrographic evidence for metamorphism, citing especially the few papers that have explicitly discussed P-T conditions. Then, using data from the literature and my own observations of metamorphic minerals in Witwatersrand quartzites to constrain metamorphic conditions, I will model the one-dimensional conductive heat flow in the basin.

Metamorphic minerals in the Witwatersrand.

The two most widely reported metamorphic minerals in the Witwatersrand are chloritoid and pyrophyllite. Chloritoid has been reported numerous times, from all of the goldfields, and from all stratigraphic levels within the basin. A review of early reports can be found in Kent (1961, p. 94-95); for a recent summary of chloritoid distribution, see table 1 of Phillips (1987). Consistent with these literature reports, I observed chloritoid throughout the stratigraphic section at Klerksdorp, a vertical range of approximately 6,000 m (see figure 2; also figure 31 in chapter 4). Pyrophyllite is also widely distributed, although less consistently reported than chloritoid, probably because pyrophyllite is difficult to distinguish from muscovite petrographically, and therefore usually misidentified as "sericite". Pyrophyllite in the Klerksdorp section, which was identified by Dr. Sally Sutton at the University of Texas-Austin with a JEOL 733 electron microprobe (Sutton et al., 1990), has the same distribution as chloritoid. Both phases are most common near the tops of formations, reflecting their formation only from aluminum-rich precursors (Sutton et al., 1990).

Pyrophyllite, in particular, constrains the peak metamorphic conditions of the Witwatersrand. Assuming a water activity near one, pyrophyllite forms from kaolinite and quartz at a temperature of about 300° C (Frey, 1987), and pyrophyllite is consumed at about 400° C (Franceschelli et al., 1986). That water activity during metamorpism was high is indicated by (1) two phase (liquid + vapor) aqueous fluid inclusions in metamorphic quartz veins, (2) the absence of carbonates in all but a few samples, and (3) the absence of any significant accumulations of organic matter from which CO_2 or CH_4 might have been generated. The temperature of formation for chloritoid has not been experimentally determined, but its first appearance is generally near the boundary between very low grade and greenschist-facies metamorphism, at a temperature between 300° and 350° C (Cruickshank and Ghent, 1978; Ashworth and Evirgen, 1984; Frey et al., 1988). The breakdown of chloritoid to staurolite occurs at about 650° C (Halferdahl, 1961), but the common co-occurrence of chloritoid with pyrophyllite and the absence of staurolite indicates that temperatures in the Witwatersrand remained well below the upper limit of chloritoid stability.

Biotite and kyanite have also been reported from various goldfields in the Witwatersrand, although neither is as widely distributed as chloritoid or pyrophyllite. Phillips (1987) recognized metamorphic biotite at the base of the Central Rand Group in the East Rand goldfield and Sutton (pers. comm., 1990) reported metamorphic biotite in the West Rand sediments from the Klerksdorp goldfield. Biotite probably formed from the breakdown of muscovite plus chlorite, both of which are abundant in the Witwatersrand, at a temperature just below 400° C (Ferry, 1984). The reports of kyanite come from near Johannesburg, at the base of the Witwatersrand Supergroup, and from Krugersdorp, where kyanite is found in quartz veins that are approximately 5000 m above the base stratigraphically (Schreyer and Bisschoff, 1982). Under conditions of water saturation, kyanite forms from the breakdown of pyrophyllite at a minimum pressure of about 3 kbar and a minimum temperature of about 400° C (Schreyer and Bisschoff, 1982; England, 1972). P-T conditions of kyanite formation probably did not exceed these minimum values significantly because pyrophyllite co-exists stably with kyanite in the veins and because the total overburden (upper Witwatersrand, Ventersdorp, and Transvaal) in this area was approximately 10 km thick (Schreyer and Bisschoff, 1982).

Finally, a suite of higher-grade metamorphic minerals has been recorded around the Vredefort dome, where the full Witwatersrand section is exposed in a structural collar that rims the northwest side of the dome (figure 1). Muscovite, chloritoid, pyrophyllite, biotite, kyanite, sillimanite, andalusite, cordierite, garnet, staurolite, cummingtonite, anthopyllite, and hornblende are all present in the Witwatersrand section at Vredefort (Bisschoff, 1982). The distribution of minerals at Vredefort suggests localized addition of heat from plutons (Bisschoff, 1982). Because the Vredefort metamorphism is apparently a local phenomenon, I will not consider it in my attempts to model the basin-wide metamorphism.

Combining all of the various observations of metamorphic minerals in the Witwatersrand, a relatively simple (but very unusual) thermal structure emerges. Pyrophyllite plus chloritoid constrains temperature to between 300° and 400° C throughout almost all of the basin. In some areas, the presence of biotite favors the high end of this temperature range, and in at least two locations near Johannesburg the presence of kyanite indicates that temperatures may have exceeded 400° C. Because the biotite and kyanite are found as high as the base of the Central Rand (almost 5,000 m above the base of the section), the 300-400° C temperature span cannot be characterized as a simple case of increasing temperature with depth. Instead, the distribution of metamorphic minerals suggests a broadly "isothermal" profile, with temperatures ranging from 300-400° C near the top and near the base of the section, a vertical distance of almost 7,500 m. The geographic distribution of temperature is equally uniform, the chloritoid-pyrophyllite assemblage having been reported from all of the goldfields (Phillips, 1987). The absence of a significant thermal gradient suggests that very unusual metamorphic conditions must have prevailed in the Witwatersrand.

The Witwatersrand mineral assemblages are much less diagnostic for pressure than for temperature. Neither chloritoid nor pyrophyllite is pressure sensitive, and without knowledge of the specific biotite-forming reaction, the presence of biotite is equally uninformative. Only kyanite, which forms from the breakdown of pyrophyllite at just over 400° C and about 3 kbar pressure (figure 2 of England, 1972), can be used to constrain pressure. Kyanite is rare in the Witwatersrand even though its precursor (pyrophyllite) is abundant. P-T conditions, therefore, must have remained below the pyrophyllite-to-kyanite reaction throughout most of the basin, making 3 kbar the maximum pressure in the basin. Considering the 7,500 m thickness of the basin and allowing for regional variability, a reasonable estimate of pressure throughout the entire basin is 1-3 kbar. This estimate agrees approximately with the 1-2 kbar estimate of Phillips (1987).

The 1dt model.

Based on the foregoing discussion of metamorphic assemblages in the Witwatersrand, the goal of the thermal modeling that follows is to establish a geologically reasonable framework in which a 7,500 m thick stratigraphic sequence might have experienced a fairly uniform T_{max} between 300 and 400° C at pressures of 1-3 kbar. The model I will use ("1dt") was developed by Haugerud (1986) for use on microcomputers. There are two important limitations of the model: It is one-dimensional and it solves for heat conduction only.

The one dimensionality of 1dt makes it a poor choice for any thermal problem in which substantial horizontal movement of heat is expected. The Witwatersrand is tabular and thin relative to its areal extent, so the assumption that most of the heat moving through the basin would travel vertically, rather than out the sides of the basin, is reasonable.

The second limitation of the model, that of solving for heat conduction only, is much more significant in the case of the Witwatersrand. Sedimentary basins undergoing prograde metamorphism can expel large volumes of fluid, composed partly of connate water and partly of the water from dehydration reactions. These fluids eventually leave the basin, carrying heat with them and thereby adding a convective component to the heat flow budget. I will return to a more thorough discussion of the possible role of convective heat transfer in the Witwatersrand after the conductive modeling has been fully explored.

The 1dt program allows the user to set up and solve problems in which thermal conductivity, density, heat capacity, distribution of radioactive elements (heat production), basal heating conditions, uplift or subsidence, and time and depth steps can all be varied. I will discuss my input for these parameters and then discuss the model results.

Thermal conductivity and density, which must be held constant throughout the modeled geologic column, have been determined for a variety of crustal and supracrustal rocks in the Witwatersrand by Nicolaysen et al. (1981) and Hart et al. (1981). Their values (K = 2.5 W/m°C; density = 2.72 gm/cm^3) are similar to average values for comparable rock types (Sharma, 1986, p. 99 and p. 356), and I will use these values in the model. Heat capacity also remains constant over the full depth of the model. I will use a value of 900 J/°CKg, which is the default value supplied by 1dt.

The distribution of the radioactive elements U, Th and K must be known to determine the heat production within the modeled column. Generally, the upper granitic crust is highly enriched in U, Th and K relative to both lower crust and supracrustal sediments, but the precise nature of their distribution is usually not known because most of the crust is inaccessible to sampling. However, the Vredefort dome exposure provides an exceptional opportunity to measure U, Th and K directly in an upper-to-lower crustal profile (Nicolaysen et al., 1981). When these measurements are added to U, Th and K concentrations in the Witwatersrand and Ventersdorp Supergroups (also from Nicolaysen et al., 1981), an exceptionally complete radioelement profile is achieved. The profile, however, is of present day concentrations and must be corrected for the radioactive decay of U, Th and K since 2.7 Ga. Figure 14 illustrates the heat production profile that results when the 2.7 Ga corrections are applied and stratigraphic thicknesses are used to assemble a 40 km thick crustal model. The choice of 40 km for the full crustal thickness is a compromise between an exceptionally thin Archean crust, as might be expected for a time when heat-producing elements were approximately twice as abundant as today, and the need for a crust thick enough to support the stable accumulation of a 10-15 km thick supracrustal sequence (the Witwatersrand plus the Ventersdorp and the Transvaal). Forty kilometers of crust beneath the Kaapvaal craton in the Archean is consistent with the work of Nisbet (1984), who favors a 35-50 km thick crust on the basis of present crustal thickness and a consideration of post-Archean tectonic activity.

In general, the heat production for the 2.7 Ga Kaapvaal craton and its volcano-sedimentary cover, as depicted in figure 14, is slightly more than twice the modern value. Especially noteworthy is the high heat production of the

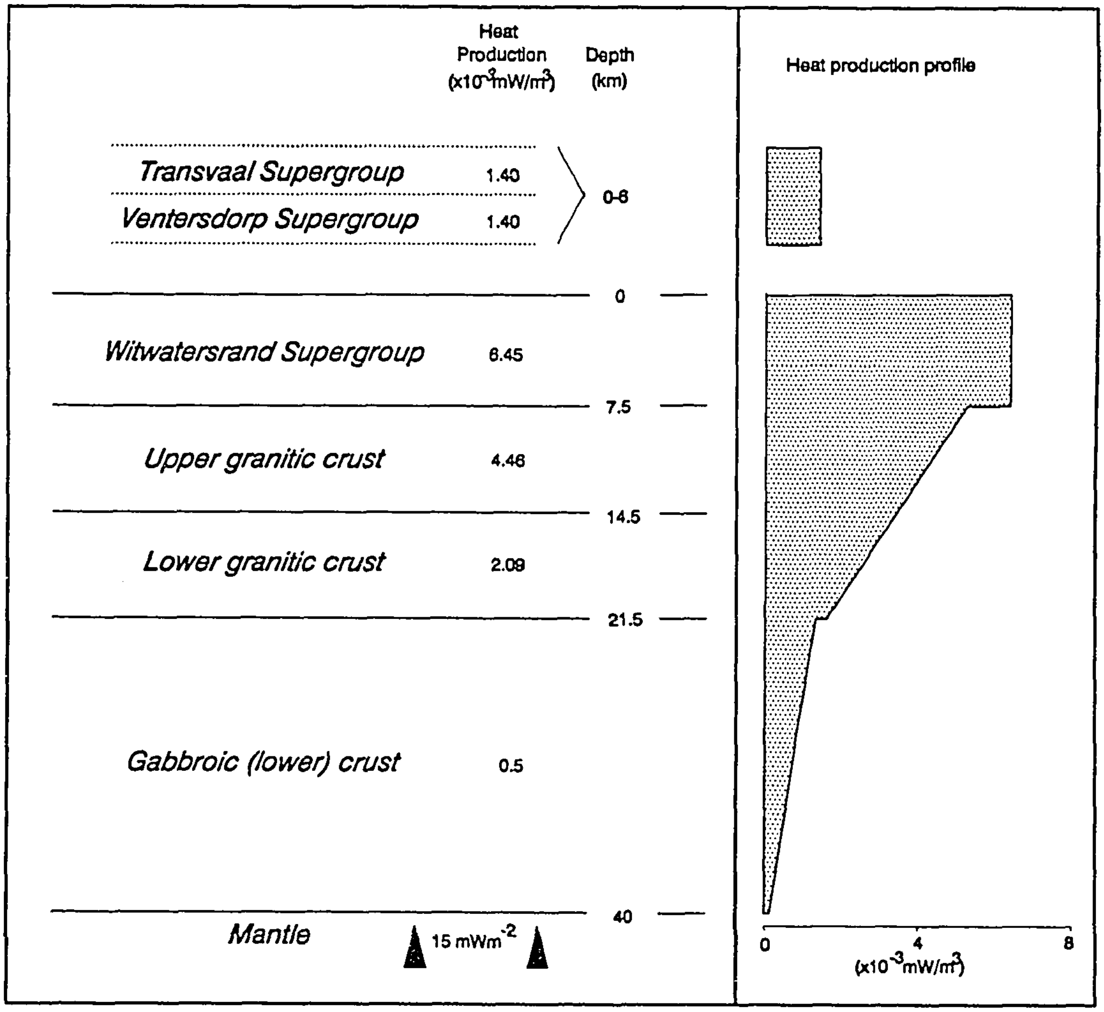

Figure 14. Crustal structure used in the thermal modeling, along with the flux from the mantle and heat production for the various crustal units (how these values were determined is discussed in the text). The heat production varies with depth as represented graphically in the vertical profile on the right (Nicolaysen et al., 1981).

Witwatersrand sediments. A typical modern shale- and sandstone-filled basin produces only one-fourth as much heat as the Witwatersrand. The anomaly is explained primarily by the abundance of detrital uranium in the Witwatersrand.

Finally, the basal heating flux (from the mantle) must be determined. Several observations enter into this determination. First, according to Nicolaysen et al. (1981) the present heat flux across the mantle in the vicinity of the Witwatersrand is 12-15 mW/m^2. If we assume that radioactive decay is the primary source of the heat flowing across the mantle-crust boundary, and that the approximate bulk composition of the core plus mantle is chondritic, then we can use the thermal half-life of a chondritic body (about 2 billion years) to estimate that sub-crustal heat production was more than twice the present value. This leads to 30 mW/m^2 as a reasonable estimate of mantle heat flux into the lower gabbroic crust of figure 14 at 2.7 Ga.

The presence of detrital diamonds in Witwatersrand sediments (Feather and Koen, 1975), however, conflicts with a mantle heat flux into the crust of 30 mW/m^2. Diamonds form in a high P, low T regime. With a 30 mW/m^2 mantle heat flux, mantle heat production equal to that of mantle peridotite at 2,700 Ma (0.032 x 10^{-3} mW/m^3), and a thermal conductivity of 2.15 W/m^2 (the conductivity of gabbro; Sharma, 1986), the geothermal gradient in the mantle is too high to enter the field of diamond stability (figure 15). A 15 mW/m^2 mantle flux, on the other hand, leads to diamond stability at

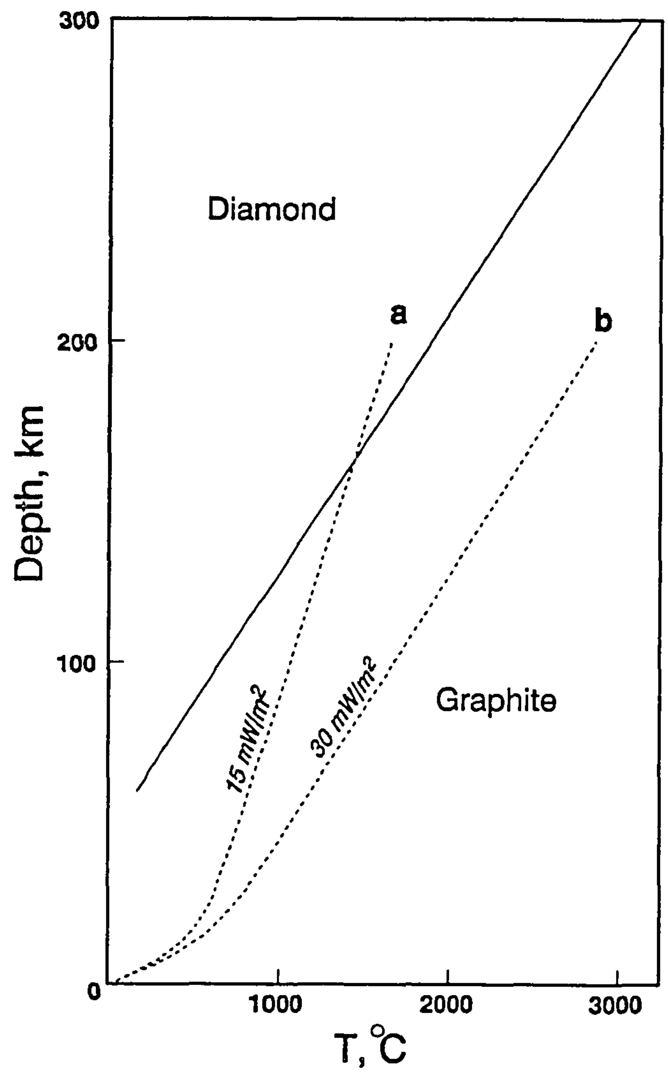

Figure 15. The geothermal gradients, (a) and (b), that correspond to a mantle heat flux of 15 mW/m^2 (the present day value beneath the Kaapvaal craton) and 30 mW/m^2 (the present value extrapolated to 3 Ga, taking into account radiocative decay), respectively. Note that gradient (b) does not enter into the field of diamond stability, whereas gradient (a) does. Because detrital diamonds have been recovered from the Witwatersrand, gradient (a), which corresponds to a mantle heat flux of 15 mW/m^2, is favored for the Archean Kaapvaal craton.

depths of 150-160 km and greater (figure 15), which is the depth range over which diamonds are believed to form in younger rocks (Wyllie, 1980). The presence of detrital diamonds in the Witwatersrand, therefore, indicates that the mantle heat flux beneath the Kaapvaal craton was no greater than 15 mW/m^2 for a period of time before 3,000 Ma (the onset of Witwatersrand sedimentation), in spite of the fact that radioactive decay dictates that approximately twice as much heat was being produced in the mantle at 3,000 Ma. The heat must have been escaping the mantle by some means other than vertical conduction up through the stable craton. Apart from conduction up through continental crust, the only other major escape for mantle heat is via oceanic crust, where heat can be lost by conduction through the thin crust, advection through basaltic magmatism, and by convection (the transport of crust from a spreading ridge to a subduction zone). Thus, either increased spreading rates, higher oceanic geotherms (implying thinned oceanic crust), and/or a greater total ridge length must have prevailed in the Archean to explain the unexpectedly low heat flow into the base of the Kaapvaal craton (see Burke and Kidd, 1978, for a supporting view).

One final consideration is the possible role of crustal thinning in increasing the basal heat flow. As discussed in chapter 2, the bi-modal Dominion volcanics are most likely a product of extension and crustal thinning. A thinned crust is compensated for in part by the upwelling of hot mantle

(McKenzie, 1978) that is out of thermal equilibrium. To return to equilibrium, higher than normal heat flow out of the mantle will result. Thus, starting at about 3,070 Ma (the time of Dominion volcanism), basal heat flow into the sub-Witwatersrand crust was probably higher than 15 mW/m^2. However, heating anomalies associated with thinned crust are transient. Even for extreme amounts of stretching, the heat flux returns to its pre-stretching value within 60-80 million years (figure 2 of McKenzie, 1978). Because Witwatersrand sedimentation persisted until some time after 2,900 Ma (the age of the Crown lava), the Dominion thermal anomaly can be safely ignored in metamorphic models of the Witwatersrand. I will therefore use 15 mW/m^2 as the basal heat flow in the models that follow.

Application of 1dt to the Witwatersrand.

With the model parameters established (figure 14), the first step in applying 1dt to the Witwatersrand is to establish an equilibrium geothermal gradient. This is the gradient that would have existed after the full Witwatersrand section had been deposited but before deposition of overlying units. As figure 16a indicates, the modeled equilibrium gradient averaged over the 7.5 km thickness of the Witwatersrand is about 40° C/km. Temperatures of 300° C and above, which are needed to generate the observed chloritoid plus pyrophyllite

Figure 16. (a) The equilibrium geothermal gradient in the Witwatersrand basin before deposition of any overlying volcanics or sediments. The model is based on the crustal structure of figure 14. At the lower right of figure 16a (also figures 16b-d) is the polychronic profile of maximum temperatures to which the Witwatersrand Supergroup would have been exposed. (b) The sequence of geothermal gradients that result from emplacing the full 2 km of Klipriviersberg basalts, at a temperature of 1,100° C, on top of the Witwatersrand, using a depth step of 50 m and a time step of 100 years. The model has the desired effect of producing a nearly isothermal T_{max} profile with peak temperatures near 300-400° C, but it is geologically not feasible to emplace a 2 km thick pile of basalts instantaneously.

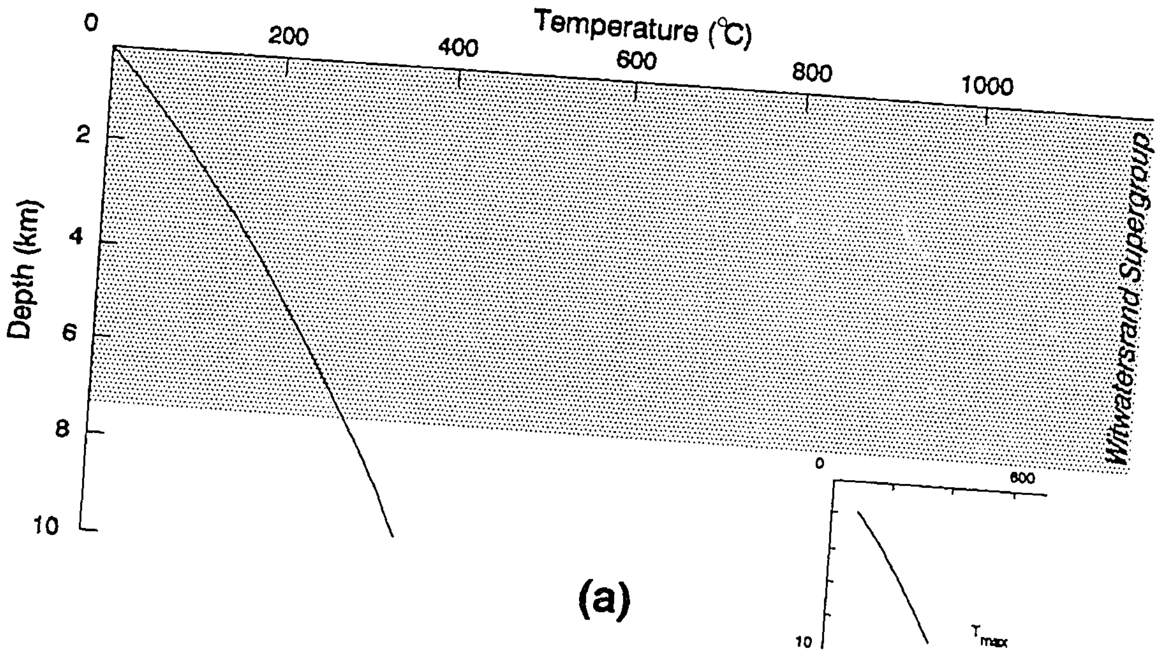
Temperature (°C)
0
200
400
600
800
1000
Depth (km)
2
4
6
8
10
Witwatersrand Supergroup
0
600
10
T max

(a)

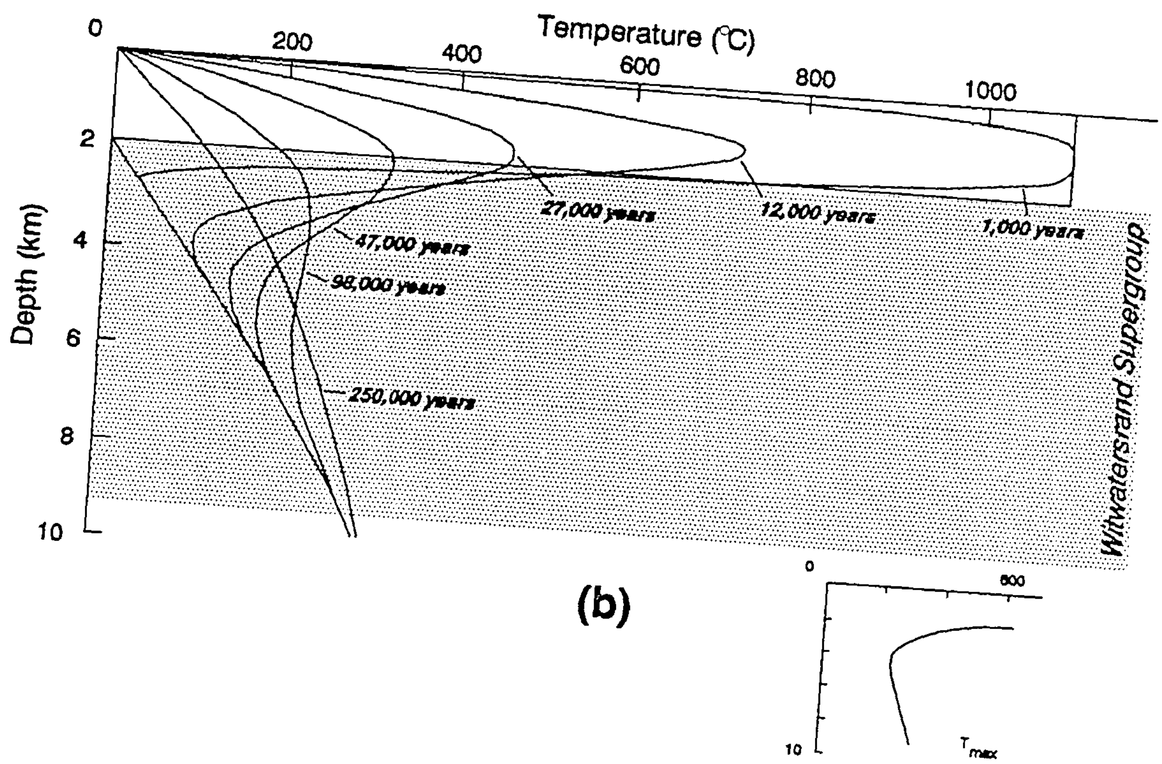
Temperature (°C)
0
200
400
600
800
1000
Depth (km)
2
4
6
8
10
27,000 years
12,000 years
1,000 years
47,000 years
98,000 years
250,000 years
Witwatersrand Supergroup
0
600
10
T max

(b)

Figure 16. (c) Thermal gradients upon cooling of a much more reasonable 200 m of lava at 1,100° C. Although some heat is conducted down into the basin, temperatures do not approach the 300-400° C required by the Witwatersrand chloritoid-pyrophyllite assemblage. (d) Thermal gradients upon cooling of the last of ten 200 m thick flows has been emplaced, each flow having been allowed to cool for 5,000 years before being buried beneath the succeeding flow. The cumulative effect of ten flows is slightly hotter than the effect of a single flow (compare to (c) above), but still is not sufficient to explain the Witwatersrand metamorphism, even with consideration of additional heat sources (see text).

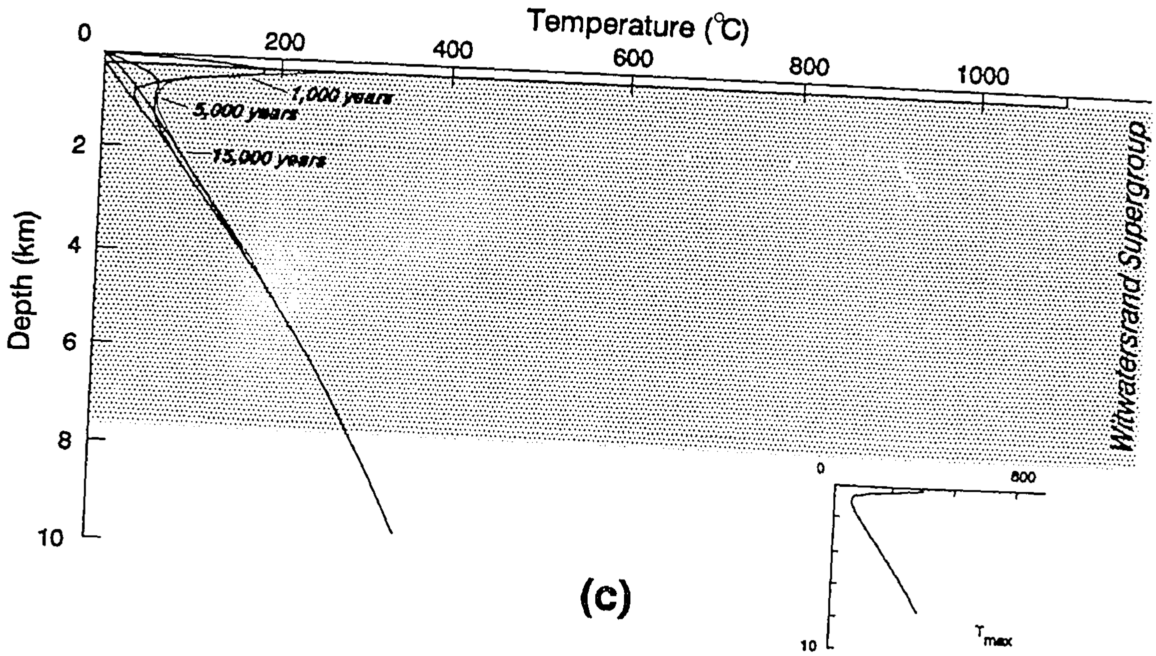

Temperature (°C)
0
200
400
600
800
1000
1,000 years
5,000 years
15,000 years
Depth (km)
2
4
6
8
10
Witwatersrand Supergroup
0
800
10
T_{max}

(c)

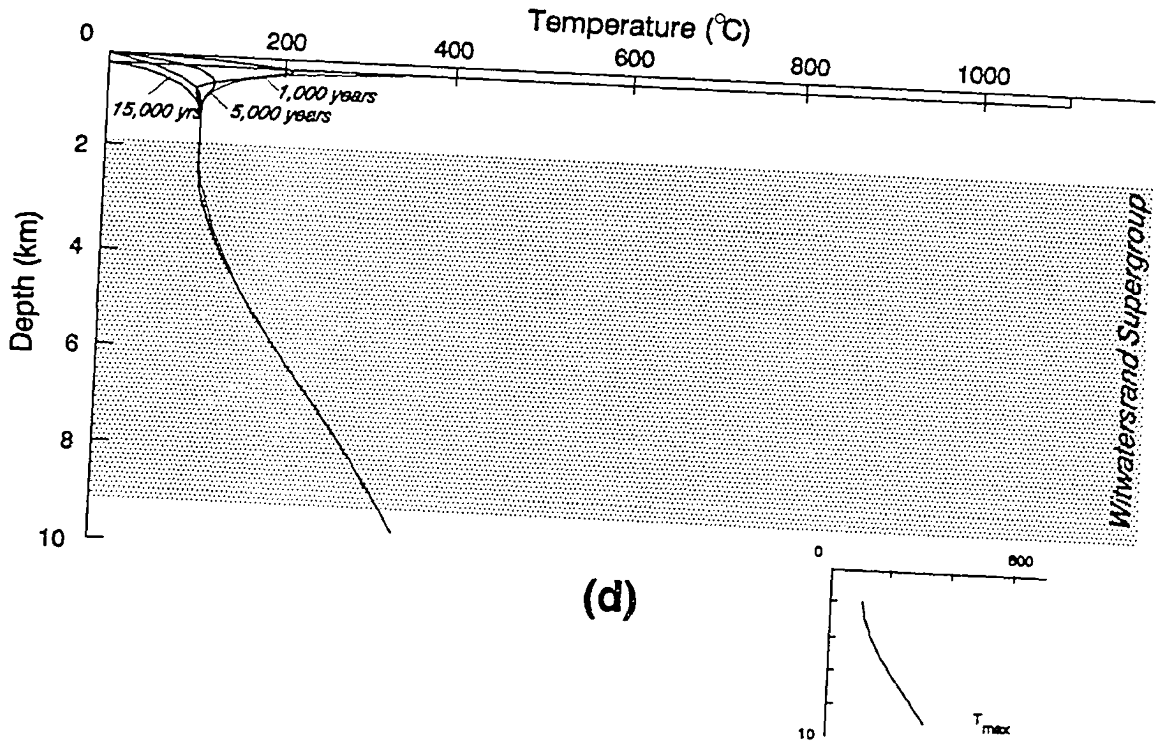

Temperature (°C)
0
200
400
600
800
1000
1,000 years
15,000 yrs
5,000 years
Depth (km)
2
4
6
8
10
Witwatersrand Supergroup
0
800
10
T_{max}

(d)

assemblage, are encountered only at the very base of the Witwatersrand section. More importantly, the 40° C/km gradient leads to a temperature difference of 300° C between the top and bottom of the basin--nowhere near the broadly "isothermal" gradient that is indicated by the distribution of pyrophyllite and chloritoid. To steepen the gradient, it will be necessary to add heat to the top--but not to the bottom--of the Witwatersrand. The Ventersdorp Supergroup, specifically the basal Klipriviersberg lavas, provides a potential source for such heating.

A review of Ventersdorp stratigraphy indicates that approximately 2 km of Klipriviersberg lavas were deposited over the Witwatersrand basin and surrounding areas (Crow and Condie, 1988; see also figure 2). These thick lavas were probably deposited rapidly, as indicated by the absence of paleosols within the Klipriviersberg Group. There is, however, a regional paleosol at the top of the Klipriviersberg, and the Ventersdorp stratigraphy above this paleosol is variable in both thickness and rock type. Importantly, there are no thick, rapidly deposited lavas similar to the Klipriviersberg above this paleosol that might have induced significant heating of the underlying Witwatersrand.

The stratigraphy of the Ventersdorp suggests that the Klipriviersberg lavas may be of primary importance in heating the Witwatersrand basin directly, whereas the remainder of the Ventersdorp (plus the overlying Transvaal) is important only in that it buried the Witwatersrand more deeply. Deeper burial will increase temperatures in the basin, but will not produce the uniform T_{max} profile that is preserved in the metamorphic assemblage.

To investigate the viability of Klipriviersberg-related metamorphism, I will use the 1dt program to place a hot (1,100° C) layer of lava on top of the basin, and then observe the thermal effect on the Witwatersrand rocks. Figure 16b illustrates the effect of emplacing a full 2 km of hot lava atop the basin. Enough heat is conducted down into the basin to raise temperatures over almost the full thickness of the Witwatersrand. More importantly, the temperature increase is greatest at the top of the section and decreases downward. When the heating from the Klipriviersberg is added to the normal geothermal gradient, the resulting vertical profile of maximum temperatures is remarkably consistent (figure 16b), in agreement with the evidence from metamorphic minerals. Although the temperatures are about 20-30° C too low in the intermediate depths of the basin, there are some additional sources of heat, most notably the latent heat of crystallization of the Klipriviersberg lavas, that could easily make up the difference. (These additional sources of heat will be discussed later.)

The results of this initial model suggest that it is geologically reasonable to expect some downwards heat conduction into the Witwatersrand from the overlying

Klipriviersberg lavas. However, the instantaneous extrusion of 2 km of lava is not likely, particularly in light of Winter's (1976) recognition of separate flows within the Klipriviersberg. To arrive at a more realistic model, I will examine the thermal effects of sequentially emplacing thinner flows atop the Witwatersrand.

Individual flood basalt flows are commonly several tens of meters thick (Williams and McBirney, 1979, p. 98), and eruptions are often episodic, with several flows erupting in rapid succession followed by a quiescent period. For modeling purposes, I will use a 200 m flow thickness to simulate the effect of several flows, each tens of meters thick, erupted in a short time interval (days or weeks). With a 200 m thick flow, there is once again a pulse of heat down into the Witwatersrand (figure 16c). However, the depth of heating is much less and the temperatures much lower than in figure 16b, in which the full 2,000 m of lava were emplaced instantaneously. The required 300-400° C temperatures are attained only within the uppermost 100 m of the Witwatersrand section, in what is probably best described as a contact metamorphic effect. Not only are temperatures insufficient, but with only 200 m of overlying lava, pressures also will be well below the 1-3 kbar range recorded by the metamorphic mineral assemblage.

To increase both temperature and pressure, I will model the effects of emplacing 2,000 m of lava in a series of ten flows, each 200 m thick. The time interval between flows becomes critical in such a model. Based on the minimal thermal impact of a single flow (figure 16c), successive flows must be emplaced rapidly, before the previous flow has cooled completely, to create a cumulative heating effect. Emplacing all ten flows in a 50,000 year interval (one flow every 5,000 years) satisfies this requirement, because the heating anomaly from a single flow will not have dissipated completely after only 5,000 years (see the 5,000 year geotherm in figure 16c). In the multiple flow model, the effects of each successive flow are similar to those of the single flow in figure 16c, but the temperatures and depth of heating into the Witwatersrand increase slightly as the volcanic pile thickens. However, even the thermal profile after the tenth flow (figure 16d) falls far short of the required temperatures. The thermal modeling thus suggests that for the Klipriviersberg lavas to have metamorphosed the basin, either the emplacement of the full 2,000 m occurred very rapidly (in much less than 50,000 years, certainly), or there were additional sources of heat.

The rate of emplacement cannot be determined directly because the lavas are too old to be dated with the needed accuracy, but it is possible to make comparisons with some younger flood basalts for which extrusion rates are approximately known. The two most thoroughly studied flood basalt provinces in the world are the Deccan traps in India and the Columbia River basalts of the northwestern U.S.. In the Deccan traps, the bulk of the 2 km thick Western Ghats lava appears to have been deposited in a single reversed polarity magnetic interval (Mahoney, 1988), the duration of which is about 600,000 years (Ness et al., 1980). A similar rate of extrusion is obtained for the Grande Ronde period of Columbia River volcanism, where one major eruption (with an average flow thickness of 30 m) occurred approximately every 10,000 years (Hooper, 1988). At this rate of extrusion it would take 600,000-700,000 years to build a section of basalt as thick as the Klipriviersberg Formation. Comparison with the Deccan traps and the Columbia River basalts thus suggests that a reasonable length of time for the eruption of the Klipriviersberg basalts is approximately 600,000 years--more than an order of magnitude longer than the 50,000 years (maximum) that the 1dt thermal modeling permits if the basalts are to have metamorphosed the Witwatersrand. Unless the Klipriviersberg eruption rates were more than ten times higher than the rates of younger flood basalts, it is unlikely that the lavas alone metamorphosed the Witwatersrand.

As alluded to earlier, there are some additional sources of heat that would have increased the thermal effect of the Klipriviersberg basalts. One such source is the intrusions (feeder dikes and sills) associated with the Klipriviersberg volcanic rocks. Such intrusions are recognized in all of the goldfields, and their distribution in the Klerksdorp goldfield has been mapped by Antrobus et al. (1986; their figure 29). Based on their map (from which the density of intrusives can be estimated) and an average thickness of 2 m for each dike or sill (Antrobus et al., 1986, and personal observations, 1988), Klipriviersberg intrusives comprise roughly 0.2% of the total volume of the Witwatersrand basin. Assuming equivalent specific heats for the intrusions and for the Witwatersrand rocks (as has been done throughout the modeling), an addition of 0.2% volume at 1100° C will translate into only a 2.2° C basin-wide temperature rise if the heat is distributed evenly. Adding the intrusions as a heat source is therefore of little consequence.

A second additional heat source is the latent heat of crystallization (H_f, or heat of fusion) of both the intrusive and extrusive Klipriviersberg rocks. For silicates, H_f averages 80 cal/gm, which is 320 times greater than their average specific heat (0.25 cal/gm C) (Williams and McBirney, 1979, p. 40). To estimate the effect H_f might have on the thermal profile, the total heat given off by crystallization can be compared to the total heat released during cooling. Cooling of a modeled sequence of Klipriviersberg lavas from 1100° to 100° C released about 250 cal/gm of heat and raised temperatures in the Witwatersrand sufficiently to establish a T_{max} of 100-200° C over most of the basin (figure 16d). Adding H_f of the magmas will supply only an additional 80 cal/gm--clearly insufficient to raise temperatures the additional 100° to 200° C needed to achieve a 300° C isothermal profile.

Finally, convection must be considered as an additional means of heating the basin. Convecting fluids cannot add heat, but convective cells can distribute heat more efficiently than conduction alone. More efficient distribution of heat could raise temperatures in two ways. First, if heat is conducted more efficiently from the Klipriviersberg into the Witwatersrand, then less heat will be conducted into the atmosphere, increasing the total addition of heat from the lavas (but only in the short term--eventually, all heat will be lost to the atmosphere). Second, heat from beneath the basin (the basal flux) will be delivered more rapidly to all levels of the basin. Although this requires that heat be extracted from the crust and mantle, these heat scurces are virtually infinite relative to the minor heat sink of the basin, so the net result on the basal flux will be insignificant. Convection will also have the effect of distributing heat more evenly through the basin, leading to more isothermal conditions than conduction alone.

That convecting (or migrating) fluids can influence thermal regimes has been demonstrated for groundwater systems (Smith and Chapman, 1983; Majorowicz et al., 1984) and for higher pressure, higher temperature diagenetic and metamorphic systems (Jowett, 1986; Hoisch, 1987; Dorobek, 1989). In all of these cases, the key to heat transport by fluids is the movement of the fluids. Either tectonic and fluid pressures or density gradients (usually owing to heating and cooling) must be present to drive the fluids, ideally in a system that permits high fluid-rock ratios in order to maximize the transfer of heat. In the Klipriviersberg/Witwatersrand system, the capping volcanic sequence makes any such system highly unlikely because the thermal structure of the basin is not conducive to the development of convective cells. Normally, a basin is hotter at the base than at the top, allowing fluids to warm at the base, rise to the top where they cool somewhat by transferring heat to the surrounding rocks, and then descend to the base again (see Jowett, 1986, for an example of a similar system in the Kupferschiefer). With the lavas on top of the Witwatersrand basin, fluids that are at the top of the basin will be heated, and will consequently remain near the top of the basin--a stable, density-stratified situation will prevail. Also, geochemical trends associated with major unconformities in the basin argue against the widespread movement of hydrothermal fluids (see chapter 6).

An alternative model.

The heat sources I have considered in this chapter include: heat flux from the mantle; radiogenic heat production in the sub-Witwatersrand crust, the Witwatersrand, and the Ventersdorp; heat released by the cooling of Klipriviersberg extrusives and intrusives; and the heat of crystallization of the Klipriviersberg extrusives and intrusives. I have quantitatively modeled the conductive transfer, and have qualitatively discussed the convective transfer of heat from these sources. Unless the Klipriviersberg lavas were erupted extremely rapidly (more than an order of magnitude faster than any reported younger flood basalts) it is unlikely that Witwatersrand metamorphism was a product of Ventersdorp volcanism, even when all additional heat sources are considered. It simply is not possible to attain the needed temperatures (300-400° C) in the upper half of the basin. Possibly, a higher basal flux such as might result from a nearby Ventersdorp magma chamber could increase temperatures sufficiently, but an inevitable consequence of increased basal heat flow would be temperatures at the base of the Witwatersrand far in excess of 400° C. Using the 1dt model, I have been unable to produce a uniform T_{max} profile through the basin.

Nevertheless, there is no doubt that Witwatersrand quartzites and shales from virtually all stratigraphic levels of the basin record a T_{max} in the range of 300-400° C. How can the metamorphic assemblages be reconciled with the apparent improbability of attaining a nearly isothermal gradient?

To answer this question, I must return to the tectonic model of the basin presented in chapter 2. Recall that the basin is asymmetric, with a steeply dipping northwest margin. Formations along the northwest margin are often truncated by erosion prior to being covered over by the next formation. Formations along the basin margin are also variable in their dip, with the deeper (older) formations generally dipping more steeply than the younger formations. Both of these observations can be explained if the Witwatersrand is a foreland basin in which older formations are uplifted, eroded and redeposited as the basin margin migrates to the southeast. A consequence of this syndepositional tectonism is that along the active northwest basin margin individual formations will not be arrayed in a typical "layer cake" stratigraphy, but will be exposed as dipping strata, with progressively older units cropping out at the surface towards the west, as illustrated schematically in figure 17. The implications of this basin margin geometry for the apparent stratigraphic distribution of metamorphic minerals can be profound. In figure 17, compare the stratigraphic section composed of samples a-f to the section composed of samples g-l. Although both sample suites fully represent the six formations, only suite g-l could actually yield useful information about the paleogeotherm. Profile a-f does not correctly sample the paleogeotherm because syndepositional tectonism has steepened bedding along the basin margin to the point where an apparently "vertical" profile of the six formations is actually a suite of samples taken from the same depth--samples that have experienced approximately the same P-T-t paths.

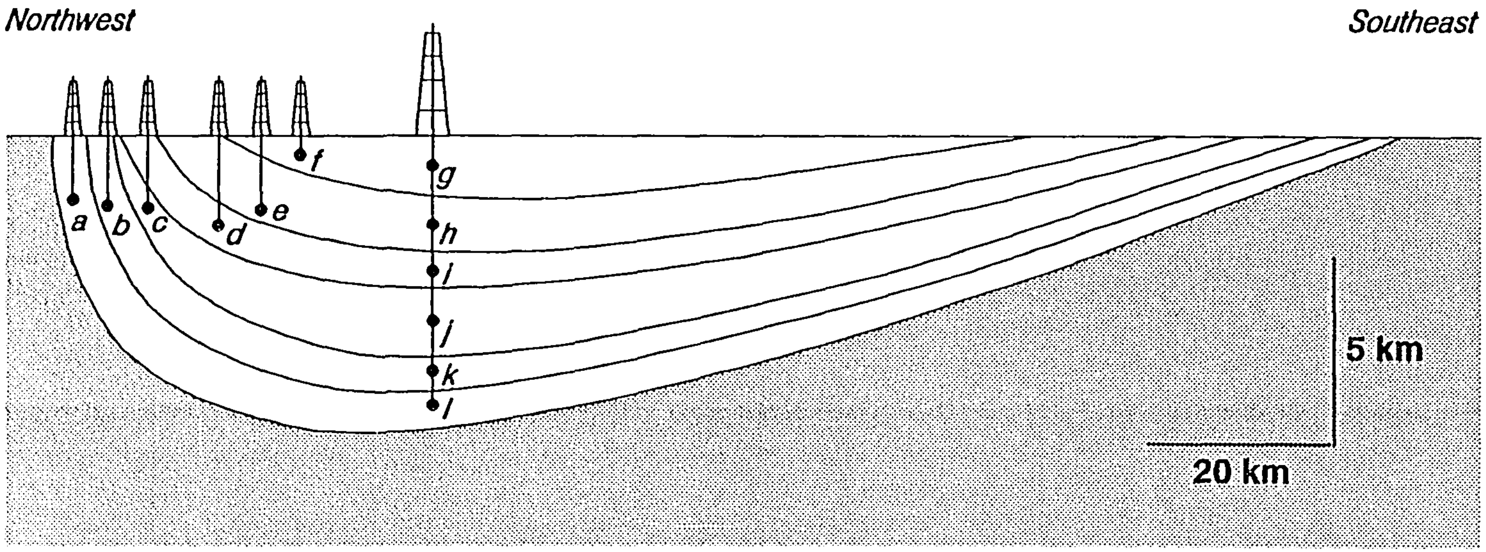

Figure 17. A schematic representation of the Witwatersrand basin. Two end member stratigraphic profiles are indicated by the sampling sequences a-f and g-l. Only sequence g-l would accurately sample the range of P-T conditions experienced by the basin during metamorphism. Sequence a-f would preserve a nearly isothermal, isobaric profile, even though the full basin is represented stratigraphically. Because Witwatersrand samples are almost entirely from mines or exploration cores, and the exploitable deposits occur only along the northwest basin margin (figure 1), it is likely that the evidence of metamorphism in the Witwatersrand has been collected from samples that approximate the a-f sequence in this figure. The apparently isothermal metamorphic conditions may therefore be an artifact of sample distribution.

The suite of samples depicted in samples a-f of figure 17 may be quite representative of typical sampling in the Witwatersrand. For the suite of samples that I investigated from Klerksdorp, inspection of the borehole records indicates that all of the samples were recovered from depths between 300 and 3,200 m (table 1), even though they represent a stratigraphic interval of 7,500 m. Also, there is no correlation between stratigraphic depth and the actual depth of sample recovery. In fact, the three stratigraphically deepest samples (DL 409-411) were recovered from only 300-400 m depth (table 1). Whether a similar situation prevails for the samples of Phillips (1987) is not clear, although it is likely. All of Phillips' samples are from the major goldfields, which are situated along the basin margin (in the proximal fan sediments), and most of his samples are from either mine exposures or from exploration cores. Mines are technologically limited to depths of about 3,000 m, and because of this limitation it is unlikely that cores (which are quite expensive) sample much below 3,000 m either. Considering these economic limitations, it is highly probable that Phillips' (1987) samples are distributed in much the same way as the Klerksdorp samples that I have studied: they represent a stratigraphic profile similar to a-f, not g-l, in figure 17.

If the widespread stratigraphic distribution of chloritoid and pyrophyllite in the Witwatersrand is not actually a <u>vertical</u> distribution, there is no longer a need

Samples	Depths (m)	Borehole #
DL 301-328	2073-2588	MMB-1
DL 329-335	2943-3066	MZA-4
DL 336-352	3126-3282	CY-1
DL 353-376	440-1258	KR-1
DL 377-394	1780-2776	G-13
DL 395-403	2336-3184	R-1
DL 404-405	2333-2380	MGR-3
DL 406-408	2765-3047	VHD-1
DL 409-411	298-461	DRH-13

Table 1. Samples from the Klerksdorp goldfield, the boreholes from which they were obtained, and the depth (below the present day surface) from which the samples were recovered. Note that the samples have all been collected from similar (shallow) depths, in spite of the fact that there is a stratigraphic difference of some 7,000 m between the top and bottom of this section. This suggests a geometric configuration similar to that portrayed in profile a-f of figure 34.

to infer a broadly uniform T_{max} over a 7,500 m vertical interval. Instead, the only requirements of a reasonable metamorphic model are that it produce peak temperatures of 300-400° C and pressures of 1-3 kbar in the upper few km of the basin, because this is where the pyrophyllite-chloritoid assemblage has been sampled.

Turning to a final 1dt model, again based on the crustal structure of figure 14, but now adding the full thickness of the Ventersdorp (3,000 m; Button, 1986) and the Transvaal (about 3,000 m based on the report of SACS, 1980, and taking into account Button's (1986) suggestion that the Transvaal thins in the Witwatersrand area), it appears that simple burial metamorphism is sufficient to generate the observed P-T conditions in the Witwatersrand (figure 18). Peak metamorphic temperatures range from 308° to 446° C in the top three kilometers of the basin, and pressures are 2-3 kbar over the same interval. Deeper in the basin both temperature and pressure are much higher (593° C and 4.5 kbar at the base), but conditions in the deep Witwatersrand are irrelevant in terms of the present data set, which is apparently drawn only from the top half or so of the basin. Metamorphic mineral assemblages in the Witwatersrand are therefore most likely the result of burial metamorphism beneath the Ventersdorp and Transvaal Supergroups.

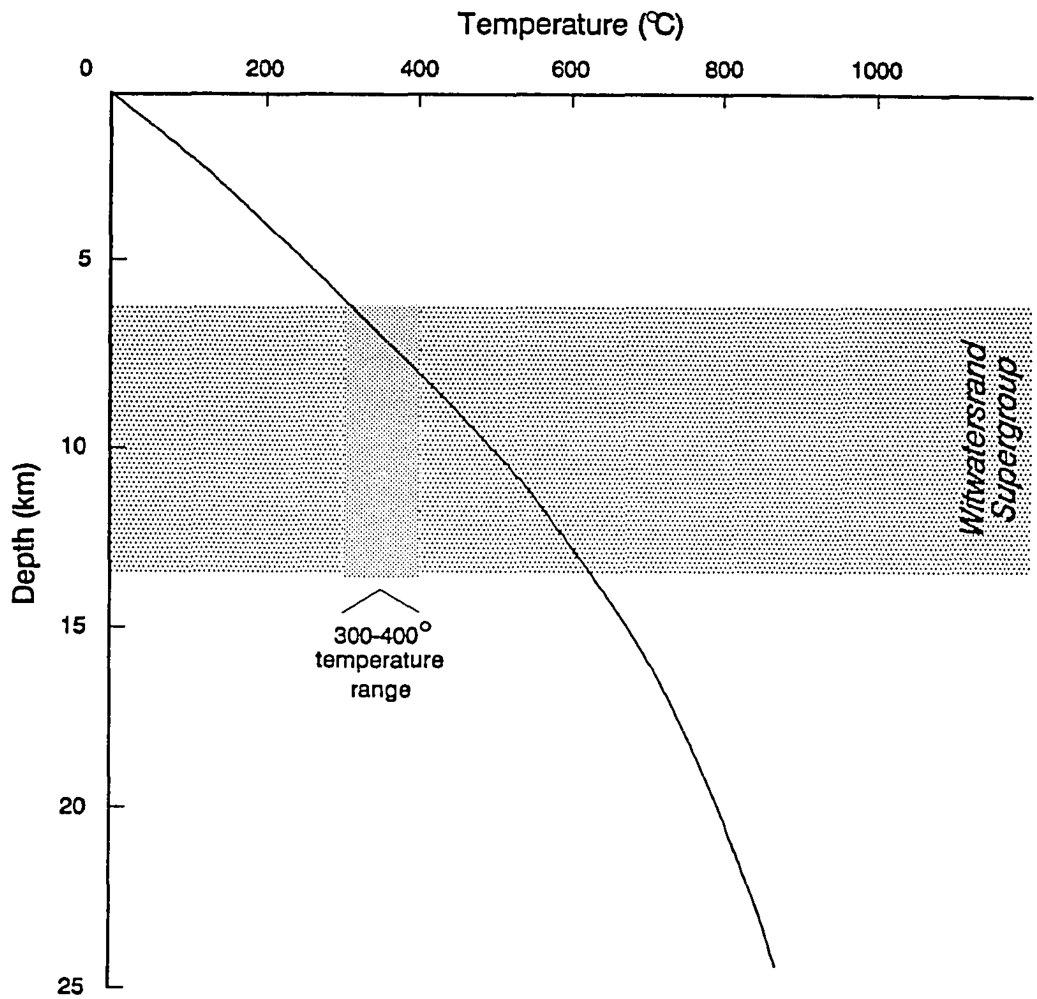

Figure 18. The geothermal gradient in the Witwatersrand after burial beneath 6 km of Ventersdorp and Transvaal sediments and volcanics. Note that temperatures of 300-400° C and pressures of 1-3 kbar prevail in the upper 2-3 km of the Witwatersrand. If Witwatersrand sampling has inadvertently been limited to these higher structural levels of the basin (see figure 34), then a simple burial metamorphism beneath the Ventersdorp and Transvaal Supergroups provides the best explanation for the widespread chloritoid-pyrophyllite assemblage in the Witwatersrand.

Chapter 4. Provenance and petrography

Considering the widespread acceptance of the modified placer theory of mineralization, the motivation behind Witwatersrand provenance studies is clear. To locate the true source of the gold, the modified placer theory dictates that we look outside of the basin, to the source rocks that supplied the gold.

Previous work on provenance in the Witwatersrand

There is an immense literature surrounding the question of provenance in the Witwatersrand basin. Most of this work takes a very direct approach: the gold is found in the conglomerates, therefore we should carefully examine the principle components of the conglomerates for any evidence as to their source area. Studies of this nature have focussed predominantly on gold particles, detrital pyrites, quartz pebbles, and the suite of assorted, unusual, heavy minerals from the conglomerates.

Hallbauer and Utter (1977), von Gehlen (1983), Hirdes (1984), and Reid et al. (1988) are all examples of studies in which gold grains were analyzed, either geochemically or morphologically. None were successful in finding unique geochemical or morphological attributes that could be recognized as characteristic of a particular source rock, or even a particular source rock type. The primary difficulty is the multi-phase history of the gold grains--not only were they weathered and transported, but they were also metamorphosed after deposition, producing recrystallization and chemical homogenization.

Examples of provenance studies of detrital pyrites include Koppel and Saager (1974), Saager (1976), Hallbauer and von Gehlen (1983), and Meyer et al. (1985). Of the four studies cited, two concluded that altered granitic terrains supplied the pyrites to the Witwatersrand (Hallbauer and von Gehlen, 1983; Meyer et al., 1985), and two concluded that greenstone belts were the principal pyrite source (Koppel and Saager, 1974; Saager, 1976). Considering that granitic and greenstone terranes are the only two major lithologies present in the Archean, the pyrite studies can be summarized as inconclusive at best.

Quartz pebbles are the volumetrically dominant constituent of the reefs, and these also have been examined for provenance. Hallbauer and Kable (1982) surveyed pebbles from 12 different stratigraphic horizons and found light REE enriched relative to heavy REE, fluid inclusions both enriched in Sn and Cs and containing cassiterite and Ba-feldspar as daughter minerals, and elevated K contents in the quartz, all of which suggest a granitic rather than a greenstone source area. Shepherd (1977) examined the distribution of five types of primary fluid inclusions in quartz pebbles from five different goldfields, and concluded that each goldfield was supplied by a unique source rock.

Neither study used a data base large enough to draw significant conclusions, and potential source rocks have not been analyzed thoroughly enough for correlations between source and sediment to be drawn. These studies thus illustrate the two main limitations of quartz pebble provenance studies: such work is extremely labor intensive and the quartz pebbles may only represent secondary vein quartz from the source area rather than the true source area lithology. The total volume of gold in the Witwatersrand basin suggests that gold quartz vein deposits alone could not have been the principal source, so the recognition of a vein component does not ultimately address the problem of gold origin.

Finally, the wide variety of rather unusual heavy minerals found in the reefs has also been used to assess provenance. The most comprehensive study using this approach was that of Viljoen et al. (1970), who concluded that the vertical stratigraphy of Witwatersrand heavy minerals could best be explained by the top-to-bottom unroofing of a Barberton-type greenstone belt. Later studies, however, dispute this interpretation (Klemd and Hallbauer, 1987; Wronkiewicz and Condie, 1987).

The contradictory results of the aforementioned studies clearly do not resolve the provenance question. About half of the studies favor granitic source areas; half favor greenstone source areas. In an attempt to break the impasse, Robb and Meyer (1990) opted for a markedly different approach to determining provenance. Using petrographic and geochemical data acquired from both surface exposures and numerous borehole penetrations through Witwatersrand and Dominion cover, they determined the approximate mineralogical and chemical composition of the Archean crust in the vicinity of the Witwatersrand basin, and then asked if this crust could reasonably account for the basin fill, both volumetrically and compositionally. The results of their lithologic survey indicated an Archean crust dominated by granitoids, with less than 20% greenstone belt lithologies. The preponderance of felsic plutonic rocks agrees well with the generally coarse-grained, quartz-rich nature of the Witwatersrand, and particularly with the sandstones of the Central Rand group. More importantly, and previously unrecognized, was the nature of the granitoids beneath Witwatersrand cover. When recovered in borehole, the granitoids were seen to be pervasively hydrothernally altered and enriched in both Au and U relative to surface granitoids (which had apparently been stripped of the altered zone by erosion). They are also Au- and U-enriched relative to the "typical" Archean granitic crust from the Barberton Mountain land.

In a follow-up study, Robb et al. (1990) dated single detrital zircons from the Witwatersrand. A large number of zircons are younger than 3,000 Ma, implying a major episode of granitization synchronous with Witwatersrand deposition. The observations of Robb et al. (1990) thus lead to a model in which high level, hydrothermally altered, Au- and U-enriched granitoids were emplaced very near to the Witwatersrand basin and eroded to fill the basin. However, a significant shortcoming of the model is its inability to account for the huge amounts of gold and uranium in the basin. As Robb and Meyer (1990) admit, the altered granites would have been inadequate and additional sources are required.

Sandstone provenance

Considering the focus on economic geology that permeates all Witwatersrand research, it is not surprising that most provenance studies to date have concentrated on the mineralized conglomerates. (Robb and Meyer, 1990, is a rare exception.) However, outside of the Witwatersrand, most recent provenance studies have been based on petrographic study of sand-sized clastic grains. The most widely applied method is that of Dickinson and Suczek (1979), in which framework grains are point-counted and plotted on quartz-feldspar-rock fragment (QFL) ternary diagrams that can be used to infer the provenance of the sands (figure 19). Further refinements are achieved by more careful consideration of the grain types. Rock fragments, for example, can be further subdivided into volcanic, metamorphic, or sedimentary classes. Feldspars sometimes can be identified petrographically on the basis of twinning, or

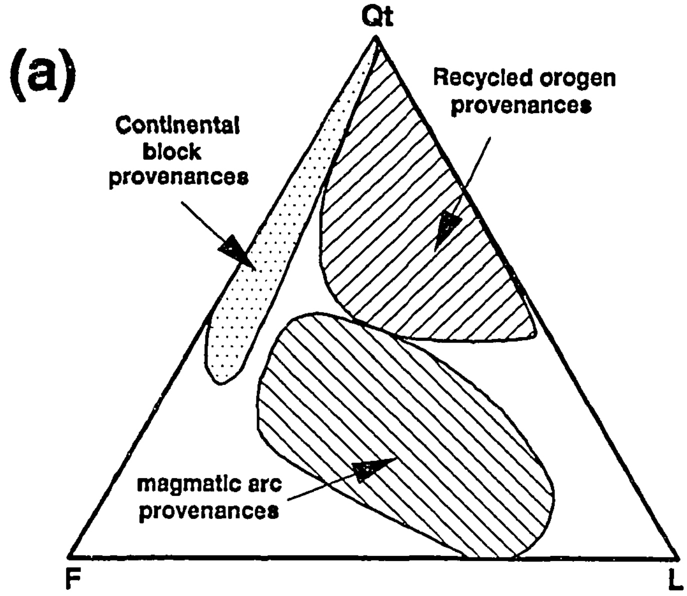

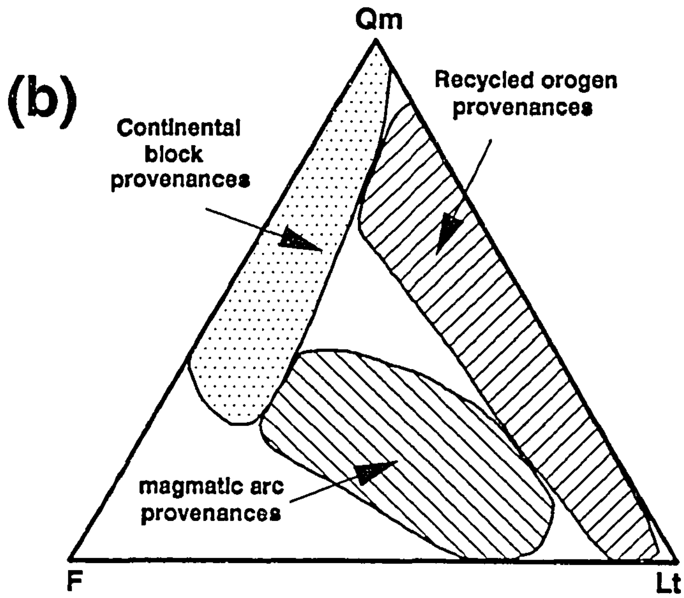

Figure 19. The QFL ternary diagrams of Dickinson (1985). The provenance fields are empirically determined. Q_t includes both mono- and polycrystalline quartz; F is feldspar; L is rock fragments (lithics); L_t includes rock fragments and polycrystalline quartz; and Q_m is monocrystalline quartz.

they can be identified more accurately with microprobe analysis. When these additional data are used in conjunction with the ternary plots of Dickinson and Suczek, provenance determinations can often be made with confidence (e.g. Graham et al., 1976; Maynard, 1984).

There are several advantages to using such a sandstone-based rather than a conglomerate-based approach to provenance in the Witwatersrand, even apart from the obvious point that the conglomerate-based studies have not been very successful. First, the sandstones constitute a much larger portion of the basin than the conglomerates--the sandstone:conglomerate ratio is 21:1 (Robb and Meyer, 1990). This ratio implies that the sandstones provide a better overall representation of the source area, simply because they are a larger sample. Second, most non-economic provenance studies have been conducted on sandstones, whereas there are few such studies of conglomerates. Physical and chemical processes of weathering and sedimentation are therefore better understood for sandstones than for conglomerates. Third, published descriptions of the Witwatersrand sandstones indicate they possess relatively common mineralogies and bulk chemistries, in contrast to the Au, U, and pyrite rich conglomerates. Consequently, there are many data available from other geologic systems for comparison to the Witwatersrand.

Before proceeding to a discussion of the Witwatersrand sandstone petrography and its consequences for provenance interpretation, a brief cautionary note is necessary: there are several processes that can modify the provenance signature, so that a simple interpretation according to the Dickinson-type model may not always be possible. In a large body of work based on the petrography of modern sands, it has become clear that weathering can alter, and perhaps even erase, the provenance signature (Franzinelli and Potter, 1983; Mack, 1984; Savage et al., 1988; Johnsson and Stallard, 1989). Equally important when working with an ancient, lithified and metamorphosed basin such as the Witwatersrand are post-depositional processes. These processes include diagenesis, metamorphism and even hydrothermal alteration. I will discuss these various alterations later in this chapter, and then again, more thoroughly, in the context of Witwatersrand sandstone geochemistry (Chapters 5 and 6 of this dissertation).

Witwatersrand sandstone provenance

For this provenance study of Witwatersrand sandstones, Keith Kenyon of Anglo-American Research Labs, South Africa, assembled a suite of 110 core samples. The samples were selected to represent the full Witwatersrand stratigraphic section at the Klerksdorp goldfield (figure 1). The economically important Central Rand Group is sampled more thoroughly than the West Rand Group (figure 20; there are 76 Central Rand samples and 34 West Rand samples). Detailed

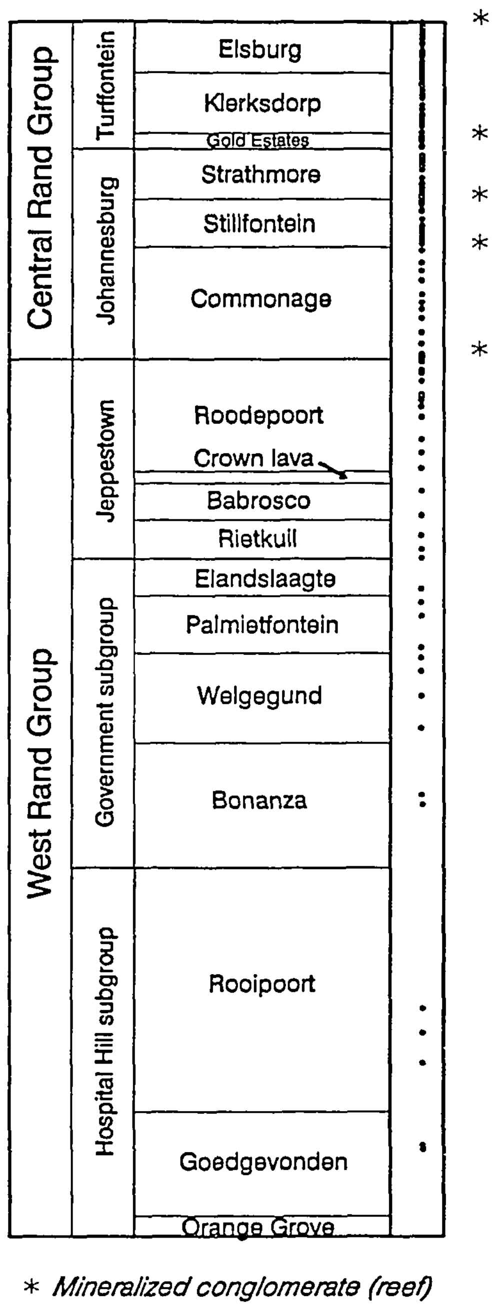

Figure 20. Stratigraphic locations of samples from the Klerksdorp goldfield. Each dot corresponds to a sample. The mineralized horizons marked on the column are, from the top down, the Ventersdorp Contact reef, the Gold Estates conglomerates, the Vaal reef, the Livingstone reef, and the Ada May/Commonage reef.

sample locations, including borehole numbers and depth of samples, are in Appendix 1.

Polished thin sections of all 110 samples were prepared. To permit microprobe analyses, the sections were not stained for feldspars. I counted 200 points per thin section according to the following eight categories: monocrystalline quartz, polycrystalline quartz, chert, matrix, feldspar, mica, calcite, and pyrite. These point count categories differ somewhat from most petrographic classification schemes, primarily because the Witwatersrand sandstones contain abundant matrix and pyrite, but no rock fragments. I will describe each category briefly.

<u>Quartz.</u> Monocrystalline quartz, polycrystalline quartz, and chert were counted separately. Monocrystalline quartz consists of a single crystal. Polycrystalline quartz is any composite of two or more quartz crystals in a single grain, regardless of the grain size. Chert is polycrystalline quartz in which individual crystals are less than 30 microns in diameter.

<u>Matrix.</u> Very fine-grained, petrographically homogeneous, sericite that fills the intergranular spaces was counted as matrix (figure 21). With microprobe and XRD analysis, this sericite proved to consist of both illite and pyrophyllite, but the two phases were not distinguishable petrographically. Rutile, as very fine, acicular aggregates, and chloritoid, as fine lath shaped crystals, are also

Figure 21. Photomicrographs of Central Rand quartzites. Photo (a) illustrates the most common matrix texture--a very fine-grained, homogeneous, mica-rich matrix. Photo (b) illustrates a rare exception--matrix which is visibly heterogeneous and may therefore be derived from rock fragments.

(a)

(b)

present in the matrix of some samples and were included as matrix in the counts.

Feldspar. Because the sections were not stained, I recognized feldspars by the presence of twinning, cleavage, and sericitic alteration. Although some untwinned, unaltered, feldspars may have been misidentified as quartz, microprobe study of point-counted sections indicated that such misidentifications were rare.

Mica. Only detrital micas are included in this category. Identification of a mica grain as detrital was based on (1) larger size than the matrix mica, (2) deformation, especially where imposed by surrounding framework grains, and (3) frayed, uneven ends. Microprobe analyses confirm that such grains are indeed detrital--they are not in chemical equilibrium with the matrix mica and they contain too much Ti to be of metamorphic origin (Sutton et al., 1990).

Calcite. Calcite does not appear as a detrital component, rather as a cement, commonly associated with albite.

Pyrite. Pyrites are rounded, compact, concentrated in laminae, slightly finer-grained than associated quartz grains, and some exhibit truncated growth zones (MacLean and Fleet, 1989), all of which suggests some of the pyrites are detrital. Other pyrites may be pseudomorphic replacements of a detrital phase such as magnetite, which is notable in its absence from the studied thin sections.

The results of the point counts are tabulated in table 2, and the framework grains are plotted on Q_tFL and Q_mFL_t ternary diagrams in figure 22. According to the Q_tFL diagram, the Witwatersrand sands are derived from a continental block source region: according to the Q_mFL_t diagram, the sands fall predominantly into the recycled orogen provenance (provenance fields as delineated by Dickinson, 1985; see also figure 19). The discrepancy between the two provenance diagrams is minor, and can be interpreted in several different ways.

One explanation lies in the nature of a continental block versus a recycled orogen (Dickinson, 1985). The continental block, or stable craton, has two primary sediment sources: low-lying granitic and/or gneissic basement rocks, and thin, flat-lying sediments (usually quartz arenites, shales, and limestones) that overlie basement. A recycled orogen has as its primary sediment source deformed and uplifted sedimentary rocks (hence the "recycled" designation). There is potentially a large overlap between sediments derived from these two sources, particularly if quartz arenites, shales and carbonates make up the recycled orogen--rocks similar to the cratonic sediments that make up the uppermost portion of the continental block source area. Thus, a source area that recycles crystalline basement plus cratonic-like sedimentary cover could produce a sediment that has the QFL composition of these Witwatersrand quartzites. A likely tectonic setting

Table 2. Point count data for 110 thin sections from the Klerksdorp goldfield. The samples are from eight different cores, and exact correlation between cores is not always possible, so the depths are approximate, particularly for the deeper samples. Those samples marked with ** are not included in the summary petrographic figure (Figure 31) because they are too fine grained (either shales or silty shales).

Sample	Depth (m)	Qm	Qp	Chert	Matrix	Fspar	Mica	Calcite	Pyrite
Elsburg:									
dl-301	3	107	51	3	39	0	0	0	0
302	16	85	62	3	49	0	0	0	1
303	25	89	42	1	68	0	0	0	0
304	39	81	74	0	45	0	0	0	0
304	59	112	27	0	58	0	0	0	3
306	77	82	64	0	54	0	0	0	0
307	96	112	21	1	66	0	0	0	0
308	99	100	63	0	36	0	0	0	1
309	122	96	46	2	56	0	0	0	0
310	127	85	40	4	71	0	0	0	0
311	160	101	54	1	44	0	0	0	0
312	176	107	51	5	37	0	0	0	0
313	190	126	36	3	35	0	0	0	0
314	219	139	38	1	22	0	0	0	0
315	235	121	38	0	41	0	0	0	0
316	249	110	46	4	39	0	1	0	0
317	265	93	62	4	40	0	1	0	0
Klerksdorp:									
318	279	93	43	3	61	0	0	0	0
319	298	85	60	3	52	0	0	0	0
320	316	98	59	3	39	0	1	0	0
321	328	92	36	8	62	0	2	0	0
322	337	90	57	1	52	0	0	0	0
323	366	83	65	2	48	0	2	0	0
324	388	106	47	4	43	0	0	0	0
325	404	94	52	2	52	0	0	0	0
326	441	88	39	3	68	0	2	0	0
327	464	69	60	3	67	0	1	0	0
328	490	64	66	2	68	0	0	0	0
329	494	79	56	5	60	0	0	0	0
330	502	150	33	0	17	0	0	0	0
331	518	156	30	3	11	0	0	0	0
332	530	99	77	4	20	0	0	0	0
333	553	113	48	1	35	1	1	0	1
Gold Estates:									
334	582	75	9	0	115	0	0	0	1
335	604	64	39	2	91	0	4	0	0
336	622	55	24	1	104	12	3	0	1
**337	627	15	1	0	182	1	0	1	0
**338	652	20	7	1	170	0	2	0	0
Strathmore 1:									
346	658	87	21	0	92	0	0	0	0
347	701	71	28	2	98	0	1	0	0
348	720	52	17	0	127	0	4	0	0
349	726	51	28	0	113	0	4	4	0
**350	739	43	9	0	130	2	12	3	1
351	755	66	33	1	72	12	6	10	0
**352	776	(shale)							

Table 2 - continued

Sample	Depth (m)	Qm	Qp	Chert	Matrix	Fspar	Mica	Calcite	Pyrite
Strathmore 2:									
339	818	65	42	0	92	0	1	0	0
340	844	63	59	0	78	0	0	0	0
341	853	79	34	1	85	0	1	0	0
342	869	71	38	0	91	0	0	0	0
343	885	66	48	0	84	0	2	0	0
344	901	84	43	2	70	0	1	0	0
345	914	103	48	0	49	0	0	0	0
Stillfontein:									
353	919	88	35	0	76	0	1	0	0
354	934	107	16	0	75	0	2	0	0
355	953	106	21	1	69	0	3	0	0
356	982	86	53	0	59	0	0	2	0
357	989	96	36	0	68	0	0	0	0
358	1030	77	33	3	78	0	2	7	0
359	1061	99	26	10	54	0	2	9	0
360	1082	82	52	1	62	0	1	2	0
361	1096	86	46	10	47	0	0	9	2
362	1118	91	45	0	61	0	1	1	1
363	1134	71	50	16	57	0	0	0	6
364	1154	92	29	0	77	0	2	0	0
Commonage:									
365	1190	86	43	4	63	0	0	4	0
366	1253	82	31	1	82	0	4	0	0
367	1293	86	52	8	53	0	0	1	0
368	1342	75	53	0	71	0	1	0	0
369	1417	87	56	1	55	0	1	0	0
370	1456	104	44	0	47	0	5	0	0
371	1489	82	48	2	66	0	2	0	0
372	1537	82	28	2	87	0	1	0	0
373	1611	80	80	3	36	0	1	0	0
374	1670	84	45	0	68	0	2	1	0
375	1723	67	11	0	120	0	2	0	0
376	1737	79	44	1	74	0	1	1	0
Roodepoort:									
377	1741	88	43	0	68	0	1	0	0
378	1752	90	22	0	87	0	1	0	0
379	1763	113	35	0	52	0	0	0	0
380	1806	78	32	0	89	0	1	0	0
381	1820	36	17	3	133	7	2	2	0
382	1862	80	17	1	65	20	4	13	0
383	1931	76	51	1	64	0	1	7	0
**384	1946	57	26	0	98	6	8	5	0
**385	1961	55	14	0	127	3	1	0	0
**386	1994	28	6	0	147	2	17	0	0
387	2050	95	35	0	26	42	2	0	0
388	2165	105	30	0	55	9	0	1	0
389	2234	98	25	0	53	23	1	0	0
**390	2316	67	22	2	70	30	5	4	0
Babrosco:									
391	2433	88	23	1	82	6	0	0	0
392	2561	83	23	0	58	33	3	0	0

Table 2 - continued

Sample	Depth (m)	Qm	Qp	Chert	Matrix	Fspar	Mica	Calcite	Pyrite
Rieutkuil:									
**393	2663	4	0	0	174	0	0	22	0
**394	2734	4	2	0	194	0	0	0	0
Palmietfontein:									
**395	2780	(shale)							
**396	2939	(shale)							
397	3007	111	48	1	36	4	0	0	0
398	3079	108	41	0	42	7	2	0	0
399	3239	96	53	0	50	0	1	0	0
Welgegund:									
**400	3294	34	18	3	136	5	0	4	0
401	3360	82	17	0	75	13	2	11	0
**402	3490	17	3	0	178	1	1	0	0
**403	3658	88	7	0	85	17	1	2	0
Bonanza:									
404	4000	82	18	1	98	0	1	0	0
405	4047	87	49	4	60	0	0	0	0
Rooipoort:									
406	5100	79	56	0	45	12	2	6	0
407	5228	84	33	0	68	6	2	7	0
**408	5382	22	6	0	156	4	2	10	0
Goedgevonden:									
**409	5800	(shale)							
**410	5811	23	3	0	165	0	0	9	0

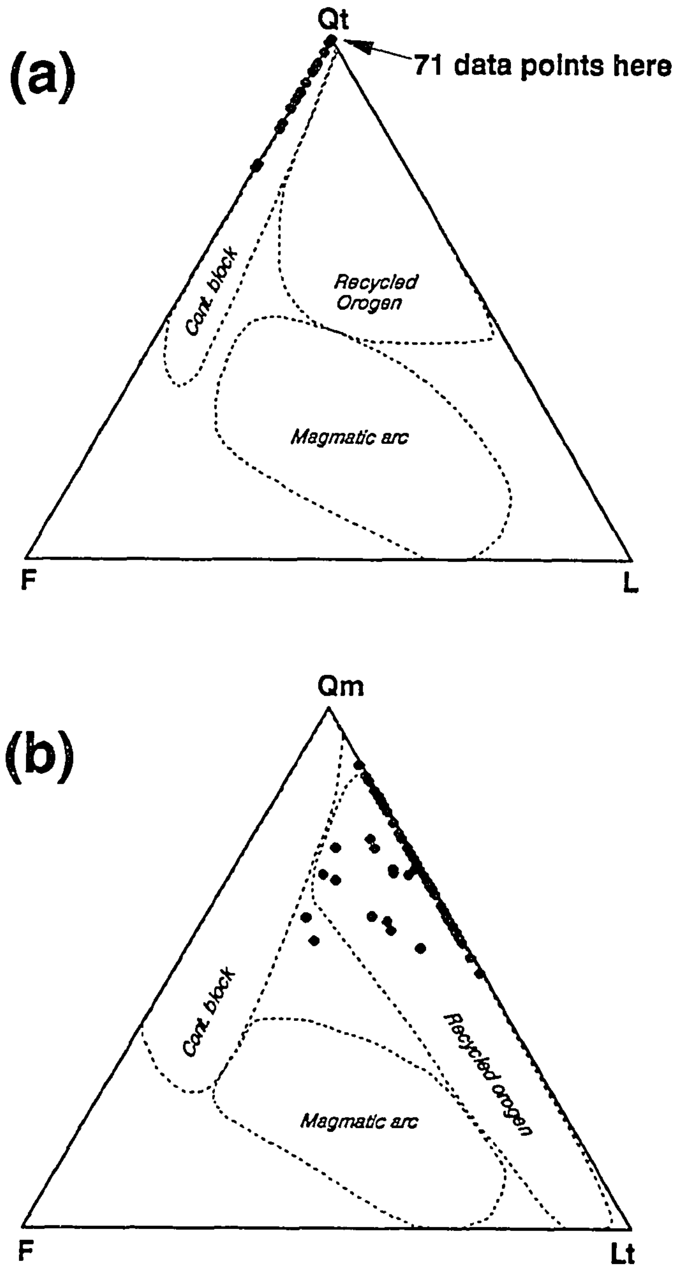

Figure 22. Point count data plotted on QFL ternary diagrams. The data fall into the continental block and recycled orogen provenance fields, respectively. However, because there is so much matrix of unknown origin in these quartzites, the interpretation could change significantly if the matrix were originally rock fragments or feldspars (fields and apices as in figure 19).

for such recycling is a foreland basin in front of a fold-thrust belt, provided basement is involved in the thrusting. A "thin-skinned" fold and thrust belt that does not expose crystalline basement would not provide the continental block signature that the QFL diagrams indicate. As discussed in chapter 2, the style of sedimentation and deformation in the Witwatersrand supports a foreland basin interpretation, and is therefore consistent with this particular QFL interpretation.

A second explanation as to why the two QFL diagrams result in slightly different provenance interpretations is that the QFL data do not accurately represent the original detrital composition of the Witwatersrand sands. One of the most striking features of the data is the complete absence of polymineralic rock fragments--the "rock fragments" that carry these quartz-rich sands into the recycled orogen field (figure 22b) are actually polycrystalline quartz grains, not polymineralic lithic grains. There is, however, abundant matrix that is not included in these framework grain ternary plots. Some of this matrix may have formed after deposition by the alteration/decomposition of detrital rock fragments. Fine-grained lithics (shales, siltstones, schists and volcanics), in particular, might not be expected to have survived the post-depositional history of the Witwatersrand, which includes compaction, diagenesis, and greenschist-facies metamorphism (Phillips, 1987). Evidence of a primary rock fragment component can be found in a few samples with sand-sized patches of visibly distinct matrix (contrast figure 21a with 21b). The maximum effect of post-depositional rock fragment destruction on provenance determinations can be demonstrated easily by assuming that all matrix was originally rock fragments, and then recalculating the QFL diagrams (figure 23). This will produce a shift toward the lithic corner of the ternary diagrams. The magnitude of the correction is limited by the percent matrix in a given sample. To construct figure 23, I have used the average QFL compositions of five formations: the Elsburg (n=17), Klerksdorp (n=16), Stillfontein (n=12), Commonage (n=12), and Roodepoort (n=10) formations. These five formations were selected because they were sampled sufficiently to calculate a meaningful average and because they were, on average, coarse-grained enough to rule out significant primary matrix (unlike the Strathmore formation, for instance, which contains some shale and silt units that contribute primary matrix).

Because some matrix will almost certainly be primary or the product of feldspar alteration, these recalculated rock fragment abundances represent hypothetical maximum values of the lithic component. The true composition of the original sand will almost certainly lie somewhere between the present QFL composition and the rock fragment-corrected QFL composition. Regardless of the precise sand composition, the effect of a rock fragment/matrix correction on both the Q_tFL and Q_mFL_t diagrams is to move the Witwatersrand sands

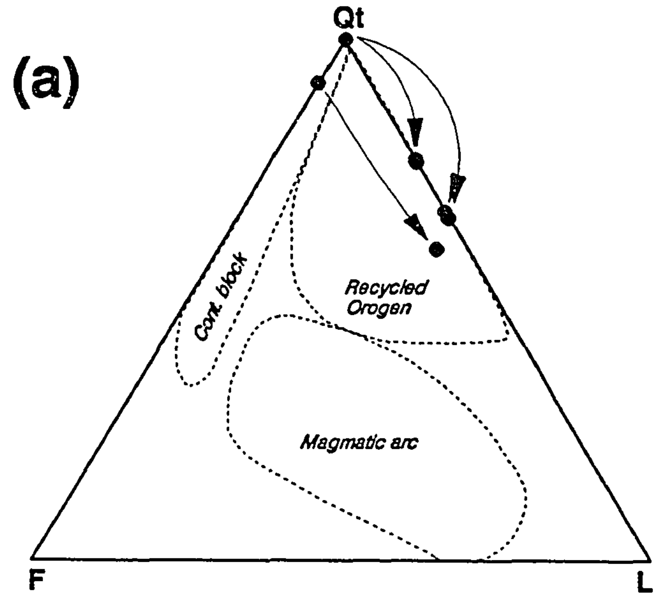

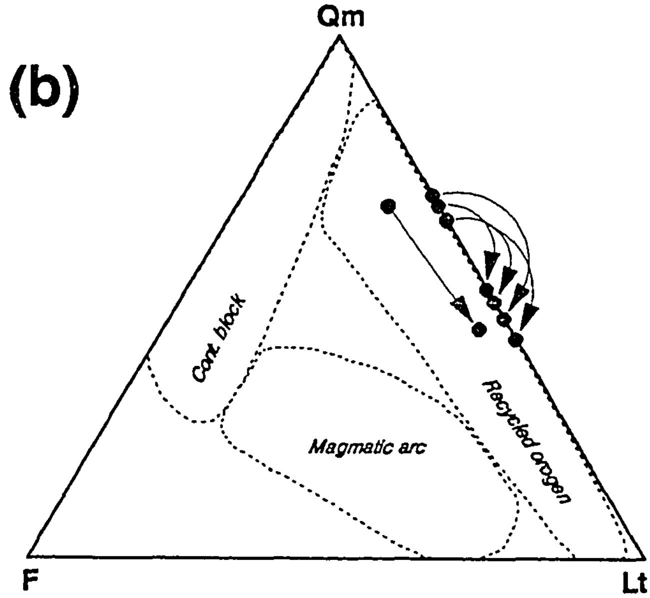

Figure 23. QFL plots of five formation averages (Elsburg, Klerksdorp, Stillfontein, Commonage, and Roodepoort). Treating the matrix as if it originally consisted of rock fragments produces the shifts indicated by the arrows.

solidly into the recycled orogen provenance (figure 23), and away from the continental block provenance indicated by the uncorrected Q_tFL diagram (figure 22a). Once again, a setting in which the Witwatersrand is a foreland basin receiving sediment from a tectonically active source area is fully compatible with the QFL recalculation.

The assumption that matrix is entirely composed of former rock fragments is almost certainly an exaggeration. There must have been some primary matrix, especially in the siltier units. Primary matrix, however, does not enter into these framework grain provenance interpretations. More importantly, some of the matrix must also be the product of feldspar alteration. Observations that favor the presence of some feldspar-derived matrix include partially sericitized feldspars, the abundance of sand-sized quartz (indicating a plutonic component to the source area, and therefore a supply of sand-sized feldspar), and the presence of patchy calcite cements. The calcite cements in the West Rand are generally associated with albite (often rimming albite) suggesting their origin as a by-product of albitization. By analogy, the presence of calcite cement in some non-feldspathic Central Rand sediments may indicate the former presence of Ca-bearing feldspar--feldspar that was first albitized, then sericitized. As with the rock fragments, it is possible to reconstruct provenance ternary diagrams allowing for the former presence of feldspar. To make this correction, it is necessary to account for the volume loss that occurs when feldspar is altered to sericite. Assuming equal parts Na-, Ca-, and K-feldspar in the original sand, the volume loss upon conversion of feldspar to sericite is from 77.4 cm^3 per mole of Al to 46.9 cm^3 per mole of Al. Thus, to calculate the original volume of feldspar that would have been present for a given volume of sericite matrix, I will multiply the percent matrix by 1.65 (77.4/46.9), and then recalculate the QFL total to 100%. This calculation simplistically assumes that all of the matrix is illitic and that it was entirely derived from feldspar.

Plotting "feldspar-corrected" QFL values produces no change in the Q_tFL continental block provenance interpretation (figure 24a). The Q_mFL_t diagram (figure 24b) undergoes a marked shift upon correction, into a rather poorly defined region that lies partly within the continental block provenance region and partly within an intermediate region that is not classified in Dickinson's diagram. Because Dickinson's fields are empirically derived, unclassified regions are present that represent QFL compositions that have not been reported from many modern sands. Rather than suggesting an extremely unusual Witwatersrand sand, this corrected plot is probably best interpreted as evidence that a simplistic, wholesale, reconstitution of the matrix to feldspar, such as I have attempted here, is not reasonable. More likely, only a

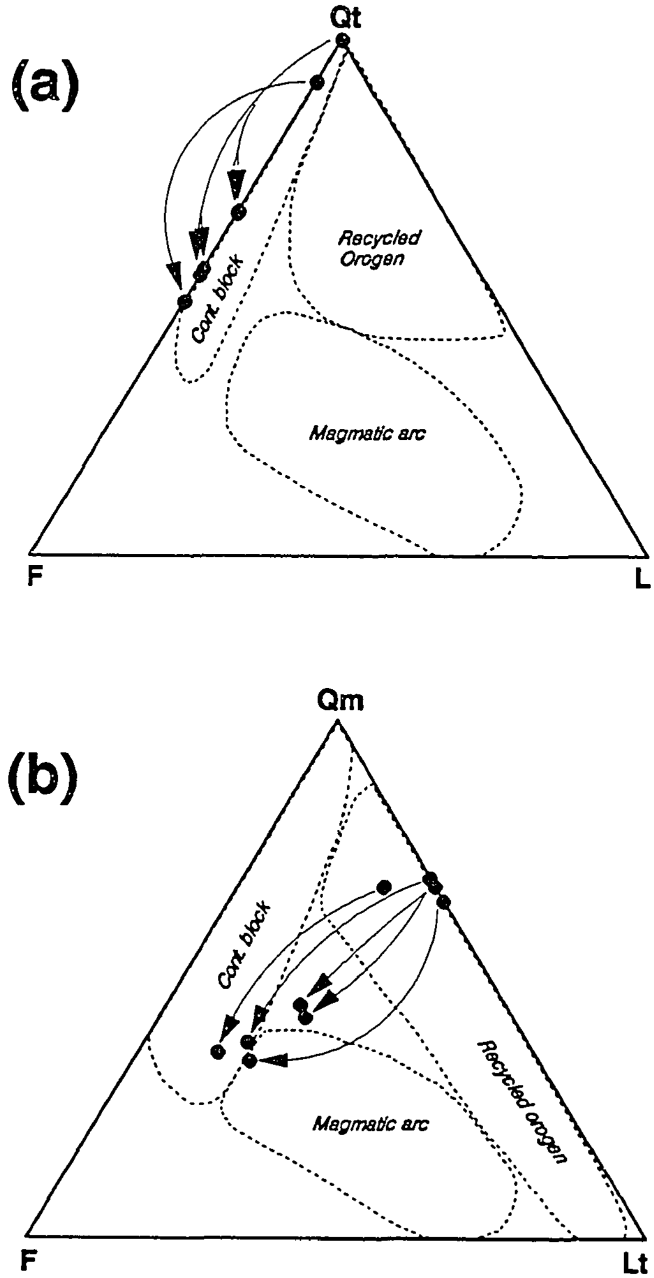

Figure 24. QFL plots as in figure 18, except that matrix is here treated as if it were entirely an alteration product of detrital feldspars.

portion of the matrix is derived from feldspar, in which case a smaller shift away from the Q_m-L_t join would occur.

The QFL data can be summarized by plotting the full range of potential feldspar-rock fragment variability on single diagrams. In other words, what interpretations are permitted by the available data, when matrix could represent original rock fragments, original feldspars, or primary matrix? To construct the diagrams, I allow each sample composition to vary between 3 end points--the counted QFL composition, the composition that assumes all matrix was originally feldspar, and the composition that assumes all matrix was originally rock fragments. The three end points define a triangle, and the true QFL composition of the original sand lies somewhere within this triangle. Figure 25 ("All samples") is the compilation of all such fields on Q_tFL and Q_mFL_t diagrams. Also in figure 25 are the fields that result when the same calculations are applied to the formation mean point count data (same formations as used in figures 22, 23 and 24). Using the formation means decreases the influence of extreme outliers in the sample set, and therefore yields a more realistic estimate of how a large number of data points might cluster. The broad areas delineated in figure 25 emphasize the difficulties involved in making a provenance interpretation for the Witwatersrand on the basis of the sand-sized detritus in the basin. The abundance of matrix, the origin of which is unresolved, makes it difficult to establish the provenance conclusively.

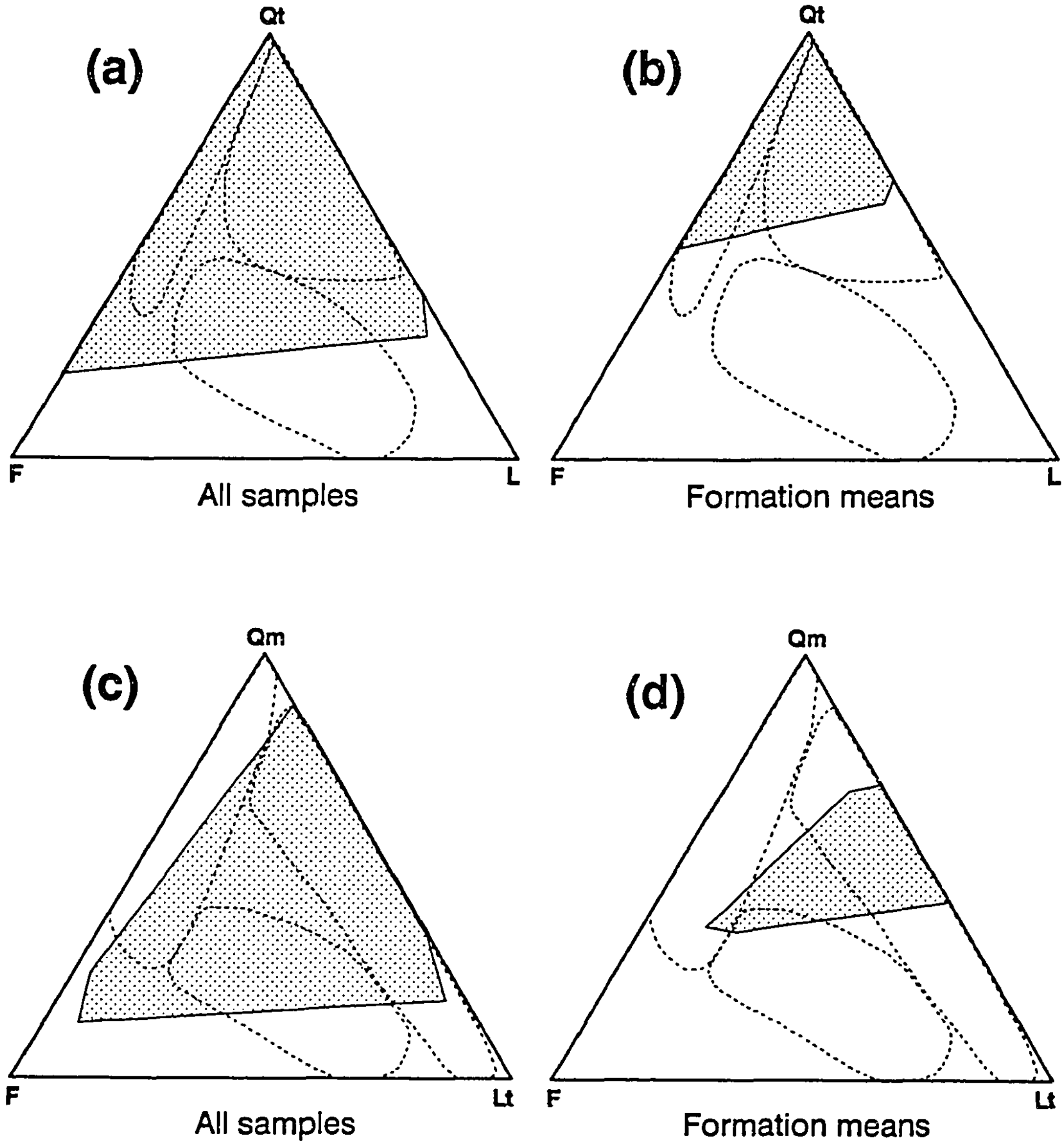

Figure 25. The fields that result when matrix is interpreted as being derived entirely from feldspar, entirely from rock fragments, or from any combination thereof. The fields defined on the basis of formation means reduce the effect of sample outliers, and therefore provide a more realistic estimate of how a large number of data points might cluster.

A magmatic arc source area is ruled out by both plots of formation means (figures 25b and 25d), and a continental block source area is marginally compatible with figure 25c but incompatible with figure 25. Only the recycled orogen field is compatible with all of the QFL plots, and so, on the whole these data favor a recycled orogenic source area.

Quartz cathodoluminescence

Although feldspar and rock fragments are commonly used to help determine provenance, in the Witwatersrand, quartz is the only detrital framework grain that is abundant. However, detrital quartz has rarely been used as a provenance tool, primarily because there are few useful, easily measured, diagnostic properties of quartz. Undulosity is difficult to quantify and is ineffective in distinguishing among source rocks; chemistry is essentially constant unless more expensive and time consuming analyses of trace elements are carried out; fluid inclusions potentially could be useful, but data collection is too time consuming to assemble a statistically significant population of grains.

One other technique that has been used sparingly in provenance studies is quartz cathodoluminescence (Owen and Carozzi, 1986). When subjected to an electron beam, quartz luminesces in both the red and the blue portions of the visible spectrum. If one peak is dominant, the grain will appear either blue or red; if the peaks are approximately equal, some shade of brown results. Although the factors that control cathodoluminescence (CL) in quartz are not well known (Zinkernagel, 1978; Sprunt, 1981), there is an empirical relationship between geologic environment and CL color: quartz from igneous and high grade metamorphic rocks luminesces blue, and quartz from low grade metamorphic rocks luminesces reddish brown (Owen and Carozzi, 1986). From these observations it follows that the CL color of quartz in sediments might be a useful provenance indicator.

Standard quartz CL methodology relies on visual study of thin sections in a luminoscope. The operator must decide whether a particular grain is red, blue, or a shade of brown. Because these color changes occur over a continuous spectrum, classification is not always obvious. To overcome this difficulty, I used a technique developed by Baker (1988) that quantitatively analyzes the CL spectrum of each grain. A Cameca SX-50 electron microprobe with a 20 micron spot and a 12.5 nA current setting was used to induce luminescence. The resulting spectrum was collected through the microprobe's optical viewing system by a fiber optics connector attached to a Princeton Instruments HR-320 optical multichannel analyzer. The analyzer collected for 20 seconds over the entire visible spectrum (from approximately 300 to 900 nm) by measuring counts per second simultaneously with 1024 diodes, each of which corresponds to a particular wavelength. The diodes were calibrated by measuring known spectra (neon and mercury vapor lamps). Figure 26 is a typical spectrum from a blue quartz grain, figure 27 the spectrum of a red grain. To quantify the CL color of each grain I used the ratio:

$$\mathrm{Intensity}_{\mathrm{Blue}} / (\mathrm{Intensity}_{\mathrm{Blue}} + \mathrm{Intensity}_{\mathrm{Red}})$$

With the single number that results (the "CL index" henceforth) it is a simple matter to compare different populations statistically. For example, the CL indices for figures 26 and 27 are 0.62 and 0.44, respectively.

I used this technique to analyze between 20 and 40 grains from each of 19 thin sections spanning the entire stratgraphic range of the Witwatersrand Supergroup. The results of these analyses are plotted stratigraphically in figure 28. A strong correlation between the thickness of the carbon coating (visually estimated) and the luminescence intensity is the most striking feature of figure 28. For example, from 950 to 1250 m depth the red and blue peak intensities are quite high. However, note that the four samples in this depth range have a relatively thin carbon coat, suggesting that the increased peak intensities are in part a function of coating thickness. The CL index, which is plotted in the last column of figure 28, eliminates the coating thickness bias and reveals that there is little variability in the CL of detrital quartz throughout the Witwatersrand section. The overall average CL index (0.57) falls within one standard deviation of the individual sample averages. There are no significant outliers amongst these

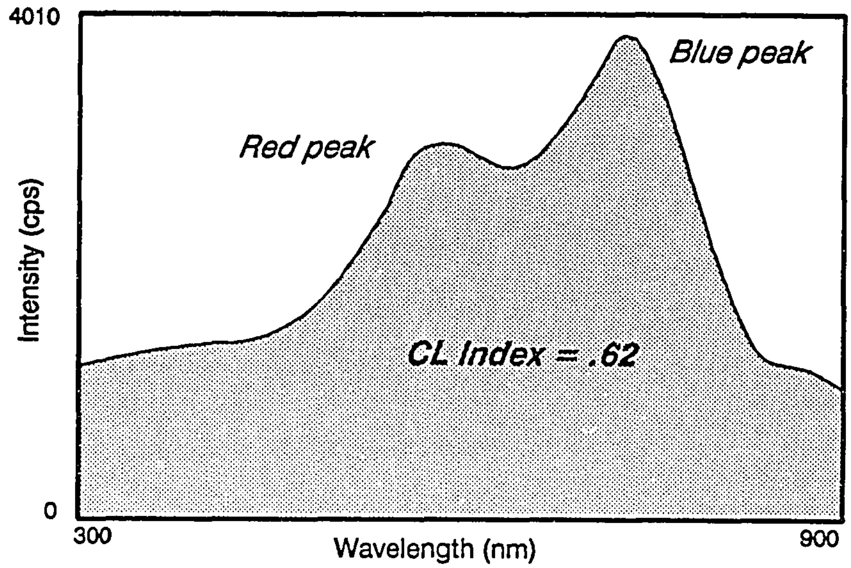

Figure 26. A cathodoluminescence spectrum from a blue luminescing quartz grain.

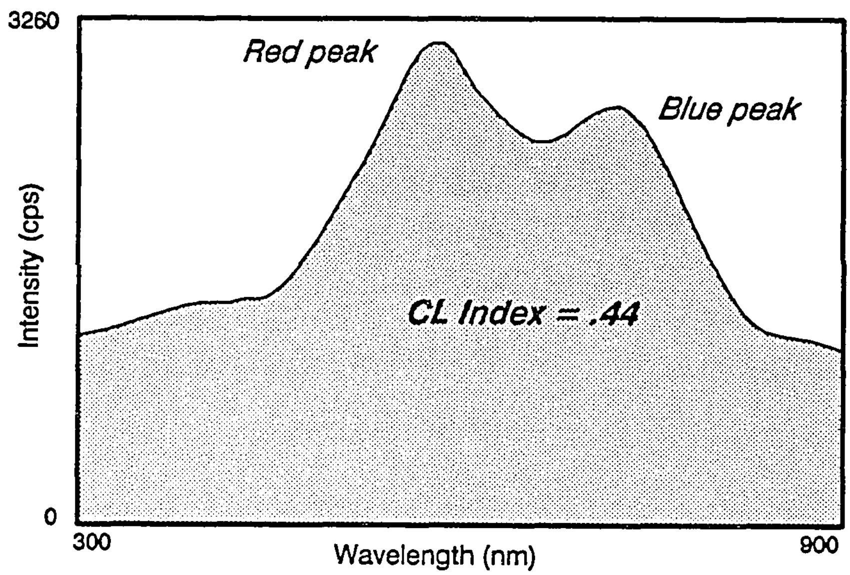

Figure 27. A cathodoluminescence spectrum from a red luminescing quartz grain.

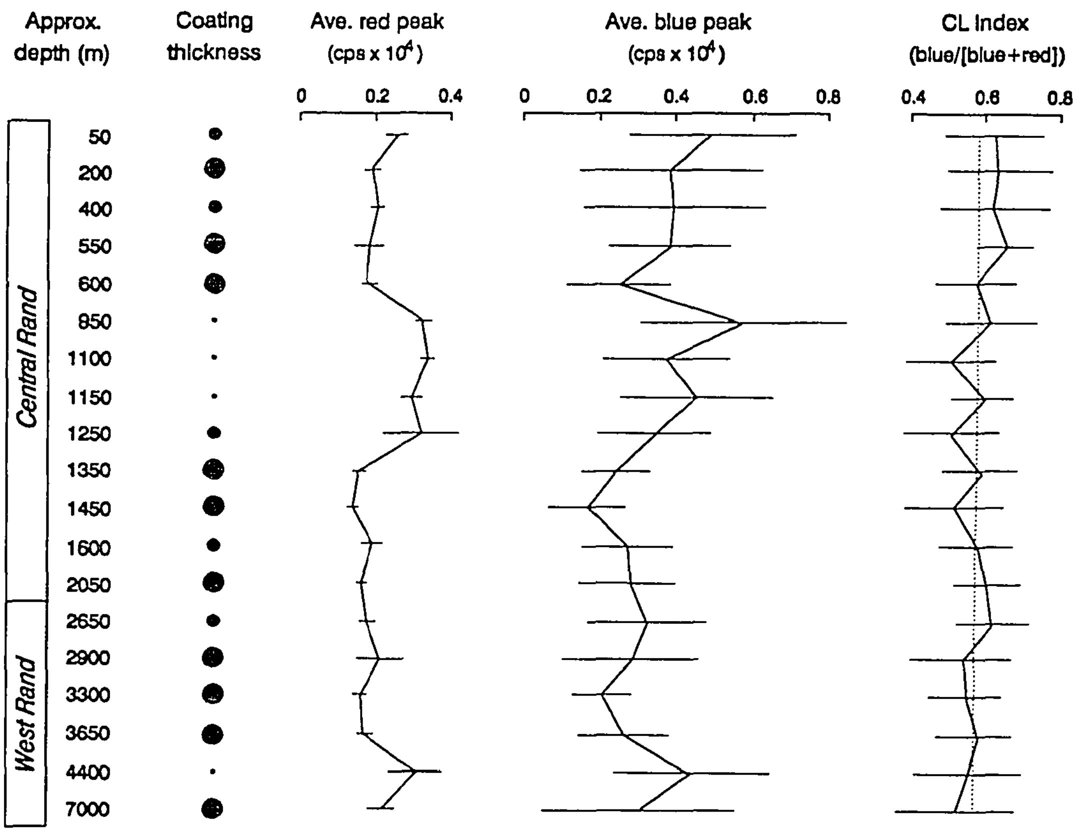

Figure 28. Quartz CL versus depth within the Witwatersrand supergroup. Coating thicknesses are visual estimates. Small dots indicate thin coatings, large dots indicate thick coatings. The peak intensities are averages obtained from 20-40 grains per sample, and the error bars are ± one standard deviation. The CL index is a ratio of the red and blue peaks (Blue/[Blue + Red]), and therefore eliminates the coating thickness bias. The dashed vertical line is the overall average CL index of Witwatersrand quartz grains.

nineteen samples, nor is there a systematic stratigraphic trend of any sort.

The uniformity of quartz CL can be interpreted in two ways. A simple and geologically reasonable explanation is that there was little change through time in the type of source rocks that were supplying sediment to the basin. This interpretation is compatible with recent suggestions that hydrothermally altered granites comprised the bulk of the Witwatersrand hinterland (Robb and Meyer, 1990; Klemd and Hallbauer, 1987), particularly because the overall tendency towards blue quartz favors an igneous or high grade metamorphic source rock. (A CL index of greater than 0.5 indicates dominance of the blue peak; the average of all grains is 0.57.) A second possible explanation is that the Central Rand sediments have been recycled from older West Rand sediments, as would be expected in the tectonic model of the Witwatersrand as a foreland basin (see chapter 2). The two interpretations are not mutually exclusive--a mixture of sediment recycling and continued addition of new granitic quartz would also produce the observed trend.

I also used quartz CL to examine "matrix" quartz--fine-grained quartz smaller than 100 microns in diameter that either is completely surrounded by matrix or is attached only nominally to larger detrital grains. In figures 29 and 30, the average of 5 to 10 matrix quartz analyses from each of 12 samples are plotted against the average detrital quartz analyses for the same samples. The CL index is

Figure 29. The CL index of matrix quartz versus the CL index of detrital quartz grains from the same sample. If the matrix quartz and the detrital quartz possessed similar cathodoluminescence properties, the points would lie on a line with slope equal to one. The direction in which the data points plot off the line indicates that detrital quartz is bluer than matrix quartz.

Figure 30. CL peaks of detrital quartz plotted against CL peaks of matrix quartz from the same sample. The red peak remains constant for both sample groups, plotting on the line with a slope of one. The blue peak, however, is much less intense for matrix quartz than for detrital quartz.

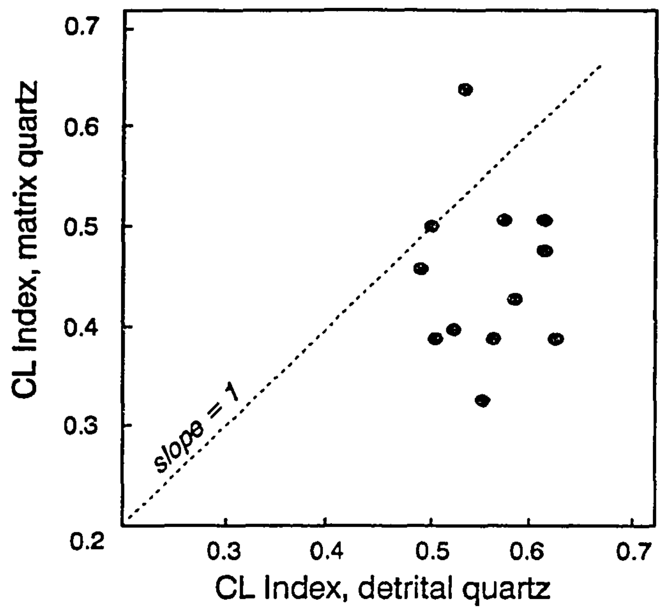

CL Index, matrix quartz
CL Index, detrital quartz
slope = 1
0.2
0.3
0.4
0.5
0.6
0.7

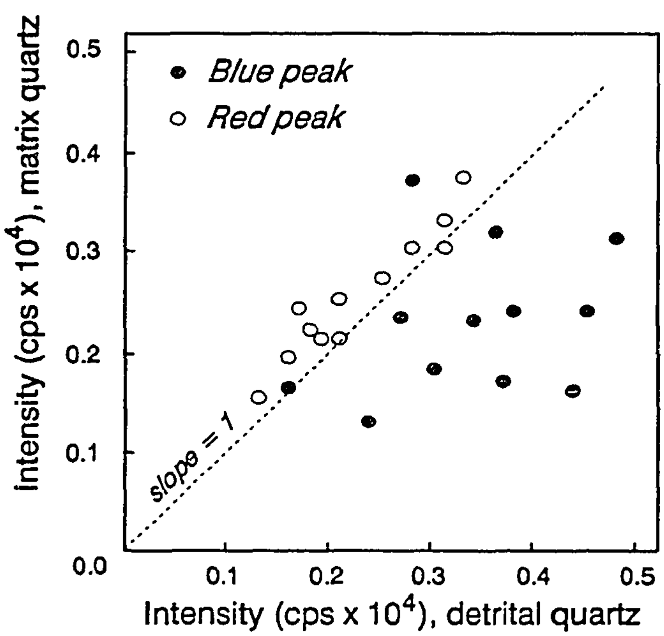

Blue peak
Red peak
slope = 1
Intensity (cps x 10^4), matrix quartz
Intensity (cps x 10^4), detrital quartz
0.0
0.1
0.2
0.3
0.4
0.5

significantly lower for matrix quartz than for detrital quartz from the same sample (confidence level of 99%). Breaking the CL peaks into their red and blue components (figure 30) can tell us whether it is the red peak, the blue peak, or some combination that leads to the CL differences between matrix and detrital quartz. The red peaks cluster about a line with slope equal to 1, indicating that the red peak is nearly equal in intensity for both detrital and matrix quartz. The plot of blue peaks, however, deviates significantly from a slope of 1, with the matrix quartz exhibiting low intensities relative to the detrital quartz.

These quantitative data reinforce qualitative relationships observed in the luminoscope, where three varieties of quartz are visible: detrital grains, which luminesce brightly; quartz overgrowths, which luminesce weakly; and the matrix quartz, which also luminesces weakly. The similar luminescence properties of matrix quartz and quartz overgrowths imply a similar mode of formation. Based on the early appearance of overgrowths in most sandstones, the mode of origin is probably diagenetic. Also, the low intensity of the blue peak in the matrix quartz is characteristic of low temperature quartz (Owens and Carozzi, 1986).

One additional conclusion that can be drawn from the differing CL properties of matrix versus detrital quartz is that metamorphism has not reset (or "homogenized") all of the quartz in the basin. Consequently, the vertical homogeneity of detrital quartz grains accurately reflects their CL provenance signature; there has been no metamorphic overprinting of their cathodoluminescence.

Vertical trends in the Witwatersrand

Although I judge my QFL plots to have been only marginally successful in assessing Witwatersrand provenance, the petrographic data can still be of considerable interest when cast into a stratigraphic framework (figure 31). Matrix decreases, and feldspars disappear almost completely in a West Rand to Central Rand traverse.

Decreasing matrix. The upwards decrease in matrix, when combined with the disappearance of feldspar, indicates that the Witwatersrand sediments are becoming more mature (i.e. more quartz rich). Mature sediments can result from both physical and chemical processes. A decrease in matrix (if the matrix is primary matrix) is an example of a physically maturing sediment. Higher energy flow conditions accompanied by more thorough fluvial (or shallow marine) reworking of the sediments will winnow out clays and silts, producing a matrix-poor, or texturally mature sediment. The many sedimentological studies that demonstrate the prevalence of vigorous fluvial activity during deposition of the Central Rand sediments (e.g., Minter, 1976; Buck and Minter, 1985;

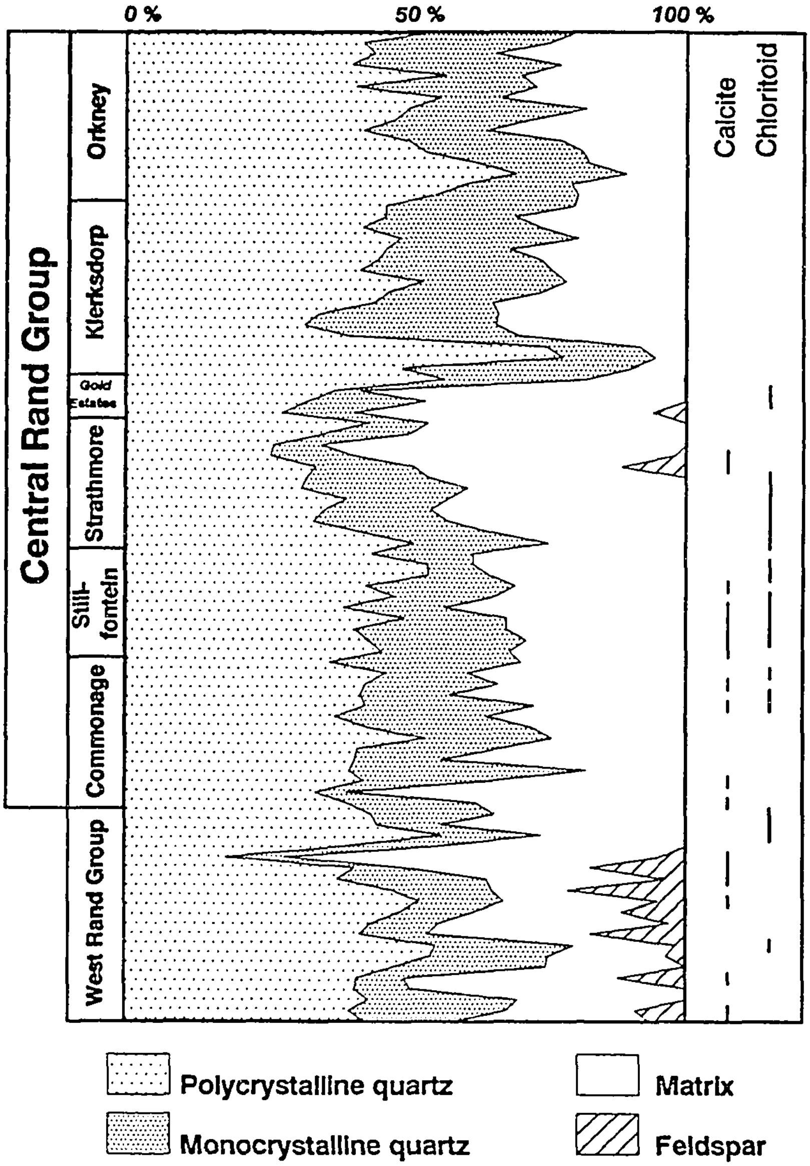

Figure 31. Summary of the petrographic data for 92 West and Central Rand quartzites from the Klerksdorp goldfield. The sample numbers, stratigraphic positions and tabulated data are in Table 1.

Els and Beukes, 1987) support this interpretation of a texturally maturing sediment in the Central Rand.

Absence of feldspars. The absence of feldspars in the Central Rand is an example of chemical maturity--there is no effective physical means for separating the hydraulically similar quartz and feldspar grains. Yet it is quite clear that the two phases do not co-exist in the Central Rand. In my examination of 76 Central Rand thin sections, I observed feldspar grains in only six samples, and the feldspar was quantitatively minor in these few samples. In an early petrographic study of the Witwatersrand, Fuller (1958) reported no feldspars in the 28 Central Rand samples that he examined.

The paucity of feldspars indicates either that they have been removed or that they were not present in the primary detrital suite of minerals. Considering the presence of feldspars in the West Rand (table 2 and figure 31), the latter scenario is unlikely. The West and Central Rand are similar in many respects, most notably in their gold and uranium mineralization, their detrital pyrites, quartz pebble conglomerates, and their overall preponderance of quartz, suggesting that they are derived from fundamentally similar source areas and should therefore have similar, feldspar-bearing framework mineralogies. Also favoring the original presence of detrital feldspars in the Central Rand is the abundance of coarse-grained (plutonic) quartz and, more generally, the large role played by granites in making up the Archean continental crust. The evidence at hand therefore favors the presence of detrital feldspar in the Central Rand. This, in turn, implies that these feldspars must have been removed post-depositionally.

Studies describing the post-depositional removal of feldspars from clastic sediments are, for the most part, found in the petroleum geology literature, where there is great interest in the secondary porosity that results when feldspars are dissolved. The prevailing view holds that this secondary porosity develops only after most of the primary porosity has been lost by compaction (Schmidt and McDonald, 1979). Generally, post-compaction secondary porosity implies feldspar dissolution at depths of several thousand meters, well into the realm of diagenesis. Two of the best documented cases of diagenetic feldspar dissolution are found in the oilfields of the Gulf coast (USA) and the North Sea. In the Gulf coast Tertiary, the percent of potassium feldspar declines markedly at a depth of 4-5 km (figure 32). A similar decline in total feldspar (from an average of about 25% to an average of 1-2%) in the Brent sandstone of the North Sea occurs between 2500 and 3500 m burial depth (figure 33). Early models explaining the deep level diagenetic dissolution of feldspar called upon CO_2 as the agent of dissolution. The source of CO_2 was suggested to be the decarboxylation of organic matter (Schmidt and McDonald, 1979; Siebert et al., 1984). Lundegaard et al.(1984) tested the hypothesis that CO_2 alone is responsible for the loss of

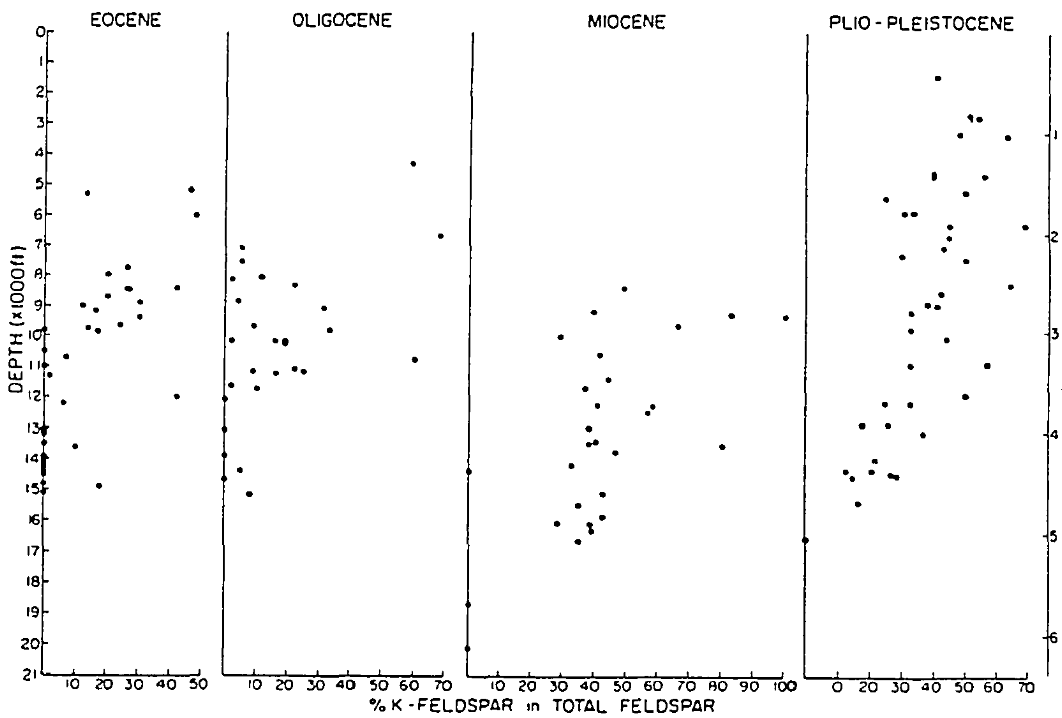

Figure 32. Potassium feldspar as percent of total feldspar in Tertiary sediments of the Texas Gulf coast. Note that K-feldspar declines to zero by about 5000 m depth in all formations. From Land et al. (1987).

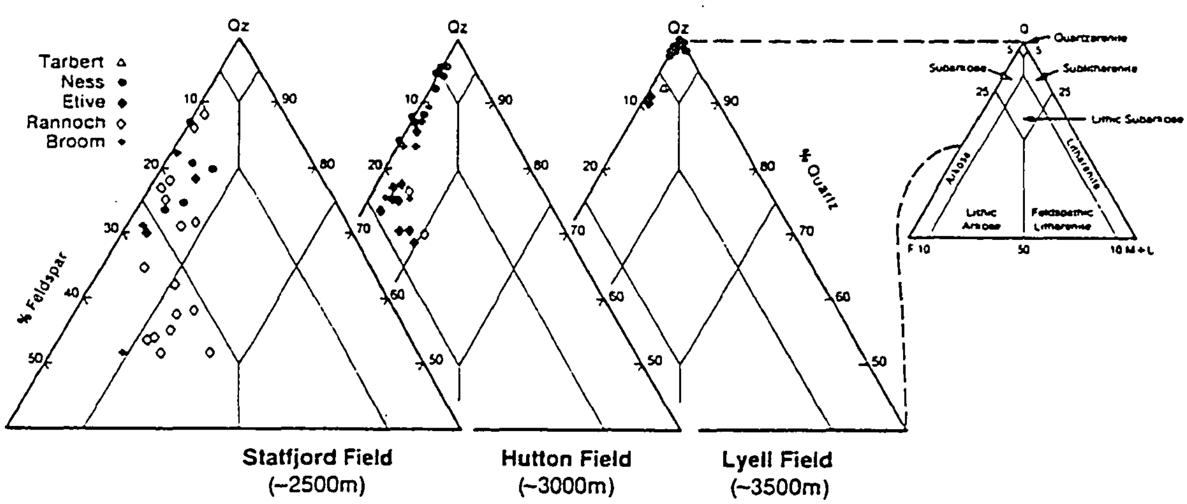

Figure 33. QFL plots of the five formations in the Jurassic Brent sandstone in the North Sea oilfields. The abundance of feldspar decreases rapidly between 2500 and 3500 m depth. By 3500 m, the sandstone is a quartzarenite.

feldspar in the Gulf coast, and found that there is insufficient organic matter in the sedimentary sequence to generate the needed volume of CO_2. To solve this mass balance problem, others have proposed dissolution driven by other, more complex, organic acids (Surdam et al., 1984; Siebert et al., 1984). At present, a comprehensive quantitative model remains elusive, but for the purposes of understanding feldspar dissolution in the Witwatersrand, two important points are: 1) most recent studies document a trend towards increasing feldspar dissolution with depth, and 2) acids (principally CO_2) produced by the maturation of organic matter are the principal agents of dissolution.

An attempt to apply a simplified deep level, CO_2-based diagenetic model of feldspar dissolution to the Witwatersrand meets with two immediate difficulties. In the Witwatersrand, feldspar has been removed from the top of the stratigraphic section, not the base of the section (compare figure 31 for the Witwatersrand to figures 32 and 33 for the Gulf coast and North Sea, respectively). Also, in the Witwatersrand it is not possible to generate CO_2 or organic acids (the agents of dissolution) from the maturation of organic matter because there was virtually no organic matter present. Three quartzite samples and one conglomerate sample that were analyzed by Richard Schultz at the University of Cincinnati yielded total C values of 0.03%, 0.04%, 0.00%, and 0.00%, indicating that there is little to no disseminated carbon in the Witwatersrand. There are also no significant localized accumulations of carbon that have been reported apart from the "carbon seams" that are found on some of the major unconformity surfaces, beneath the mineralized conglomerates. These seams are generally only one to several millimeters thick, and a few centimeters to several meters in length (Hallbauer and Van Warmelo, 1974). Because they are thin, laterally discontinuous, and occur at only a few stratigraphic horizons in the basin, the carbon seams represent volumetrically insignificant accumulations of organic matter in the context of the total basin fill.

Although the feldspar distribution and lack of carbon make deep-level diagenetic destruction of feldspar in the Witwatersrand unlikely, the basic principles can be used to develop an alternative scenario. Rather than dissolving feldspar at depth with a deep CO_2 source, it may be possible to do almost the opposite in the Witwatersrand: dissolve feldspar in the shallow subsurface with a shallow, atmospheric CO_2 source. Such a model superficially resembles weathering, but there are some fundamental differences between modern theories of weathering and the meteoric leaching that I propose for the Central Rand. First, feldspar has been leached from almost 2,000 m of sediment in the Rand--a much thicker profile than has ever been reported for weathering profiles. Second, weathering depends heavily on the terrestrial biota. In modern soils and groundwaters, the principal weathering acids are organic acids and carbonic acid (which is a product of root respiration and organic matter oxidation; Wood and Petraitis, 1984). In the Witwatersrand, with no significant terrestrial biota, a different source of weathering acid is needed.

Theoretical and geochemical considerations suggest that atmospheric CO_2, of inorganic origin, was probably the major weathering acid in the Archean. Holland (1984, p. 79) calculated that upon initial accretion and degassing of the Earth, approximately one-third of the total terrestrial CO_2 may have accumulated in the atmosphere (in contrast to the <0.01% of total terrestrial CO_2 that is present today in the atmosphere and ocean combined). Initial CO_2 levels were therefore very high. But how rapidly did atmospheric CO_2 decline to modern levels? Was the concentration of atmospheric CO_2 high enough during the time of Central Rand sedimentation for significant meteoric leaching to occur? We can gain some insight from consideration of the sun's evolution.

Based on the sun's present luminosity and total mass, it has been determined that total solar luminosity has increased roughly 20% in the past 3 billion years (Hart, 1978). In spite of the cooler Archean sun, there is ample evidence of water-lain deposits (the Witwatersrand, for example), implying temperatures about the same as today's. To maintain above-freezing temperatures, atmospheric greenhouse processes must have been more effective in the Archean. The dominant greenhouse gas is CO_2, and Owen et al. (1979) have calculated that atmospheric CO_2 must have been

100 times more abundant 3 billion years age than it is today (.033 bar CO_2 versus .00032 bar CO_2) to maintain an average surface temperature of about 20° C. Also favoring high CO_2 levels in the Archean is the absence of photosynthesizers. Geological evidence (an abundance of banded iron formation and changing iron behavior in paleosols; Holland, 1984) and paleontological evidence (Schopf, 1975) indicate that photosynthesis probably was not an important global O_2 source and CO_2 sink until after about 2,000 Ma. If the concentration of CO_2 in the Archean atmosphere was indeed 100 times higher than present levels, the amount of CO_2 dissolved in meteoric water would have been proportionately greater. When CO_2 dissolves in water it forms carbonic acid, H_2CO_3. Carbonic acid can convert feldspar to kaolinite:

$KAlSi_3O_8 + H_2CO_3 + 4.5H_2O$ -----> $0.5Al_2Si_2O_5(OH)_4 + K^+ + 2H_4SiO_4 + HCO_3^-$ (equation 1)

$NaAlSi_3O_8 + H_2CO_3 + 4.5H_2O$ -----> $0.5Al_2Si_2O_5(OH)_4 + Na^+ + 2H_4SiO_4 + HCO_3^-$ (equation 2)

$CaAl_2Si_2O_8 + H_2CO_3 + H_2O$ -----> $Al_2Si_2O_5(OH)_4 + Ca^{++} + CO_3^{--}$ (equation 3)

These reactions, of course, may proceed by way of intermediate products such as illite and smectite. I have chosen to write them as a single-step process.

The reactions can take place only if CO_2-enriched groundwater is brought into contact with feldspathic sediments. For a basin such as the Witwatersrand, the movement of groundwater is quite predictable. Recharge occurs along the basin margins. This is because the greater elevation of the basin margin/source area induces maximum precipitation, and the basin margin sediments are the coarsest (most proximal to the source area), thus allowing maximum infiltration. Because the basin margin is topographically higher than the more distal (downslope) basin fill, a hydraulic head is established that causes the infiltrating groundwater to flow basinward. Eventually, near the center of the basin, the groundwater discharges. Two examples of this general flow pattern are shown in figure 34. Figure 34a is from the Central Valley of California, a particularly well-studied hydrologic system, and figure 34b is from the Smith Creek valley, Nevada. Both of these basins are similar to the pre-consolidation Central Rand. They have an essentially impermeable basement, mountainous source areas, and unconsolidated basin fill consisting of proximal, coarse-grained alluvial fan deposits grading basinward into finer-grained equivalents. It is apparent from the flow patterns in figure 34 that carbonic-acid charged groundwater would be most active in the shallow, proximal regions of the basin, where it begins its subsurface journey in equilibrium with atmospheric CO_2. As the first pulse of groundwater flows down into the sediment column and then basinward,

Figure 34. Groundwater flow patterns in the Central Valley, California (a) and the Smith Creek valley, Nevada (b). Recharge is predominantly along the basin margins, the groundwater then flows basinward, and discharge occurs near the center of the basins. (a) is from Williamson et al. (1989). (b) is from Thomas et al. (1989).

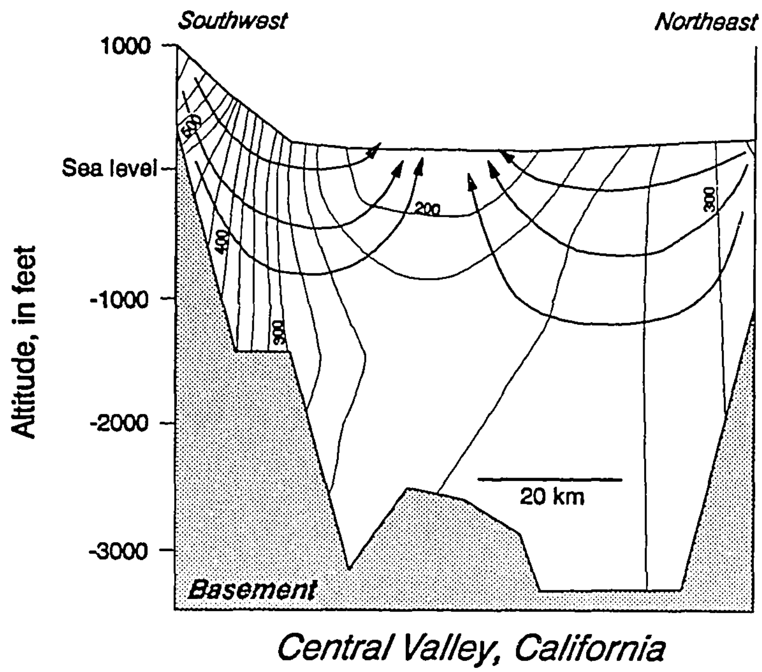

Central Valley, California

(a)

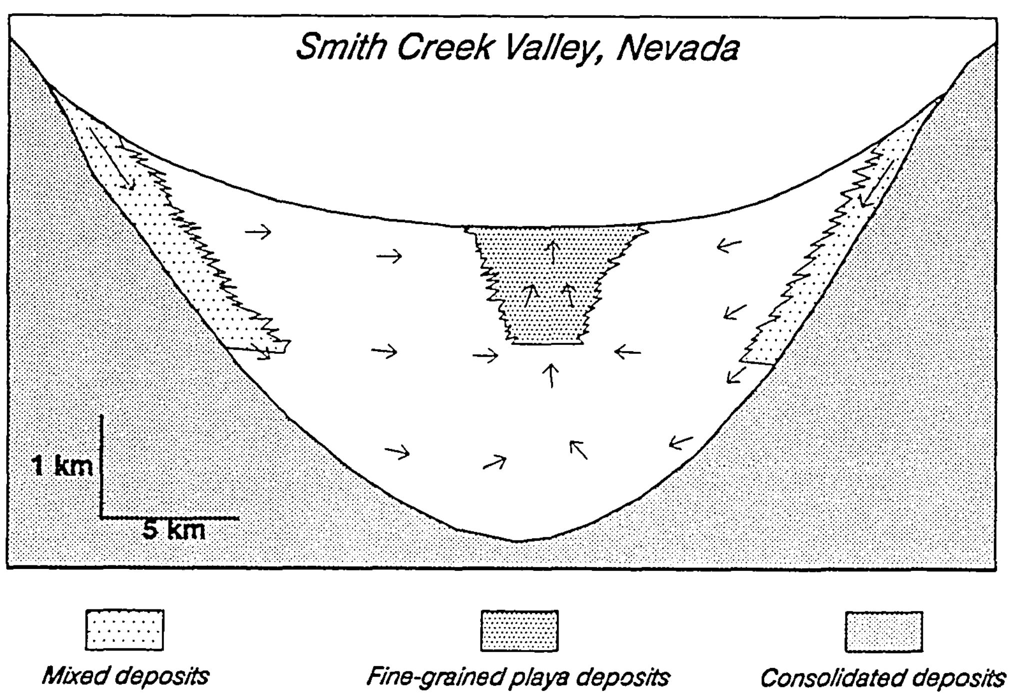

(b)

continuously reacting with feldspar, it would gradually attain equilibrium with the feldspar as a result of rising pH and cation concentrations brought about by reactions 1-3. Thus, the most intense leaching would initially be nearest the surface. The next pulse of groundwater following approximately the same path would first encounter leached sediments, through which it would travel with little chemical effect, the leached sediments already having been brought into equilibrium with acid groundwaters by the first pulse of groundwater. Over time, each new pulse would travel farther through leached sediments before encountering chemically reactive (feldspathic) sediments, thereby advancing the front along which feldspar dissolution occurs. This is, of course, not a process carried out by discrete pulses of groundwater, rather a continuous process operating along a "front" that is gradational--the most soluble feldspars being leached at the distal end of the front, the least soluble remaining until the front has all but passed, thereby encountering the most reactive groundwater.

The degree to which feldspars can be leached, or the depth to which the front can penetrate, is not limited by the equilibrium chemistry of the CO_2-H_2O system. As groundwater continues to flow through the system, reaching greater depths (and therefore higher pressures and temperatures), the solubility of CO_2 increases because the rising pressure raises CO_2 solubility more than the rising temperature lowers CO_2 solubility (Lundegaard et al., 1984).

Thus, the CO_2 that dissolved in the groundwater initially (that is, the $CO_2(aq)$ that is in equilibrium with atmospheric CO_2) will be fully retained in solution. Indeed, were more CO_2 available at depth, the $CO_2(aq)$ could increase.

The depth of leaching is, however, limited to some degree by time and the hydrologic system. Only in a very stable, long-lived hydrologic system will there be enough time available to cycle large volumes of groundwater through deep basin sediments. There are several reasons for this. First, the deep groundwaters will initially be approximately in equilibrium with feldspar. Only after shallow sediments have been leached will acid groundwaters penetrate deeply. Second, the flow of groundwater is faster in the shallow subsurface because the sediments are less compacted and therefore possess greater hydraulic conductivities. A higher flow rate will cycle more dissolved CO_2 through the sediment, leading to increased feldspar removal. Third, hydraulic conductivities in bedded sediments are anisotropic, with higher conductivities parallel to bedding than across bedding. With essentially flat-lying sediments such as were present in the Central Rand soon after deposition, this anisotropy will limit the rate of vertical flow.

Considering the potential hydrologic difficulties involved in leaching deep sediments, it is probably unreasonable to expect almost 2,000 m of virtually feldspar-free sediment from a single episode of groundwater leaching. However, the episodic style of sedimentation in the Central Rand permits a more reasonable interpretation. As discussed in the tectonics section, there are numerous unconformities within the 2,000 m or so of sedimentary section, the stratigraphic locations of which are plotted on figure 35. Because each unconformity marks a period of subaerial exposure and erosion, each unconformity also marks the topmost horizon of a meteoric/groundwater leaching regime. Thus, the Central Rand may have been leached of feldspars in eight sequential groundwater regimes rather than a single, 2,000 m thick leaching episode. Because unconformities correlate approximately with formation boundaries, each formation would have been leached individually, prior to deposition of the next formation. By this model, only the topmost sediments need be leached in a particular groundwater regime. As discussed earlier, it is precisely the topmost sediments that are most easily leached.

Within the Central Rand there is one particularly thick (about 500 m) interval of conformable sediments between the Commonage and Livingstone reefs (figure 35). Feldspar has been reported as an important accessory mineral in the lower half of this interval (Antrobus et al., 1986). A similar exception to the trend of complete feldspar dissolution is sample DL-333 from the very base of the Klerksdorp formation. In both of these examples, feldspar is preserved

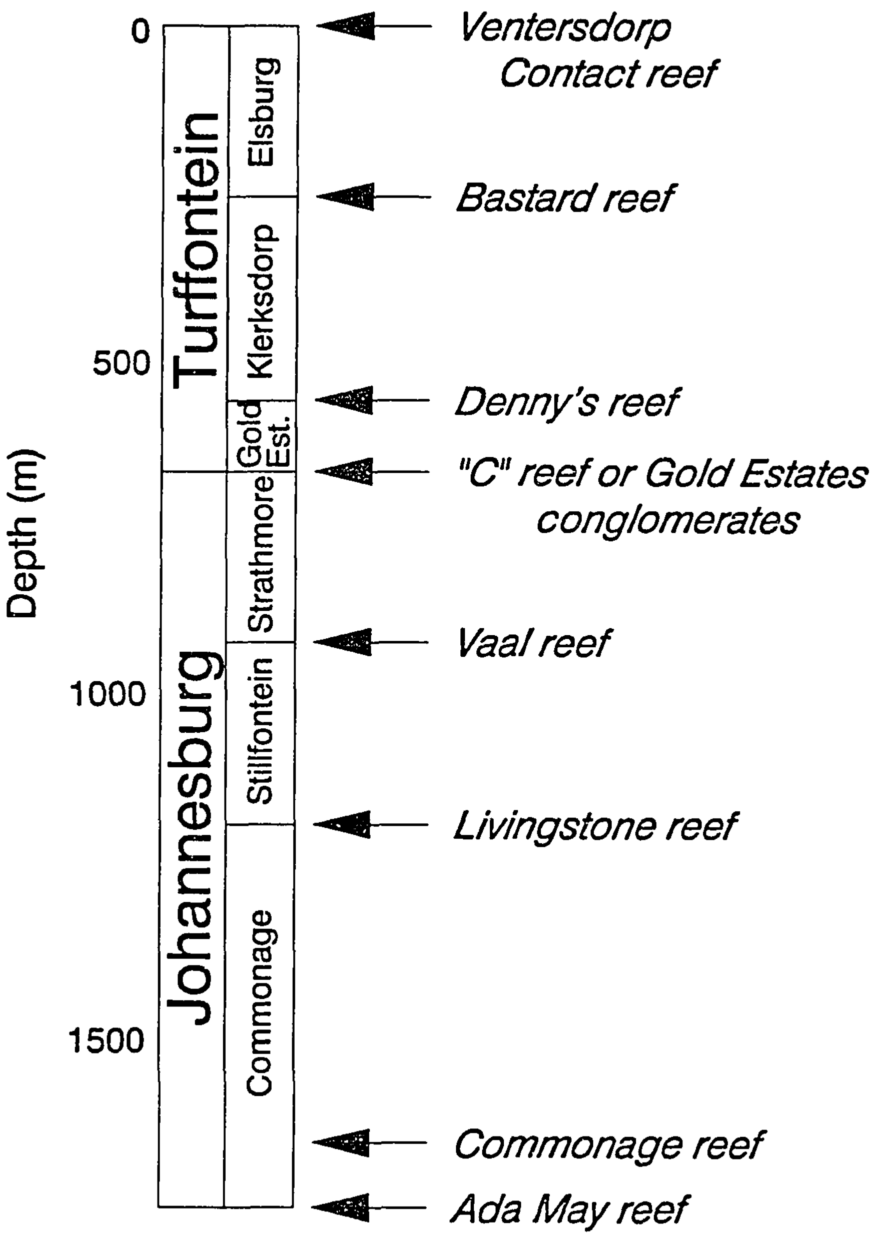

Figure 35. The stratigraphic positions of major uncomformities in the Central Rand (arrows). The uncomformities are recognized on the basis of carbon seams, basal conglomerates (the "reefs"), and erosional surfaces.

only well beneath the overlying unconformity (approximately 250 and 300 m beneath the unconformities, respectively).

The four remaining samples in which feldspar is found are DL-336 and DL-337 from the Gold Estates formation and DL-350 and DL-351 from the Strathmore formation. These feldspathic sands are unusually fine-grained (average grain sizes of 250, 100, 150, and 200 microns, respectively, compared to a typical range of 500 to 1500 microns for other samples) and they are exceptionally matrix rich (52%, 91%, 75%, and 36% matrix, respectively). These textural characteristics lead to low hydraulic conductivities, which will in turn lead to reduced groundwater flow. The few horizons that preserve feldspar can thus be explained in the context of the meteoric/groundwater model as being either too deep or too impermeable to permit complete feldspar dissolution.

An additional observation in support of this qualitative groundwater model is the absence of feldspar from the top of the West Rand. The first appearance of feldspar beneath the West/Central Rand unconformity is in sample DL-381, at a depth of 80 m beneath the unconformity. The leaching at the top of the West Rand is thus consistent with the stratigraphic trends in the Central Rand.

The discussion of feldspar dissolution has to this point been only qualitative. To permit a more quantitative analysis of the problem, I will discuss the geochemistry of these Klerksdorp quartzites.

Chapter 5. Formation-scale geochemical trends: Evidence for meteoric leaching

As discussed in chapter 4, the distribution of feldspar in the upper half of the Witwatersrand section from the Klerksdorp goldfield appears to be stratigraphically controlled--feldspar is present near the base of several formations, but not at the formation tops. Taking the loss of feldspar as an indicator of chemical alteration, the feldspar trend suggests that individual formations are more highly altered at their tops than at their bases, an observation that led me to propose in chapter 4 that leaching by meteoric water, one formation at a time, was the mechanism of chemical alteration. In this chapter I will integrate bulk chemistry of the quartzites and total CO_2 availability to demonstrate that leaching by meteoric water is a reasonable explanation for the chemical alteration of the Witwatersrand quartzites.

Bulk chemistry of the quartzites

Most of the thin sections from the Klerksdorp goldfield that were studied petrographically (see chapter 4) have also been analyzed geochemically with an electron microprobe by Dr. Sally Sutton at the University of Texas at Austin. Methods, results, and interpretations of this work can be found in Sutton et al. (1990). I will review Sutton et al.

briefly and then discuss Sutton et al.'s results in the context of meteoric leaching.

Geochemical analyses were conducted on a JEOL 733 microprobe operating at 15 kV with a current of 45 nA on brass and a beam diameter of 100 microns. Because the beam diameter was much larger than most matrix mineral grains, each of the 20 to 50 analyses per thin section is an average analysis of a multigrain region. The regions were selected randomly, but any region with more than 50% quartz was not analyzed, and the final results are recalculated on a SiO_2-free basis to emphasize chemical patterns in the non-quartz fraction.

The results of these analyses are reproduced here in table 3, which is taken directly from Sutton et al. (1990). Chemical trends in table 3 that Sutton et al. emphasized include upwards enrichment in Al and K, and upwards depletion in Ca, Na and Mg. These trends, manifest within individual formations and in the stratigraphic section as a whole, were interpreted by Sutton et al. as the likely result of intense source area weathering. Sutton et al. also studied the chemistry of individual mineral phases and concluded that pre-metamorphic bulk chemistry, not metamorphic alteration (as proposed by Phillips, 1988), was the controlling factor in determining the composition of the metamorphic assemblages.

To assess chemical alteration in the Witwatersrand quartzites quantitatively, it is essential to know, at least

sample	depth m	Ti	Al	Fe[1]	Mg	K	Na	Ca
Elsburg:								
dl301	3	0.83	70.2	2.64	2.00	23.6	0.43	0.35
dl301	16	0.67	70.5	3.01	1.83	23.3	0.54	0.22
dl303	25	0.55	69.1	2.94	1.81	22.9	0.52	2.22
dl304	39	0.56	68.3	1.71	1.30	22.1	0.65	5.37
dl305	59	2.76	69.1	3.49	1.92	21.6	0.60	0.57
dl306	77	4.24	70.3	1.39	1.18	22	0.62	0.19
dl307	96	6.69	68	2.12	1.48	20.8	0.66	0.17
dl308	99	19	57.4	3.08	1.94	17.9	0.54	0.18
dl309	122	0.81	71	2.99	1.95	22.3	0.64	0.23
dl310	127	0.97	70.5	4.08	2.36	21.1	0.68	0.24
dl311	160	0.47	73.3	1.19	1.14	22.7	0.70	0.54
dl312	176	0.31	72.6	0.89	1.14	23.9	0.67	0.47
dl313	190	0.35	71.4	2.42	2.45	22.3	0.68	0.38
dl314	219	0.48	60.5	13.1	10.5	14.1	0.68	0.45
dl315	235	1.07	72.4	0.82	1.07	21.9	2.33	0.44
dl316	249	8.65	68.1	0.88	0.83	18.6	1.93	0.94
dl317	265	0.18	75.2	0.45	0.37	22.1	1.26	0.45
Klerksdorp:								
dl318	279	0.90	84.7	1.01	0.41	11.5	0.72	0.46
dl319	298	0.27	81.3	1.54	0.67	14.8	0.87	0.53
dl320	316	0.96	76.3	6.11	2.11	13.2	0.81	0.46
dl321	328	1.70	71.7	8.70	3.21	13.4	0.84	0.46
dl322	337	0.83	77.9	3.81	1.60	14.6	0.88	0.41
dl323	366	0.45	76.1	3.63	1.54	16.6	1.18	0.33
dl324	388	0.56	75.8	1.67	0.91	19.4	1.26	0.44
dl325	404	0.42	66.8	12	5.17	13.9	1.12	0.44
dl326	441	0.65	70.9	7.98	2.36	16.3	1.17	0.37
dl327	464	0.58	60.4	19.9	6.66	11.1	0.83	0.28
dl328	490	0.29	63.9	14.8	5.62	13	1.20	0.83
dl329	494	1.22	70.2	6.92	2.33	17.4	1.70	0.30
dl330	502	0.26	71.1	3.74	1.46	20	2.38	0.99
dl331	518	0.41	47.1	34.5	13.5	3.45	0.43	0.43
dl332	530	2.80	70.7	7.41	1.85	15	1.49	0.56
dl333	553	0.46	78.5	0.46	0.27	15.6	4.36	0.42
Gold Estates:								
dl334	582	1.22	95.3	0.7	0.14	1.36	0.89	0.28
dl335	604	0.09	95.6	0.51	0.23	1.77	1.35	0.28
dl336	622	0.59	55.6	14.5	11.9	4.68	11.9	0.55
dl337	627	1.75	56.1	16.9	12.6	8.21	3.00	1.36
dl338	652	2.23	48.4	29.5	11.2	6.18	1.24	0.76
Strathmore 1:								
dl346	658	0.29	77.8	4.09	1.8	13.5	2.22	0.23
dl347	701	0.40	59.7	22.5	4.43	11	1.61	0.20
dl348	720	1.25	61.9	16.4	5.28	13.5	1.46	0.06
dl349	726	0.37	58.9	13.2	4.44	13.2	1.68	8.05
dl350	739	0.74	57.4	15.7	6.04	11.5	2.93	5.48
dl351	755	0.41	53.6	9.03	3.77	10.6	7.29	15.1
Strathmore 2:								
dl339	818	1.01	65.8	14	3.25	13.3	2.30	0.27
dl340	844	0.30	58.4	22.1	6.24	11	1.23	0.30
dl341	853	2.96	65.7	10.9	3.2	15.3	1.54	0.28
dl342	869	1.35	69.2	7.99	2.29	17.1	1.58	0.40
dl343	885	1.09	67.5	11.2	2.53	15.8	1.32	0.35
dl344	901	1.59	64.1	16.9	2.43	13.2	1.26	0.24
dl345	914	0.16	80.1	4.09	0.32	13.5	1.53	0.23
Stilfontein:								
dl353	919	0.42	88.8	0.45	0.27	9.54	0.70	0.10
dl354	934	1.52	81.3	1.56	0.53	13.7	0.96	0.46
dl355	953	0.62	72	18.6	2.53	5.47	0.45	0.17
dl356	982	0.67	52.2	31.8	4.55	8.72	0.48	0.24
dl357	989	0.49	58.1	24.1	3.40	11.9	1.14	0.53
dl358	1030	3.59	75.9	20.7	2.16	15.1	0.81	0.31
dl359	1061	0.40	53.4	22.8	1.83	13.6	0.63	0.23
dl360	1082	0.29	67.1	12.8	1.15	17.5	0.83	0.26
dl361	1096	3.18	59.9	20	3.48	12.3	0.88	0.10
dl362	1118	3.47	48.2	31.8	2.60	10.5	0.69	2.12
dl363	1134	4.43	59.8	18.7	3.89	11.4	1.12	0.54
dl364	1154	0.50	68.4	12.7	2.97	14.2	0.75	0.27
Commonage:								
dl365	1190	0.18	77.6	7.14	1.81	12	0.78	0.28
dl366	1253	3.53	70.1	11.4	2.93	10.8	0.58	0.43
dl367	1293	0.55	65	16.8	4.60	12.5	0.53	0.19
dl368	1342	1.03	65.6	11.8	5.08	15.1	0.84	0.39
dl369	1417	0.51	68.5	9.20	4.10	16.4	0.85	0.29
dl370	1456	0.64	63.1	14.5	8.96	10.5	0.90	1.01
dl371	1489	0.89	64.7	12.9	7.61	12.9	0.80	0.40
dl372	1537	0.83	62.8	14.2	8.54	12.2	0.79	0.37
dl373	1611	0.58	62.1	16	6.49	13.3	0.86	0.42
dl374	1670	1.02	65.4	9.28	6.80	15.9	0.90	0.47
dl375	1723	0.71	65.6	10.8	6.62	14.5	0.89	0.38
dl376	1737	1.22	67	7.38	7.38	15.8	1.03	0.40
Roodepoort:								
dl377	1741	0.60	76.8	9.71	0.92	9.39	1.40	0.92
dl378	1752	0.23	74.2	12	1.06	10.3	1.52	0.41
dl379	1763	1.34	65	14.2	4.19	13.7	1.16	0.22
dl380	1806	4.40	66.6	7.18	2.28	17	1.79	0.54
dl381	1820	1.64	44.7	18.2	16.8	5.6	7.28	5.40
dl382	1862	1.45	52.9	9.64	4.37	8.44	12	10.8
dl383	1931	0.36	48.9	12.1	7.82	10.9	0.82	18.2
dl387	2050	0.40	53.6	9.63	6.41	4.18	15.1	10.4
dl388	2165	5.29	52.7	9.75	5.08	8.50	13.3	5.15
dl389	2234	1.76	47.9	7.47	3.41	4.31	16.8	17.8
dl390	2316	0.86	51	10.7	9.32	7.44	15.7	4.62

Ti, Al, Fe, Mg, K, Na, Ca: oxides

1. All Fe as FeO

Table 3. Bulk chemical analyses of Witwatersrand quartzites from the Klerksdorp goldfield, recalculated on an SiO_2-free basis. The data were obtained by "wide-beam" electron microprobe analysis (see text). From Sutton et al. (1990).

approximately, the composition of unaltered Witwatersrand quartzites. From comparison of tables 2 and 3 there are a number of chemically analyzed quartzite samples that contain feldspar (DL-333, 336, 337, 350, 351, 381, 383, 387, 388, and 389). I will assume that these feldspar-bearing samples are the least altered in the Klerksdorp section and will use their average bulk chemistry to represent the original pre-alteration composition of all other analyzed quartzites. The mean composition of the remaining quartzites, which are all feldspar-free, is taken to represent the average composition of altered Witwatersrand quartzites.

Comparison of the Witwatersrand samples to average sands from active continental margins and to average upper crustal rocks (table 4) indicates that the feldspathic Witwatersrand sands are indeed very nearly unaltered. There is a slight (~10%) aluminum enrichment and a small loss of the alkalis, but the degree of alteration is significantly less than in the feldspar-free Witwatersrand quartzites, which exhibit a 40% aluminum enrichment relative to average continental sands and, most notably, an almost complete loss of Na and Ca. Also, the stratigraphic positions of the "altered" and "unaltered" sample suites are appropriate for the meteoric leaching model because all of the "unaltered" feldspar-bearing samples are either so fine-grained so as to be relatively impermeable or are from at least 250-300 m below the nearest overlying unconformity (see discussion in chapter 4). For alteration by meteoric leaching, it is

Wt. % oxide	Feldspar-bearing Witwatersrand quartzites	Feldspar-free Witwatersrand quartzites	Active continental margin sands	Average upper crustal rocks
Al	54.4	68.9	49.3	47.1
K	8.3	14.9	11.1	9.7
Na	9.2	1.0	10.6	11.2
Ca	7.9	0.6	9.5	10.3
Fe	11.2	10.0	10.5	13.2
Mg	7.3	3.1	4.7	6.8
Ti	1.3	1.5	1.8	1.8

Table 4. Bulk chemistry normalized to zero SiO_2 of Witwatersrand quartzites (separated into feldspar-bearing and feldspar-free populations), average active continental margin sandstones, and average upper crustal rocks. The Witwatersrand chemical data are from Sutton et al. (1990), the active margin sandstone data are form Bhattia (1983), and the average crustal rock data are from Taylor and McLennan (1981). Note that the feldspathic Witwatersrand quartzites are compositionally similar to average sands from active continental margins (a tectonic classification that includes foreland basins; Bhattia, 1983) and to average upper crustal rocks. This similarity suggests the unleached quartzites are representative of unaltered Witwatersrand detritus. Feldspar-free Witwatersrand quartzites are Al-rich and Ca-, Na-, Fe-, and Mg-poor, indicating they have undergone chemical alteration of some sort.

precisely the deepest and least permeable samples that should be least altered.

Using the average composition of both altered and unaltered quartzites (table 4) and assuming aluminum immobility, it is possible to quantify the chemical effects of alteration. The first step in doing so is to reconstruct the unaltered quartzite composition including SiO_2. To do so, SiO_2 in quartz and SiO_2 in other minerals must be added to the compositional data in table 4. From petrographic analyses (table 2), SiO_2 in quartz makes up 46% of the 12 unaltered quartzite samples. Non-quartz SiO_2 is contributed by feldspar, which constitutes 6% of the rock (also from table 2), and muscovite, which is the predominant matrix mineral (as determined by XRD analysis). Muscovite comprises 48% of the unaltered rock. The SiO_2:Al_2O_3 ratio (in weight percent) for feldspar is 3.54:1 (assuming equal proportions of Na-, Ca-, and K-feldspar), and for muscovite is 1.18:1. Considering the ratio of feldspar to muscovite (6%:48%), the average SiO_2:Al_2O_3 ratio in the matrix of these quartzites is 1.44:1. Multiplying 1.44 by the percent Al_2O_3 (54.4) yields 78.3, the SiO_2 that must be added to the average analysis in table 4, column 1. The new total is then normalized to 54% (the percent matrix) and brought to 100% by the addition of 46% SiO_2 (the average percentage of free quartz in these quartzite samples). The SiO_2-inclusive composition that results (table 5, column 1) is close to the average composition of active continental margin sands

Wt. % oxide	1	2
Si	69.9	73.9
Al	16.5	12.9
K	2.5	2.9
Na	2.8	2.8
Ca	2.4	2.5
Fe	3.4	2.7
Mg	2.2	1.2
Ti	0.4	0.5

Table 5. Comparison of the average composition of unaltered Witwatersrand quartzites (column 1) to the average composition of active continental margin sands (column 2; Bhattia, 1983). The Witwatersrand compositions are recalculated from the data in table 4, column 1 to include SiO_2. See text for calculations.

(table 5, column 2), again confirming the plausibility of this approach.

CO_2 demand

To determine CO_2 demand from bulk chemical data, weight percent oxides must be converted to molar quantities. The foregoing reconstruction of an SiO_2-inclusive unaltered Witwatersrand sandstone composition produced 16.5 weight percent Al_2O_3, and the density of wet sand is about 1.8 x 10^3 kg/m^3 (Sharma, 1986), so there was a total of 297 kg, or 2,910 moles, of Al_2O_3 in every cubic meter of sediment. When the compositional data for altered and unaltered Witwatersrand quartzites in table 4, columns 1 and 2 are converted to mole fractions and normalized to one mole of Al_2O_3, gains and losses of the major elements in molar quantities can be determined. For each mole of Al_2O_3 present in the weathered rock, the alteration resulted in a gain of 0.07 moles of K_2O and losses of 0.25 moles of Na_2O, 0.25 moles of CaO, 0.09 moles of FeO and 0.22 moles of MgO. Thus, for the Witwatersrand sands to have been altered to their present composition, 730 moles of Na_2O, 730 moles of CaO, 260 moles of FeO, and 640 moles of MgO per cubic meter of sediment had to be removed. Gain or loss of SiO_2 cannot be determined because there is free quartz in all altered and unaltered samples; consequently SiO_2 variations might be either sedimentological or chemical in nature. Addition of

K_2O probably occurred during diagenesis or later (MacFarlane and Holland, in prep) and will not be discussed further in this chapter. I will, however, return to the topic of Potassium addition in chapter 6.

The removal of cations from their host sediment depends on first, being liberated by hydrolysis or carbonation reactions (see equations 1-3 in chapter 4, for example), and second, being carried out of the weathering zone in solution. The transport of cations can take place only if balanced by the transport of anions. In a meteorically-dominated system at normal pH levels, particularly one in which CO_2 is the principal weathering acid, HCO_3^- is the anion that provides charge balance. Thus, one mole of CO_2 was required for each mole of positive charge removed from the basin. With this relationship in mind, a total CO_2 budget can be calculated. For each cubic meter of sediment, the removal of 730 moles of Na_2O required 1,460 moles of CO_2, 730 moles of CaO required 1,460 moles of CO_2, 260 moles of FeO required 520 moles of CO_2, and 640 moles of MgO required 1,280 moles of CO_2, for a total CO_2 demand of 4,720 moles. (For a similar mass balance approach to determining CO_2 demand see Holland, 1984, or Lundegaard et al., 1984.)

CO_2 availability and implications for meteoric water fluxes

As discussed in chapter 4, the partial pressure of CO_2 in the Archean atmosphere was probably about 0.033 atm, approximately 100 times higher than in the modern atmosphere. This atmospheric CO_2 dissolves in water to form carbonic acid:

$$CO_2 + H_2O \longrightarrow H_2CO_3$$

The extent to which this reaction proceeds is expressed by:

$$KCO_2 = H_2CO_3 / \alpha PCO_2 \alpha H_2O$$

For rainwater, the activity of H_2O is 1, and at 15°C the equilibrium constant is 0.0479 (Drever, 1982), so the activity of H_2CO_3 would have been:

$$H_2CO_3 = (0.0479)(0.033) = 0.00158 \text{ moles/kg}$$

For an uncharged solute in an extremely dilute solution the difference between activity and concentration is insignificant. Therefore, each liter of Archean rainwater potentially supplied 1.58×10^{-3} moles of CO_2. To satisfy the CO_2 demand as calculated in the previous section (4,720 moles/m^3), a total of 3×10^6 liters of CO_2-charged meteoric water must have been flushed through each cubic meter of sediment.

In this model meteoric water is delivered to the Witwatersrand sediments across subaerially exposed unconformity surfaces, so it is useful to think of the total flux in terms of precipitation and infiltration across a unit surface area (figure 36). To do so, I will consider a total volume of sediment that is 250 m deep, 22.5 km long (measured perpendicular to the basin margin), and 1 km wide (measured parallel to the basin margin). A depth of 250 m represents the approximate maximum depth of leaching. In the two thickest conformable sequences (the Commonage and the Klerksdorp), feldspar first appears approximately 250 m beneath the overlying unconformity (see table 1, samples DL-318 to 333 for the Klerksdorp Formation and p. 557 of Antrobus et al., 1986, for the Commonage Formation). The 22.5 km length reflects the total down-dip extent of leaching, from the basin margin (which coincided with the present location of Klerksdorp throughout Central Rand deposition; see figure 3) to the southeasternmost limit of active mining, where 60% of the samples in table 3 were obtained (see appendix 1). Leached sediments may well extend even further downdip, but Witwatersrand sampling presently is confined to the more proximal regions of the basin for economic reasons. The 1 km width is an arbitrary choice selected for ease of calculation, but the underlying assumption is that the degree and depth of leaching does not change significantly in moving northeast or southwest along the basin margin. This assumption is reasonable considering the remarkable geographic uniformity of the Witwatersrand; aluminous metamorphic assemblages reflecting similar

Figure 36. The geometric configuration of the meteoric leaching model. (a) is a schematic block diagram of the Klerksdorp alluvial fan that extends from the basin margin to the furthest down-dip extent of active mining (also the limit of sample coverage), a distance of about 22.5 km. (b) is the stratigraphic section (Roodepoort through Elsburg Formations) to which the leaching model is applied. Formation thicknesses and the distribution of feldspar are drawn to scale. Note that feldspar is found only at depths greater than ~250 m below the nearest unconformity (unconformities coincide with formation boundaries). (c) is the idealized stratigraphic unit on which the mass balance calculations of CO_2 demand vs. CO_2-charged meteoric water influx are based. In effect, (c) can be taken to represent the feldspar-free portion of any of the 7 formations in (c).

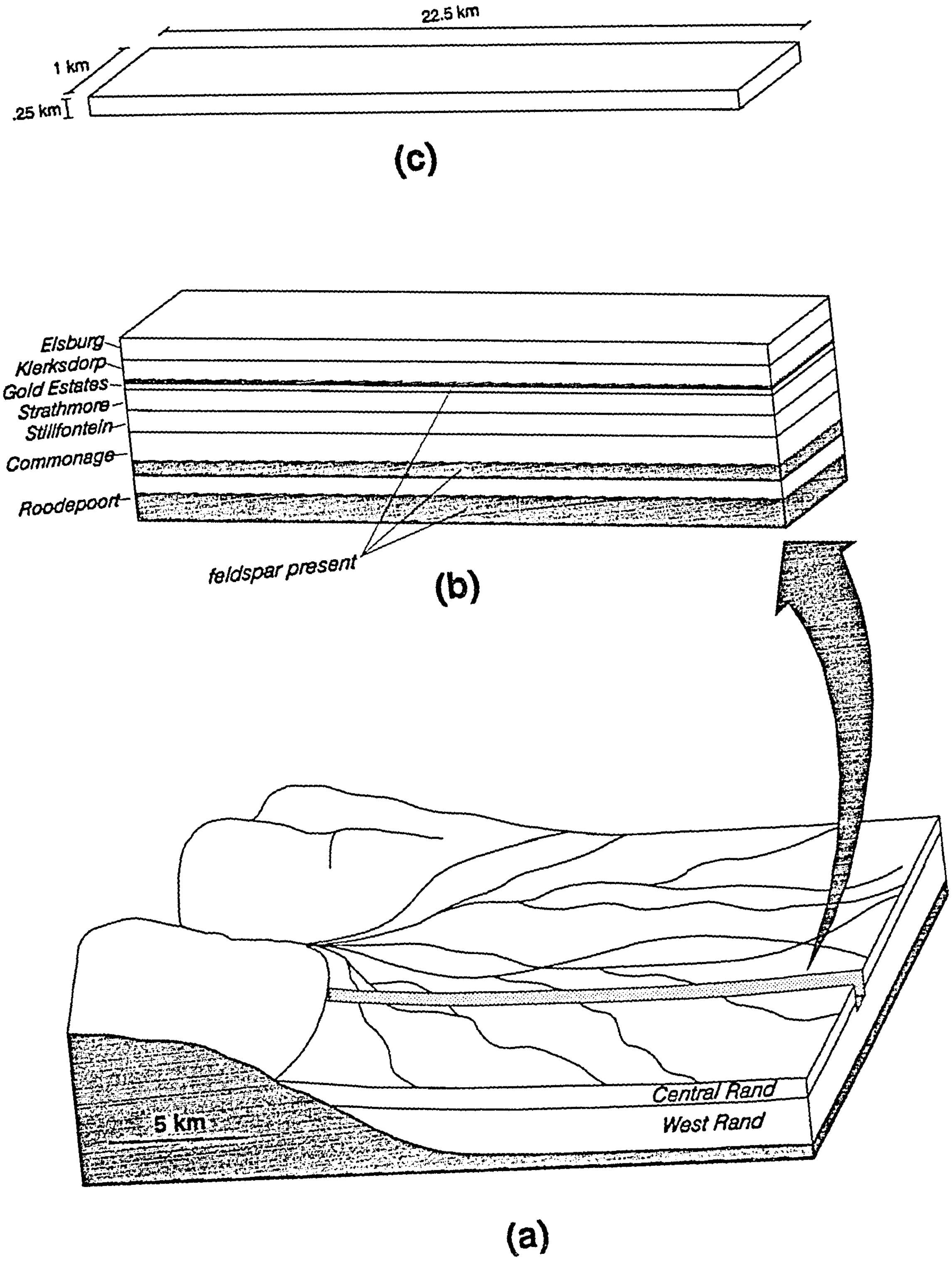
22.5 km
1 km
.25 km
(c)
Elsburg
Klerksdorp
Gold Estates
Strathmore
Stillfontein
Commonage
Roodepoort
feldspar present
(b)
Central Rand
West Rand
5 km
(a)

aluminous bulk compositions are reported from all of the major goldfields (Phillips, 1987).

The total volume of sediment in the 22.5 x 1 x 0.25 km section of figure 36 is 6.75×10^9 m^3. Based on the calculations of meteoric water flux, a total of 2.03×10^{16} liters ([6.75×10^9 m^3] x [3×10^6 liters/m^3]) of CO_2-charged groundwater would have been needed to balance the loss of Ca, Na, Fe and Mg from a section of this size. To investigate the plausibility of meteoric leaching on this scale, it will be necessary to consider rates of precipitation and infiltration.

Rainfall in the Archean

The average rainfall on land masses today is about 66 cm/year (Garrels and MacKenzie, 1971). However, on average only about 4% of the total precipitation actually infiltrates the soil zone to become groundwater. Of the remaining 96%, two-thirds is lost to evapotranspiration and one-third to surface runoff (figure 4.2 of Garrels and MacKenzie, 1971). Consequently, only 2.6 cm of meteoric water are added to the groundwater supply each year (4% of the 66 cm/year total precipitation).

In the Witwatersrand, both precipitation and infiltration rates may have been substantially greater than the modern average values, leading to a larger flux of meteoric water into the groundwater system. Evidence for higher infiltration rates comes from consideration of the textural characteristics of the Central Rand sediments. As is typical of alluvial fan sediments, and proximal fan sediments in particular, conglomerates and sandstones are the dominant lithologies. The high permeability and porosity of such sediments leads to infiltration rates greater than the 4% average value. Returning to the example of California's Central Valley (figure 34a), the infiltration rate along the eastern margin, which is proximal to the Sierra Nevada mountains, is 20% (see figure 19 of Williamson et al., 1989). An even higher infiltration rate of 39% is reported from the Gangetic alluvial sediments that are being shed off of the Siwalik range in the Nepal Himalayas (Gupta and Paudyal, 1988). Both of these examples involve unlithified, proximal, clastic alluvial sediments such as were present beneath each of the major unconformities in the Central Rand. Consequently, 30% is a reasonable infiltration rate for the Witwatersrand sediments. Absence of vegetation in the Archean probably had little net effect on infiltration rates, because, on the one hand, vegetation increases infiltration by slowing surface runoff, and on the other hand, it decreases infiltration by evapotranspirating.

Estimating precipitation for the Witwatersrand is much more problematic. Even the modern global average of 66 cm/year is applicable to only a few continental areas, because local and regional variations in rainfall are extremely high. However, from what is known of precipitation patterns today, it is possible to make some reasonable predictions of Archean continental precipitation. Based on Holland's (1984) reconstruction of the degassing of the early Earth (which is based primarily on the volcanic flux of rare gases), most of the Earth's volatiles, including water, had approached their present levels by about 4,000 Ma. Walker (1977) concluded, on the basis of lead isotopic evidence, that degassing was complete within the first 100 million years of Earth history, and on the basis of sedimentary rock distributions, that the oceans were filled within the first 1 billion years of Earth history. The total volume of H_2O in the hydrologic cycle at 2,800 Ma was therefore probably about the same as today's total volume. The manner in which this water was distributed to the continents, however, may have been quite different.

On a global basis, evaporation dominates over the oceans and precipitation dominates over the continents, with a net transfer of 3.6 x 10^{16} liters of water to the continents each year (figure 4.2 of Garrels and MacKenzie, 1971). Atmospheric physics can be used to explain this precipitation imbalance. Moisture is added to the atmosphere by evaporation, which occurs predominantly over the oceans because they cover most of the Earth's surface and because there is always a supply of water to evaporate (unlike the continents). Moisture is removed from the atmosphere by precipitation, which occurs when air masses rise, adiabatically cool, condense into clouds, and finally release their water as rain or snow, a process that occurs more readily over continents for two reasons: continents are elevated above sea level, so moisture-laden oceanic air is physically forced to rise when it encounters a continent, and continents heat more rapidly and to greater extremes on a daily basis than do oceans, resulting in more vigorous convective rise of air masses. Because the present-day landward net transfer of precipitation is based on physical processes (which presumably have not changed in the past 3 billion years) a similar process of net transfer must have existed in the Archean. The scale of transfer, however, might have been much greater in the Archean because total continental area was much smaller. Figure 37 indicates that the total continental area at 2,800 Ma was only about 10% of the present value. Oceans must have been correspondingly larger, the net result being a 39 to 1 ratio of ocean to continent rather than the 3 to 1 ratio that exists today. If the total volume of water moving through the hydrologic system was similar, as suggested above, then the order of magnitude decrease in continental area might have led to an approximately order of magnitude increase in continental precipitation.

Further support in favor of increased continental precipitation comes from the relationship that exists between the size of a land mass and precipitation rate (figure 38). At a given latitude, small continents are subject to more precipitation than large continents. This is

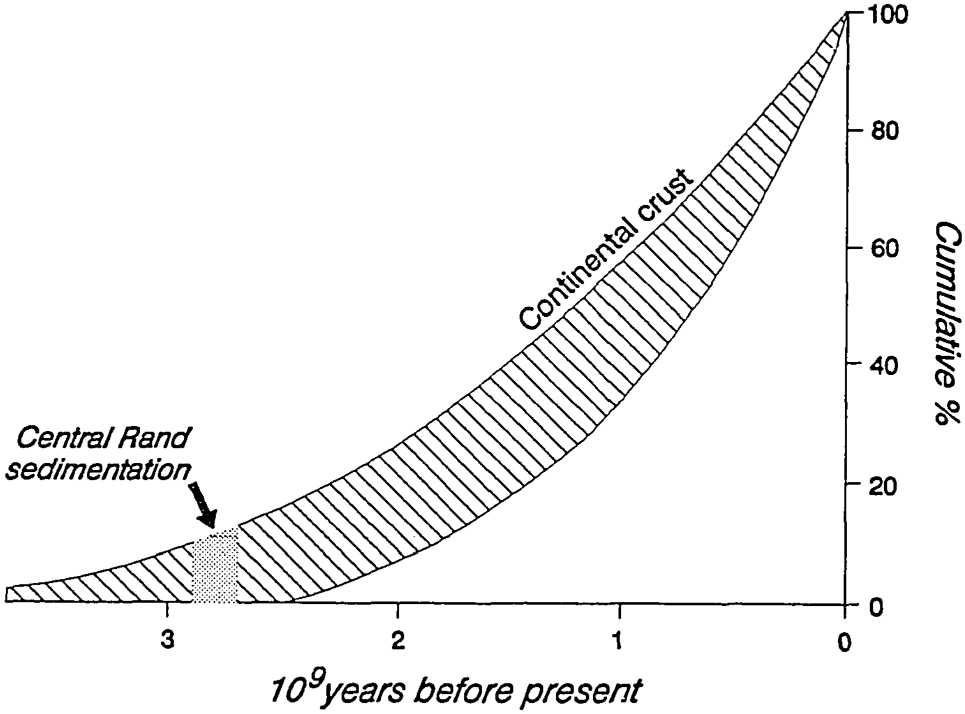

Figure 37. Cumulative area versus age distribution of continental crust, after figure 5.7 of Veizer (1986). The upper and lower limits encompass several different estimates--see Veizer (1986) for references. Note that the total continental area at 2,800 Ma was approximately 10% of the present day continental area.

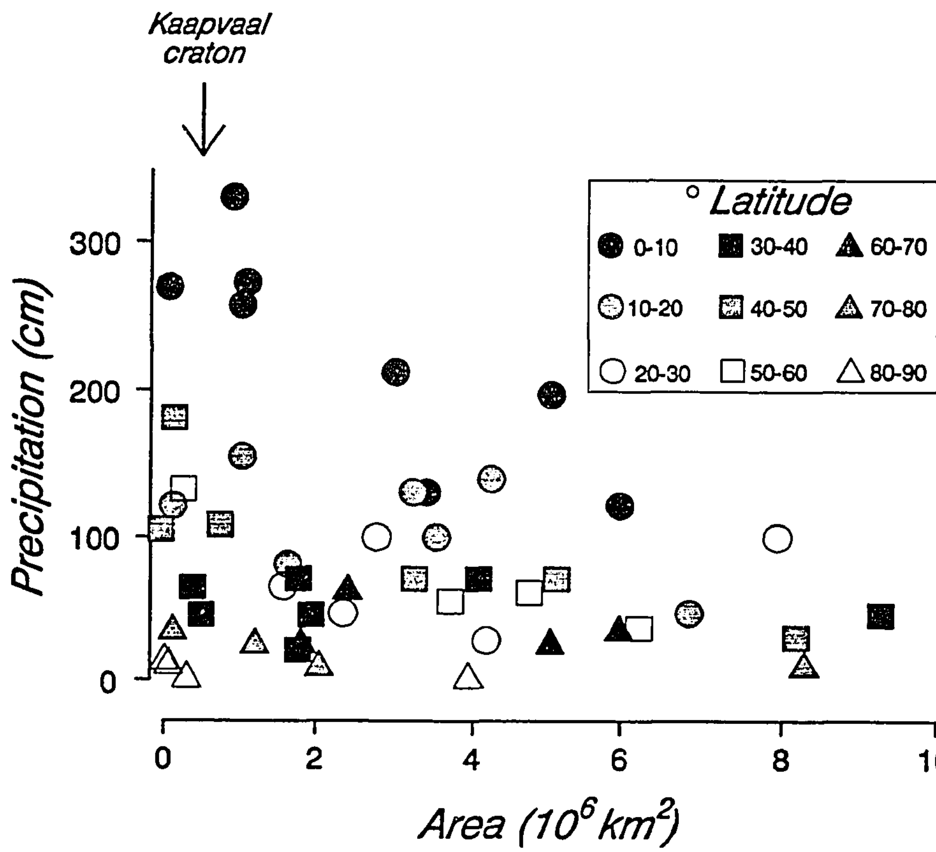

Figure 38. The relationship between average annual rainfall and continental area, from Tardy et al. (1989). At a given latitude, smaller continents experience greater rainfall. The Kaapvaal craton, on which the Witwatersrand basin was situated, has a total area of only 500,000 km^2, placing it at the far left-hand side of this plot, where annual rainfall for non-polar latitudes is 2 to 5 times greater than the present day continental average of 66 cm/year.

because small continents lack the large interior deserts that develop inboard of precipitation-inducing mountain ranges on larger continents. Again, because the size/rainfall relationship is based on simple physical processes, a similar situation must have prevailed in the Archean. The Kaapvaal craton (about 500,000 km^2) is quite small relative to modern continents (e.g., Africa has an area of about 30,000,000 km^2; Australia an area of about 8,000,000 km^2) and plots at the far left edge of figure 38, where annual rainfall rates for non-polar latitudes are from two to five times the continental average of 660 mm/year. The size/rainfall relationship is much less significant for near-polar latitudes (greater than 60° N or S), but the Witwatersrand was probably not polar. There are no glacial deposits (the diamictites in the basin are interpreted as debris flows; Tankard et al., 1982); there are carbon seams that are interpreted as the remains of surficial algal mats; and simple probability discounts the likelihood of a polar setting (only 13% of the Earth's surface area lies above 60° N or below 60° S).

In sum, consideration of modern patterns of rainfall distribution leads to the conclusion that small continents in the Archean may have experienced rainfall rates 20 to 50 times higher than the average modern continental rate of 66 cm/year. Most of this increase (a factor of 10) is attributed to a smaller total continental area in the Archean. The remainder (a factor of 2 to 5) is attributed to the small size of Archean continents, and of the Kaapvaal craton in particular. Admittedly, these semi-quantitative estimates of Archean rainfall are highly speculative. Nevertheless, they are based on physical principles that can be reasonably extrapolated back into the Archean. To err slightly on the conservative side, I will choose an average rainfall rate of 660 cm/year, ten times greater than the modern average rate, but still significantly lower than the rainfall recorded in many places today (Cherrapunji, India, for example, averages 2,647 cm/year). Combining 660 cm/year of rainfall with an infiltration rate of 30% (as previously discussed) yields an influx of meteoric water of 2 m/year, which is equal to 4.5×10^{10} liters/year when summed over the entire 2.25×10^{7} m^2 area of the model (figure 36).

With an influx of meteoric water equal to 4.5×10^{10} liters/year, 450,000 years would be required to supply the 2×10^{16} liters of CO_2-charged groundwater needed to convert the unaltered Witwatersrand sands to the altered Witwatersrand sands in a 250 m thick interval. The validity of the model thus depends on whether 450,000 years is a reasonable length of time for subaerial exposure of the unconformity surfaces in the Central Rand Group.

<u>Time constraints</u>

The stratigraphic section over which this meteoric leaching model is being applied extends from the base of the

Roodepoort Formation (at the top of the West Rand Group) to the top of the Elsburg Formation (at the top of the Central Rand Group). Conveniently, this interval is bracketed by volcanics. The Crown lava lies immediately beneath the Roodepoort Formation, and has been dated by single zircon ^{206}Pb-^{207}Pb methods at 2,900 Ma (Minter, pers. comm., 1990). The Klipriviersberg and Makwassie volcanics, which overly the Central Rand Group, yield single zircon ^{206}Pb-^{207}Pb ages of 2,709 $\pm$ 4 Ma (Armstrong et al., 1990). The total time available for deposition plus intervening periods of erosion and meteoric leaching is therefore approximately 190 million years. Even allowing for considerable periods of inactivity (e.g., perhaps several tens of millions of years elapsed before the Ventersdorp volcanics covered the already filled Witwatersrand basin), the 450,000 years required for my model of meteoric water leaching beneath each of the eight major unconformities is clearly within the time constraints provided by the bounding volcanics.

Another approach to testing the validity of the 450,000 year time span is to consider the likelihood of a particular unconformity remaining exposed subaerially for such a lengthy time span. This can be done both for the Witwatersrand basin and for younger, more precisely-dated, basins. Within the Witwatersrand, Hallbauer and Barton (1987) have estimated the minimum period of time required to form an "average" Witwatersrand placer. Taking into account source area gold grades, weathering and transport rates, and the total "concentration factor" required to produce a high-grade placer, they calculated that a minimum of 250,000 years would be required to form a single placer--a time period that agrees remarkably well with my estimate of the time required to leach a single unconformity-bound formation.

Four hundred and fifty thousand years also falls within the time constraints imposed by data from younger, more precisely-dated foreland basin sequences. In the Ebro foreland basin of Spain, Aradon et al. (1986) studied syntectonic unconformities and concluded, on the basis of paleontological data, that the unconformities develop rapidly: for the unconformity depicted in figure 39 they estimate that 2 million years is required. A similar time frame arises from magneto-stratigraphic dating in the Andean foreland basin by Johnson et al. (1986). Sediments at the top of the Rio Jachal Formation and at the base of the Mogna Formation were deposited during seafloor anomaly 2A. Because anomaly 2A spans approximately 1 million years, the unconformity that separates these two formations must represent a hiatus of less than 1 million years. The time available for leaching in younger foreland basins therefore appears to be roughly 0.5-2 million years for each unconformity-bound unit. If exposure times on the Witwatersrand unconformities were similar to those reported from younger foreland basins, it would appear that there was

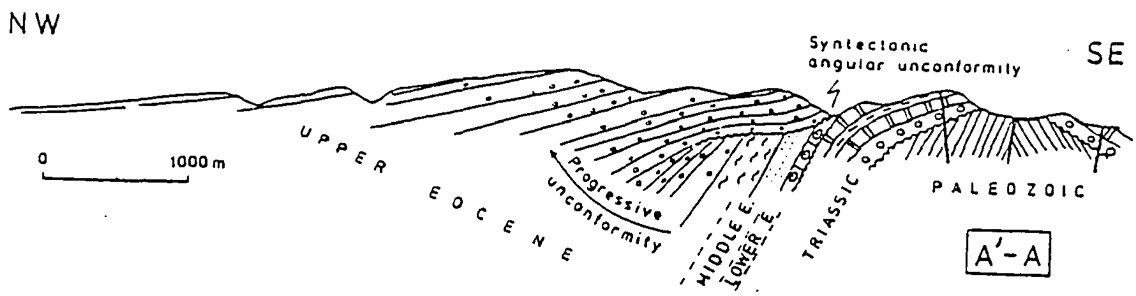

Figure 39. A syntectonic angular unconformity in the Ebro foreland basin of Spain that is similar to the angular unconformities in the Witwatersrand. On the basis of paleontologic evidence, Aradon et al. (1986) suggest that the unconformity must have developed within 2 million years. From Aradon et al. (1986).

enough time available to alter the Witwatersrand quartzites meteorically.

As a final test, I will briefly investigate the sensitivity of the meteoric leaching model to changes in the input parameters. The parameters in this model that have the potential to change the 450,000 year outcome are rainfall rate, partial pressure of atmospheric CO_2, infiltration rate, depth of leaching, and chemistry of the Witwatersrand sands. The depth of leaching and the chemistry of Witwatersrand sands (pre- and post-leaching) are based on data collected from 110 thin sections from the Klerksdorp goldfield. Unless additional data are collected (perhaps from another goldfield), there is no basis for adjusting these parameters--they are rather firmly fixed by the data at hand. The three remaining parameters (infiltration rate, partial pressure of atmospheric CO_2, and rainfall rate) are all related to the time required for leaching by a reciprocal--a 50% decrease in any of these parameters, for example, will result in a doubling of the time required for leaching. The infiltration rate of 30% is probably quite accurate because it is based on hydrologic data collected from modern basins that are very similar to the Witwatersrand. Partial pressure of CO_2 and rainfall rate, however, have the potential to vary significantly from the values that I have chosen, resulting in a much different outcome. For example, substituting modern values (330 ppm atmospheric CO_2 and 66 cm/year rainfall) results in a thousand-fold increase in the time required for leaching--from 450,000 years to 450,000,000 years. Clearly, therefore, it is the rainfall rate and the atmospheric CO_2 that most strongly influence the model. Considering the potential difficulties involved in estimating these parameters for the Archean Earth, this model for meteoric leaching of the Witwatersrand must be considered rather speculative.

Alternatives to the meteoric leaching model

The meteoric leaching model presented here is built upon bulk chemical and stratigraphic data from the Witwatersrand quartzites and estimates of atmospheric CO_2 in the Archean, continental rainfall in the Archean, and the infiltration rate of meteoric water into the Witwatersrand sands. When reasonable values are chosen for each of these parameters, the mass balance modeling indicates that the Witwatersrand sands could have been leached by meteoric water, one formation at a time, in a geologically reasonable time frame.

Other alteration schemes for the Witwatersrand quartzites have also been suggested, but there are problems with each. Vos (1975) proposed that Central Rand sediments were simply reworked proximal West Rand sediments--the reworking process leading to increased maturity. Although the concept of reworking is fully consistent with my tectonic reconstruction of the basin in chapter 2, several lines of evidence suggest that the recycling did not significantly mature the sediments. First, a West Rand-to-Central Rand recycling does not explain the alteration at the top of the West Rand's Roodepoort Formation, or the consistent intraformational trend towards increasing alteration upwards. Meteoric leaching, on the other hand, explains both observations quite well. Second, the transport distance involved in recycling West Rand sediments into the Central Rand Supergroup is very short--on the order of 50 km according to Pretorius' reconstruction of the migrating basin margin (figure 3). Cameron and Blatt (1971) reviewed studies of feldspar destruction during fluvial transport and concluded that no significant feldspar loss occurred in most streams over even hundreds of miles of transport, and that even the feldspar loss reported in high gradient streams was suspect because there was no control in these studies for the effects of dilution by the downstream addition of quartz. Finally, if the Central Rand sediments had matured during transport, an exceedingly quartz-rich sediment would have resulted because other minerals would have been removed prior to deposition. The presence of 35% matrix (on average) suggests instead that minerals other than quartz were a major component of the Central Rand sediments at the time of deposition.

Source area weathering was proposed by Sutton et al. (1990) to explain the aluminous composition of Central Rand quartzites, and more specifically, to explain the trend towards increasing alteration upwards within individual formations. Certainly source area weathering was a factor in the chemical evolution of these sediments, considering the CO_2-enriched atmosphere of the Archean. In fact, the slightly aluminous composition of even the least altered Central Rand sediments relative to average active continental margin sands (table 4) might well be a result of source area weathering. Nevertheless, the stratigraphic trends and the overall high aluminum content of the Central Rand quartzites argue against a major role for source area weathering. The stratigraphic trend expected from the periodic uplift and erosion of a deeply weathered source area is one in which the most altered sediments would be deposited at the base of each formation (because the most altered sediments would be at the top of the source area). Each source area uplift event (corresponding to a thrust sheet emplacement in the foreland basin model) would likely generate a new pulse of more altered (first transported) to less altered (last transported) sediment, with each pulse corresponding to a single unconformity-bound formation (see figure 4 of Graham et al., 1986, for example). This pattern is contrary to the trend in the Central Rand, where the most altered sediments are at the tops of the formations. The high aluminum content of the Central Rand is also difficult to reconcile with source area weathering because it is unlikely that aluminous, deeply weathered sediments could be transported en masse to the depositional site. An aluminous residuum, consisting of clay minerals, would be separated during transport from a sand-sized fraction in which quartz and any remaining feldspars or rock fragments would be carried.

Finally, Phillips (1987, 1988) proposed that alteration in the Witwatersrand was a product of hydrothermal alteration. Again, the intraformational stratigraphic trends are not consistent with alteration by hydrothermal fluids, which would presumably crosscut stratigraphic boundaries while exploiting faults, shear zones, and permeable horizons (Phillips, 1988). Further evidence against hydrothermal alteration will be examined in the next chapter, in which geochemical profiles supporting the presence of paleosols in the Witwatersrand will be discussed.

Chapter 6. Paleosols in the Witwatersrand

If chemical alteration of the Witwatersrand sediments were a result of meteoric leaching, as proposed in chapter 5, the most intense alteration would be found immediately beneath major unconformities. Intense alteration by meteoric waters beneath an unconformity is more commonly referred to as soil formation. In this chapter I will examine chemical trends that are similar to those described in chapter 5, but because the sampling is on a smaller scale (a scale compatible with modern soil-forming processes), "altered sediments" become "paleosols".

The primary objective of this paleosol study is a better understanding of the chemical evolution of the Witwatersrand basin. Palmer et al. (1989) and Phillips (1987, 1988) recognized aluminous horizons within the basin and interpreted them as products of hydrothermal alteration formed during peak greenschist facies metamorphism. In Phillips and Myers (1989), this metasomatic model was extended to include even the gold mineralization of the basin, marking a return to the "hydrothermalist" viewpoint after many years of widespread acceptance of the modified placer theory. Because this revived hydrothermal model is based on a fluid-dominated, chemically-altering metamorphism, it is essential that the evidence for such open-system metamorphism be scrutinized carefully, and the contribution of other alteration processes, including weathering, be fully assessed. Whereas other responses critical of the revived hydrothermalist model have concentrated primarily on the mineralization of the basin (Minter, 1988; Smith, 1989; Reimer and Mossman, 1990), I will here engage the hydrothermalist vs. placerist debate in the context of the basin's unmineralized aluminosilicates.

The interpretation of Witwatersrand paleosols in a larger global context is another aim of this chapter. There is a growing data base of Precambrian paleosols from which we can obtain some measure of atmospheric oxygen levels through time (Holland at al., 1989). The Archean Witwatersrand, thought to have been deposited in a low oxygen atmosphere on the basis of detrital pyrite and uraninite, is a potentially valuable addition to this data base.

Sampling strategy

Palmer et al. (1989) in a recent investigation of sub-unconformity alteration zones sampled in sufficient detail to identify the small scale (<10 m) geochemical trends that are characteristic of paleosols, but only samples from beneath the purported weathering surface were collected ("footwall" sampling). When only the footwall is sampled, alteration can be ascribed either to weathering or, as by Palmer et al. (1989), to metasomatism by hydrothermal fluids that are focussed along the unconformity and its associated, permeable, overlying basal conglomerate. To eliminate this ambiguity, I have sampled both the footwall and hanging wall of several reefs in the basin. Metasomatism should alter both hanging wall and footwall sediments--the alteration "halo" should extend to both sides of the fluid-concentrating conglomerate. Weathering, on the other hand, will alter only the footwall.

In addition, I examine two footwall profiles developed on basalt from the Evander goldfield. These basalt profiles are from Palmer et al. (1989), and although there are no corresponding hanging wall profiles, the basalts are particularly useful because they provide a fixed parent rock composition against which alteration can be quantitatively measured.

Sample collection and methods

The Vaal reef, its footwall, and its hanging wall provide most of the data for this study. Profiles M, V2, VR, V3, and V4 are from the Vaal reef in the Klerksdorp goldfield. Profiles V2 and M are complete profiles through the hanging wall and footwall of the Vaal reef; V2 (11 samples) was collected underground and extends 80 cm into the hanging wall and 80 cm into the footwall; M (8 samples) was collected from core and extends 15 m into the hanging wall and 14 m into the footwall. Profiles VR (6 samples spread over 35 cm of reef plus 25 cm of hanging wall), V3 (7 samples collected over 300 cm of footwall), and V4 (6 samples collected over 250 cm of footwall) make up a composite profile: they were collected underground and within several hundred meters of one another because limited exposure did not permit collection of a single continuous profile.

Two reefs from the Welkom goldfield, the Ada May and the Commonage, were sampled from core. The Ada May profile (WAM), from the base of the Johannesburg subgroup, consists of 10 samples from 2.2 m of hanging wall and 2.4 m of footwall. The Commonage profile (WC), which lies about 150 m higher in the section, consists of 10 samples from 5.2 m of hanging wall and 3.2 m of footwall. The stratigraphic positions of all of these profiles are shown on figure 40.

Also, I include data from two profiles of the Bird metabasalt from the Evander goldfield. Palmer (1986) collected and analyzed the samples and reported the data; geochemical data for these profiles also appear in table 2 of Palmer et al. (1989), but with a different numbering scheme. I have returned to the original sample numbers and stratigraphy as reported in Palmer (1986). The two Bird footwall profiles sample 4.4 and 5.8 m (borehole 84 and borehole 326, respectively) of basalt beneath the Kimberley reef.

All samples were cleaned, crushed and ground, then pressed into powder briquettes for XRF analysis on a Rigaku 3070 spectrometer. Powder briquettes were used rather than

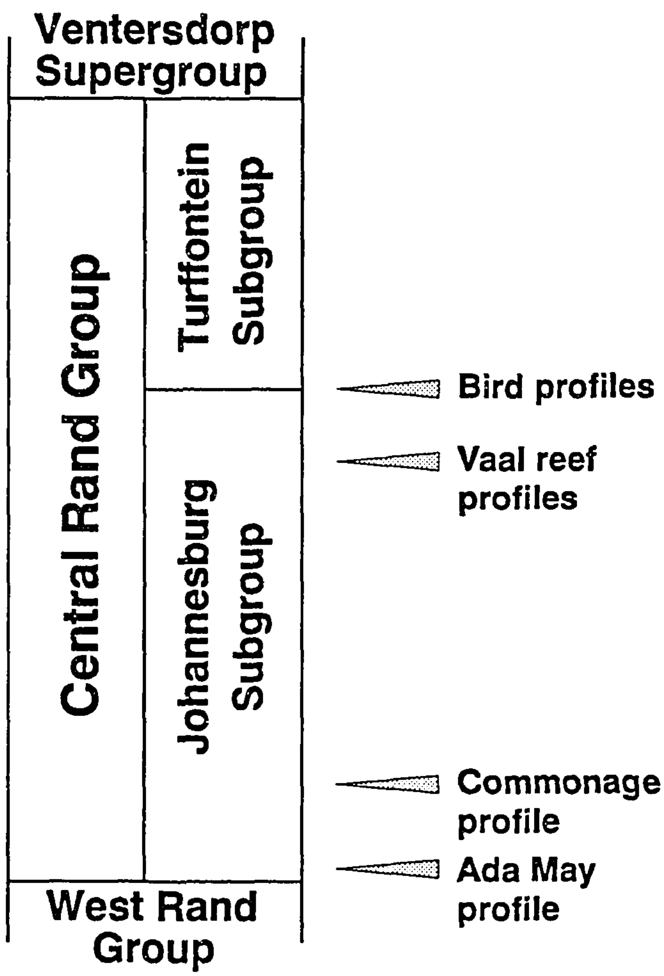

Figure 40. Stratigraphic position of the studied profiles.

glass discs because the high iron and sulfur contents of the pyrite-rich samples are not amenable to fusion in Pt-Au crucibles, and because sample preparation is greatly simplified. However, considerable grain size and matrix effects can result from the analysis of powders (Potts, 1987, p. 245-247). To overcome grain size effects, samples were uniformly ground until no particles larger than 30 microns remained (equivalent to passing a 400 mesh sieve). To overcome matrix effects, calibration curves were based on a large number of standards (N = 15 to 20) chosen for their chemical and mineralogical similarity to the unknowns.

Analytical totals reported here do not include H_2O^+ and therefore do not sum to 100%. H_2O^+ was, however, determined on ten samples using the Penfield technique. Water content from these ten samples was plotted against (Al_2O_3 + FeO) to derive an empirical equation for water content based on the assumptions that only micas make a significant contribution to the water content of the whole rock, and that (Al_2O_3 + FeO) is an accurate measure of mica content. When the resultant correction factor is applied to the analyses reported here, the mean of all analytical totals is 99.72 (N = 58), with a standard deviation of .61, indicating that the anhydrous totals reported here are reasonable.

Iron appears in the analytical results as both FeO and pyrite. These values were determined by first using all analyzed sulphur to make pyrite, and then reporting all remaining iron as FeO. Ferric/ferrous ratios were not determined. Analytical results are presented in Table 6.

Results

Primary homogeneity

To interpret the geochemical data (table 6) it is important first to recognize and to minimize primary textural and compositional differences between and within hanging wall and footwall rocks. For the Vaal, Ada May and Commonage reef profiles, sedimentologic, petrographic and geochemical data demonstrate any primary differences to be minimal.

Sedimentologically, the depositional environment of footwall and hanging wall rocks for each of the reefs is similar. For the Vaal reef, both were deposited in a marginal marine (or inland sea) setting, and both are dominated by unimodal pi cross beds. The primary difference is that the footwall cross beds are smaller and less consistently oriented than those of the hanging wall, reflecting a regressing fluvio-deltaic footwall environment versus a transgressing, longshore current dominated, hanging wall environment (Minter, 1976). Nevertheless, for both units, sediment originated in a northwesterly source area, was transported across a broad fluvial plain, and was deposited at or near the interface between the fluvial and

Table 6. Whole rock XRF analyses. Depth is relative to the reef, so that negative depths represent footwall and positive depths hanging wall samples. Profiles 84 and 326 are from Palmer (1986) and also appear in Palmer et al. (1989). See text for locations of other profiles.

Sample	Depth (m)	Si	Ti	Al	Fe	Mn	Mg	Ca	Na	K	P	FeS2	LOI	Total	CIA
V-2-1	0.75	92.6	0.04	4.7	0.7	0.02	0.29	0.01	0.07	0.7	0.01	0.14	n.d.	99.3	84
V-2-2	0.61	87.8	0.26	7.6	1.0	0.02	0.36	0.03	0.12	1.2	0.02	0.41	n.d.	98.7	83
V-2-3	0.46	90.1	0.36	5.9	0.7	0.01	0.23	0.02	0.07	0.9	0.02	1.14	n.d.	99.5	84
V-2-4	0.30	85.6	0.24	10.2	0.4	0.01	0.21	0.05	0.15	1.5	0.03	0.14	n.d.	98.5	84
V-2-5	0.20	90.3	0.13	6.7	0.3	0.03	0.18	0.09	0.09	1.0	0.01	0.11	n.d.	98.9	83
V-2-6	0.10	68.9	0.36	23.0	0.5	0.01	0.29	0.03	0.54	3.9	0.04	0.09	n.d.	97.7	82
V-2-9	-0.15	76.8	0.46	17.3	0.2	0.00	0.17	0.01	0.25	2.2	0.03	0.37	n.d.	97.8	86
V-2-10	-0.30	74.1	0.44	19.1	0.3	0.00	0.21	0.02	0.32	2.9	0.03	0.18	n.d.	97.5	84
V-2-11	-0.46	78.6	0.32	16.2	0.1	0.00	0.15	0.01	0.20	1.7	0.02	0.13	n.d.	97.4	88
V-2-12	-0.61	74.3	0.47	19.9	0.1	0.00	0.18	0.01	0.25	2.1	0.03	0.09	n.d.	97.4	88
V-2-13	-0.75	75.1	0.45	19.0	0.1	0.00	0.17	0.01	0.21	1.8	0.03	0.14	n.d.	97.0	89
M-20	14.50	84.5	0.09	8.8	2.6	0.02	0.68	0.00	0.13	1.4	0.02	0.03	n.d.	98.3	84
M-21	10.90	81.7	0.48	9.9	3.3	0.03	0.78	0.00	0.13	1.5	0.02	0.05	n.d.	97.8	84
M-22	8.50	85.3	0.38	8.8	1.9	0.02	0.47	0.00	0.13	1.5	0.02	0.17	n.d.	98.7	83
M-23	4.90	80.8	0.20	12.3	1.9	0.02	0.43	0.00	0.22	2.2	0.02	0.10	n.d.	98.2	82
M-24	-3.10	82.9	0.22	13.2	0.2	0.00	0.13	0.01	0.19	1.0	0.02	0.05	n.d.	97.9	90
M-25	-5.00	87.8	0.49	9.2	0.4	0.00	0.14	0.00	0.15	0.9	0.03	0.06	n.d.	99.3	88
M-26	-9.00	88.4	0.13	8.8	0.5	0.00	0.16	0.00	0.14	0.9	0.02	0.02	n.d.	99.1	88
M-27	-14.00	89.0	0.16	8.5	0.2	0.00	0.13	0.00	0.19	1.5	0.01	0.03	n.d.	99.8	81
VR-1	1.10	90.1	0.18	6.6	0.5	0.00	0.27	0.01	0.14	1.2	0.02	0.53	n.d.	99.5	81
VR-2	0.90	89.9	0.07	7.0	0.4	0.00	0.24	0.01	0.17	1.3	0.01	0.10	n.d.	99.1	81
VR-3	0.60	84.2	0.33	8.6	1.2	0.01	0.53	0.06	0.24	1.5	0.03	1.59	n.d.	98.3	80
VR-4r	0.35	82.7	0.22	10.3	1.4	0.01	0.66	0.19	0.33	1.7	0.02	0.16	n.d.	97.6	79
VR-6r	0.09	97.4	0.02	1.6	0.3	0.00	0.19	0.00	0.04	0.2	0.01	0.47	n.d.	100.2	84
VR-7r	0.03	90.2	0.09	3.4	0.8	0.01	0.29	0.01	0.10	0.5	0.03	3.71	n.d.	99.1	82
V-3-7	-0.05	76.9	0.26	17.7	0.1	0.00	0.16	0.01	0.12	1.3	0.02	0.15	n.d.	96.7	92
V-3-6	-0.50	75.4	0.41	19.2	0.1	0.00	0.16	0.00	0.08	1.1	0.02	0.13	n.d.	96.6	93
V-3-5	-1.00	78.5	0.32	16.2	0.1	0.01	0.15	0.01	0.07	0.9	0.02	0.11	n.d.	96.5	93
V-3-4	-1.50	78.6	0.29	16.3	0.2	0.01	0.16	0.01	0.06	0.8	0.02	0.13	n.d.	96.6	95
V-3-3	-2.00	78.2	0.40	16.4	0.2	0.01	0.16	0.01	0.06	0.8	0.02	0.45	n.d.	96.6	95
V-3-2	-2.50	83.7	0.27	12.3	0.2	0.01	0.15	0.01	0.03	0.6	0.01	0.27	n.d.	97.5	94
V-3-1	-3.00	78.5	0.35	16.4	0.1	0.01	0.16	0.01	0.06	0.8	0.02	0.16	n.d.	96.6	94
V-4-1	-0.05	72.0	0.52	21.1	0.2	0.00	0.21	0.03	0.27	2.0	0.03	0.26	n.d.	96.6	89
V-4-2	-0.50	82.4	0.29	14.4	0.2	0.00	0.15	0.01	0.05	0.6	0.02	0.14	n.d.	98.2	95
V-4-3	-1.00	80.2	0.32	15.2	0.2	0.00	0.18	0.01	0.08	0.7	0.02	0.23	n.d.	97.2	94
V-4-4	-1.50	69.9	0.74	23.5	0.4	0.00	0.26	0.02	0.24	2.1	0.03	0.23	n.d.	97.4	90
V-4-5	-2.00	77.5	0.53	17.2	0.3	0.00	0.20	0.01	0.10	0.9	0.02	0.47	n.d.	97.1	94
V-4-6	-2.50	84.5	0.30	12.4	0.2	0.00	0.16	0.01	0.06	0.6	0.02	0.20	n.d.	98.5	94
WAM-1	2.20	86.3	0.18	6.7	0.9	0.02	0.63	0.74	1.47	1.1	0.02	0.23	n.d.	98.3	57
WAM-2	1.50	79.0	0.21	11.7	1.3	0.02	0.95	0.47	1.90	2.2	0.03	0.37	n.d.	98.1	65
WAM-3	1.10	76.4	0.24	13.7	1.5	0.03	0.99	0.43	1.97	2.8	0.02	0.26	n.d.	98.3	66
WAM-4	0.60	78.4	0.20	10.9	1.8	0.03	0.93	0.37	1.41	2.4	0.02	1.86	n.d.	98.2	66
WAM-5	0.40	85.0	0.19	8.0	0.9	0.02	0.60	0.41	2.02	1.3	0.02	0.22	n.d.	98.7	59
WAM-6	-0.50	76.7	0.20	14.8	0.9	0.01	0.77	0.21	1.00	3.7	0.02	0.14	n.d.	98.4	71
WAM-7	-0.80	72.8	0.29	17.3	1.5	0.02	1.06	0.34	1.14	4.2	0.03	0.32	n.d.	98.9	71
WAM-8	-1.30	79.1	0.18	12.0	1.3	0.03	0.93	0.26	1.37	2.7	0.02	0.12	n.d.	98.0	68
WAM-9	-1.70	84.0	0.14	8.9	1.1	0.02	0.77	0.26	1.09	2.0	0.02	0.20	n.d.	98.4	67
WAM10	-2.40	84.5	0.13	8.5	1.0	0.02	0.70	0.27	1.15	1.9	0.02	0.11	n.d.	98.2	66

Table 6 - continued

Sample	Depth (m)	Si	Ti	Al	Fe	Mn	Mg	Ca	Na	K	P	FeS2	LOI	Total	CIA
WC-1	5.20	80.7	0.29	10.3	1.6	0.05	1.16	0.52	0.23	2.3	0.03	0.62	n.d.	97.7	73
WC-2	3.80	76.4	0.29	13.9	2.0	0.05	1.42	0.06	0.30	3.0	0.03	0.12	n.d.	97.6	78
WC-3	2.60	59.9	0.55	24.7	3.0	0.06	2.05	0.04	0.50	5.0	0.03	0.13	n.d.	95.9	80
WC-4	1.60	86.6	0.19	6.7	1.0	0.02	0.74	0.03	0.16	1.5	0.02	0.55	n.d.	97.4	78
WC-5	1.00	89.8	0.12	5.6	0.6	0.01	0.44	0.02	0.12	1.2	0.02	0.25	n.d.	98.1	78
WC-6	0.30	84.0	0.23	9.5	0.8	0.02	0.63	0.04	0.24	2.2	0.03	0.35	n.d.	98.1	77
WC-7	-0.10	91.5	0.04	4.4	0.7	0.02	0.55	0.04	0.09	0.9	0.02	0.06	n.d.	98.3	78
WC-8	-0.70	84.6	0.10	9.5	0.6	0.01	0.50	0.02	0.25	2.2	0.02	0.05	n.d.	97.8	77
WC-9	-1.70	78.8	0.23	13.6	1.0	0.02	0.79	0.03	0.34	2.9	0.03	0.28	n.d.	98.0	78
WC-10	-3.20	87.3	0.08	7.1	0.6	0.01	0.39	0.03	0.19	1.6	0.02	0.04	n.d.	97.4	77
84-112	-0.10	55.5	1.88	26.7	2.4	0.03	1.28	0.63	0.39	7.8	0.02	n.d.	3.91	100.6	72
84-113	-0.20	47.6	2.26	31.9	1.7	0.02	1.05	1.31	0.43	9.5	0.02	n.d.	4.30	100.1	70
84-114	-0.30	45.8	2.34	32.8	1.8	0.01	0.73	1.66	0.32	9.6	0.03	n.d.	4.29	99.3	70
84-115	-0.90	53.9	1.60	22.0	7.4	0.09	2.44	2.03	0.30	5.7	0.03	n.d.	4.48	100.0	68
84-116	-1.20	47.6	0.94	13.6	9.9	0.17	3.84	9.47	1.32	0.9	0.10	n.d.	9.95	97.8	40
84-117	-2.90	54.9	0.90	13.5	8.2	0.16	3.18	16.06	0.39	0.0	0.11	n.d.	2.24	99.7	31
84-118	-3.90	51.4	0.99	14.8	9.7	0.17	4.12	14.25	0.37	0.1	0.12	n.d.	3.99	99.9	36
84-119	-4.40	52.3	1.17	16.9	13.3	0.19	4.38	2.73	2.72	0.1	0.12	n.d.	4.31	98.2	64
326-120	-0.30	56.0	1.22	29.4	0.7	0.00	0.19	0.16	1.14	6.9	0.05	n.d.	4.32	100.1	75
326-121	-0.60	52.9	1.80	30.9	0.3	0.00	0.00	0.02	0.79	8.0	0.04	n.d.	3.98	98.7	76
326-122	-0.70	50.3	1.83	33.4	0.3	0.00	0.08	0.06	1.16	8.4	0.02	n.d.	4.34	99.9	75
326-123	-0.90	48.3	1.98	34.2	0.7	0.01	0.09	0.08	1.16	8.3	0.02	n.d.	4.61	99.3	76
326-124	-1.10	47.8	1.87	34.3	1.1	0.01	0.14	0.08	1.05	8.7	0.06	n.d.	4.62	99.7	75
326-125	-1.50	50.4	1.85	31.6	2.5	0.01	0.17	0.04	0.75	7.7	0.06	n.d.	4.10	99.2	77
326-126	-1.90	47.0	1.90	34.8	1.9	0.01	0.14	0.06	0.88	8.4	0.02	n.d.	4.62	99.7	76
326-127	-2.30	43.5	1.53	26.1	15.6	0.08	1.24	0.07	0.53	4.0	0.04	n.d.	4.79	97.6	83
326-128	-3.30	49.1	1.41	25.3	11.4	0.09	1.39	0.23	0.57	4.4	0.12	n.d.	4.59	98.6	81
326-129	-3.80	43.4	1.09	18.1	24.2	0.21	3.59	0.20	0.14	0.7	0.12	n.d.	5.11	96.8	93
326-130	-4.30	51.1	0.83	14.8	11.0	0.21	6.88	5.47	2.42	0.1	0.11	n.d.	6.70	99.6	51
326-131	-5.30	51.1	0.87	15.2	10.4	0.18	7.15	7.63	2.83	0.1	0.11	n.d.	3.25	98.8	45
326-132	-5.80	50.7	0.87	15.4	9.8	0.18	6.50	8.34	3.12	0.0	0.09	n.d.	3.25	98.2	43

marine environments. There is, therefore, no reason to suspect major sedimentological differences between the hanging wall and the footwall of the Vaal reef.

The Ada May and Commonage reefs from the Welkom goldfield also provide no sedimentologic evidence for primary differences between hanging wall and footwall rocks. Within the intervals sampled, both reefs are very thin (<10 cm), oligomictic, uranium-mineralized conglomerates with traces of gold mineralization and carbon (Minter et al., 1986). The depositional environment of footwall, reef, and hanging wall for both the Commonage and Ada May sequences is inferred to be one of fluvial fans prograding into a shallow sea (Minter et al., 1986), presumably in a continuous depositional sequence--there is no obvious sedimentologic break, nor is there a significant unconformity beneath either reef (Minter, pers. comm., 1990).

Hanging wall and footwall samples from each sampled reef are also very similar petrographically. Excepting the reef samples VR-4, VR-5, and VR-6, each of which consists of .5 to 2 mm pebbles in a sand-sized matrix, only sandstones were sampled. Amongst the sandstones (table 7) there are no statistically significant, systematic grain size differences between hanging wall and footwall sediments for either the Ada May or Commonage reefs, and for the Vaal reef the difference between hanging wall (average grain size of 950 microns) and footwall (625 microns) is statistically significant (at a confidence level of 0.99) but not of

	Ave. grain size (microns)	Ti/Al ratio
Vaal reef		
Hanging wall (n=13)	*950*	*0.027*
Footwall (n=22)	*625*	*0.023*
Ada May reef		
Hanging wall (n=5)	*480*	*0.021*
Footwall (n=5)	*470*	*0.015*
Commonage reef		
Hanging wall (n=6)	*525*	*0.024*
Footwall (n=4)	*500*	*0.012*

Table 7. Comparison of footwall and hanging wall sediments. Two of the comparisons differ significantly (confidence level = 99 %): the Vaal reef hanging wall sediments are coarser than the Vaal reef footwall sediments, and the Commonage hanging wall sediments are richer in Ti than the Commonage footwall sediments.

sufficient magnitude to induce major porosity/permeability differences across the reef. As is true of the bulk of Witwatersrand quartzites, feldspars and rock fragments are almost totally absent (see chapter 4 and Sutton et al., 1990). Instead, both hanging wall and footwall rocks of the three reefs examined here consist of quartz grains and a sericite (muscovite and pyrophyllite) matrix, with relative abundances ranging from 60-90% quartz and 10-40% sericite matrix, plus minor amounts of pyrite, chlorite, chloritoid, and rutile.

Examination of Ti/Al ratios provides a geochemical test of primary homogeneity. Titanium and aluminum are strongly separated by sedimentologic processes because they occur in phases that are hydraulically very different. Also, a change in sediment source may change primary Ti/Al ratios. In either case, the primary Ti/Al ratio should be preserved because both Ti and Al are relatively immobile during chemical alteration (Palmer et al., 1989; Nesbitt and Young, 1989). In the Vaal reef profiles, Ti/Al ratios indicate that there are no major primary compositional differences between Vaal reef footwall and hanging wall sediments (table 7). In the Ada May and Commonage profiles, there is approximately 30% and 50% more Ti relative to Al, respectively, in the hanging wall than in the footwall (table 7), indicating a small primary compositional difference across these reefs. In light of the textural and sedimentologic homogeneity of these two profiles, these changes in Ti/Al ratios are probably a source area effect rather than the result of different hydrodynamic environments.

Major element ratios

To correct for the significant primary variations in quartz/matrix content, I will work with major element ratios that do not include SiO_2. Single elements, particularly iron, will be considered in ratio to aluminum, and the alkalis as a group (Na, Ca, and K) will be considered by use of the Chemical Index of Alteration (Nesbitt and Young, 1982).

The Chemical Index of Alteration (CIA) is calculated using mole fractions according to the formula

$$Al_2O_3 \,/\, (Al_2O_3 + K_2O + Na_2O + CaO).$$

Originally applied to shales by Nesbitt and Young (1982), the CIA has more recently been used to assess weathering in modern soils developed on granites (Nesbitt and Young, 1989) and in transported sediments from the Indus river and the Witwatersrand basin (Maynard et al., 1991).

The CIA values obtained in this study (table 6) are commonly greater than 80, indicating highly altered--very aluminous--sediments. The stratigraphic distribution of CIA values in each hanging wall to footwall profile across the Vaal reef indicates that alteration is markedly asymmetric, with intense footwall alteration but little hanging wall alteration (figure 41). Ada May reef alteration (figure 42a) is somewhat asymmetric, but less so than in the Vaal reef. Commonage reef alteration (figure 42b) is flat, and therefore symmetric. Each of the two basalt profiles (figure 43) is highly altered immediately beneath the unconformity, but unaltered by 1 and 4 m depth, respectively. One of the Bird metabasalt profiles (Figure 43a) has a 3 m zone of depressed CIA values. These anomalous values are a result of Ca contents higher than normal for unaltered basalt, indicating Ca addition to this portion of the profile.

The Fe/Al ratio reveals stratigraphic patterns that parallel those of the CIA index. The Fe/Al ratio across the Vaal reef (figure 44) is distinctly asymmetric, with an almost complete loss of iron in the footwall of all 3 profiles. There is a slight iron depletion in the uppermost 1 m of Ada May footwall (figure 45a), but no significant iron loss in the Commonage footwall compared to the Commonage hanging wall (figure 45b). Iron depletion in the two Bird metabasalt profiles (figure 46) extends approximately 1 m and 3.5 m beneath the unconformity, respectively, corresponding very closely to the depth of alteration observed in the CIA plots (compare figure 43). Because FeO and MgO values correlate closely (table 6), a similar series of plots of Mg/Al ratios shows the same stratigraphic trends as Fe/Al ratios.

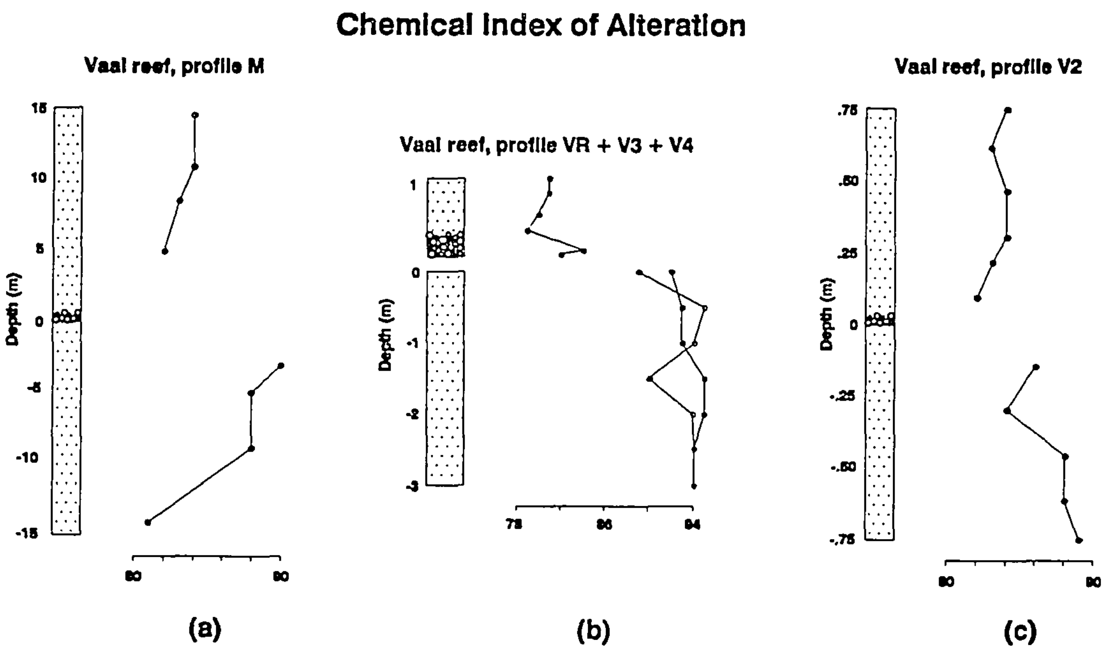

Figure 41. CIA index across the Vaal reef from three locations in the Klerksdorp goldfield (See text for an explanation of the CIA index). Profile M is from core, profile V2 from mine exposure, and profile VR + V3 + V4 is a composite of three profiles collected underground and within several hundred meters of one another--VR-1 to VR-6 of hanging wall, V3-1 to V3-7 (solid circles) of footwall, and V4-1 to V4-6 (open circles) of footwall. The asymmetry of alteration (footwall sediments are highly altered, hanging wall sediments are not) in conjunction with the observation that the Vaal reef marks a major uncomformity suggests weathering as the agent of alteration. Hydrothermal alteration by fluids that are focussed along the conglomeratic reef would have altered both the hanging wall and footwall sediments.

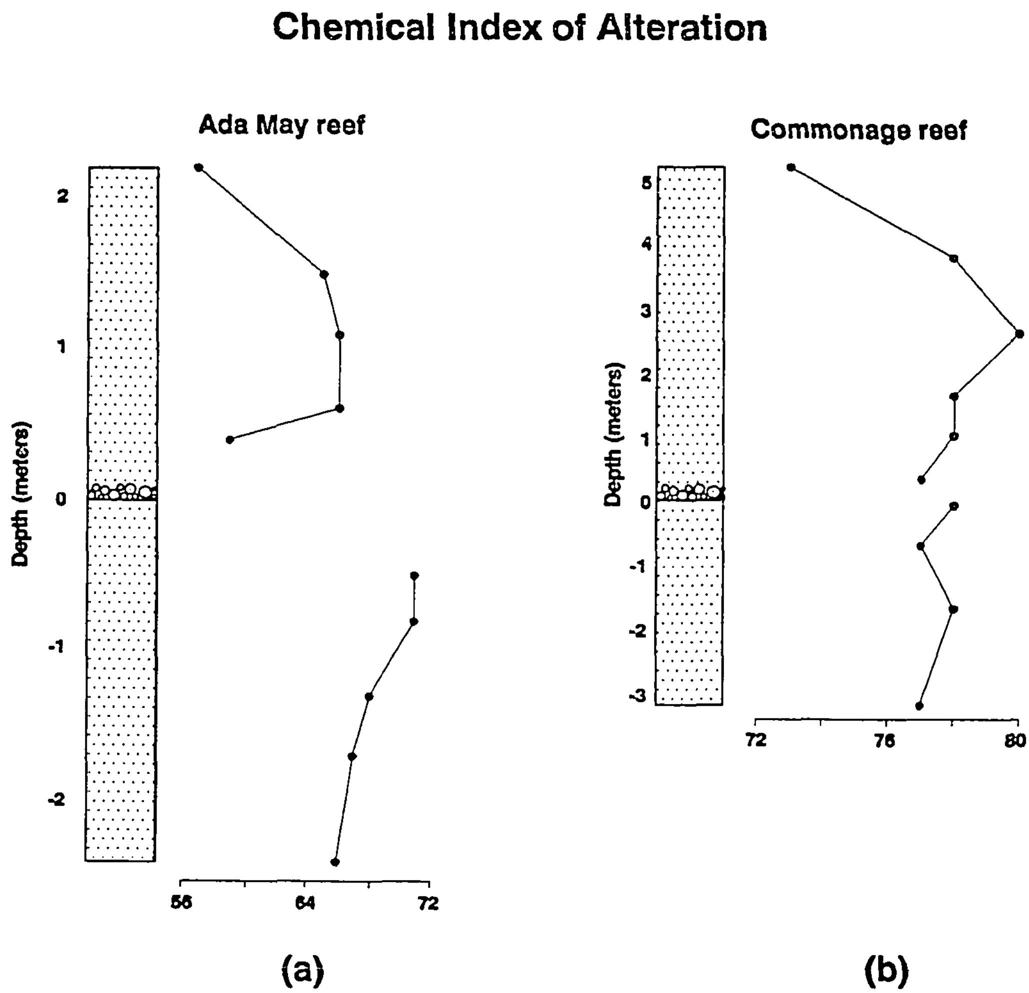

Figure 42. CIA index across the Ada May and Commonage reefs in the Welkom goldfield. Both profiles were collected from core. The Ada May profile exhibits a slight, 1 m deep, footwall alteration seen in the two uppermost footwall samples. The Commonage profile exhibits no footwall alteration. Unlike the Vaal reef paleosurface, there is no marked uncomformity beneath either of these reefs (Minter et al., 1986). Thus, deep footwall weathering would not be expected.

Chemical Index of Alteration

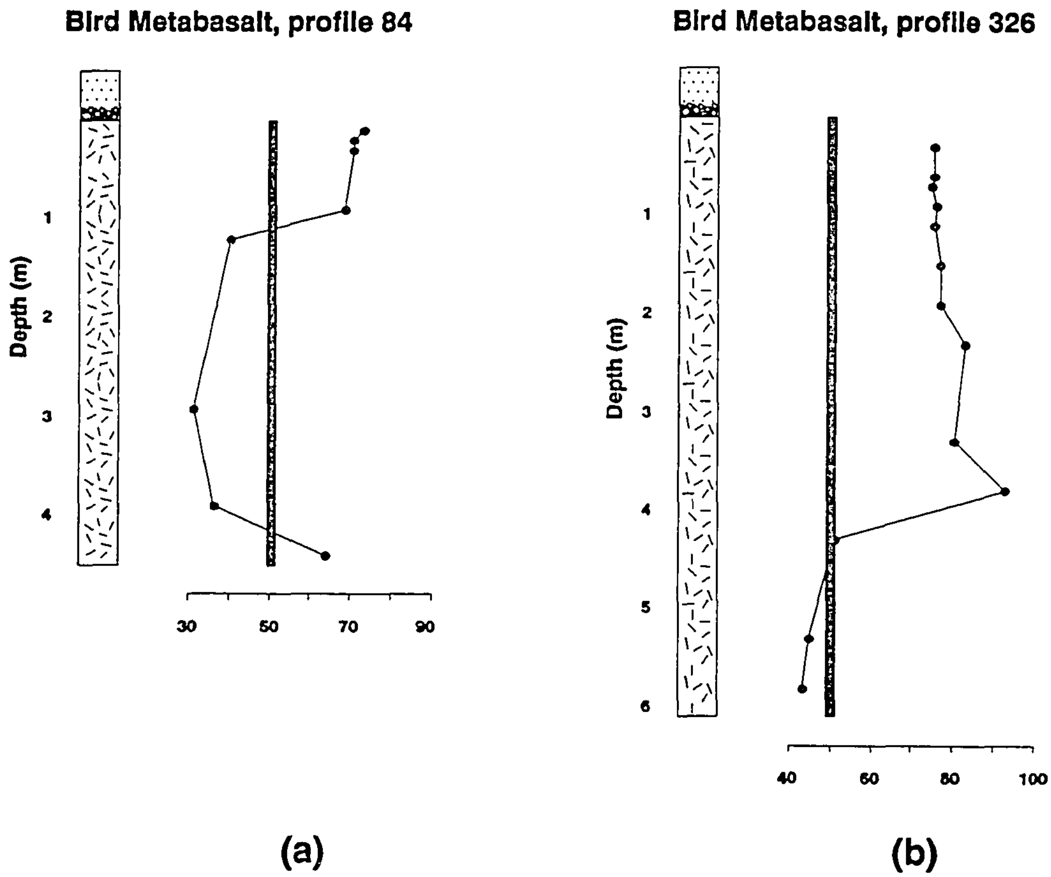

Figure 43. CIA index in the Bird metabasalt from the Evander goldfield. The data are from Palmer (1986). The vertical stippled bar represents the CIA index of average, unaltered basalt. Profile 84 is alkali-depleted to a depth of 1 m beneath the uncomformity surface; profile 326 to a depth of 4 m.

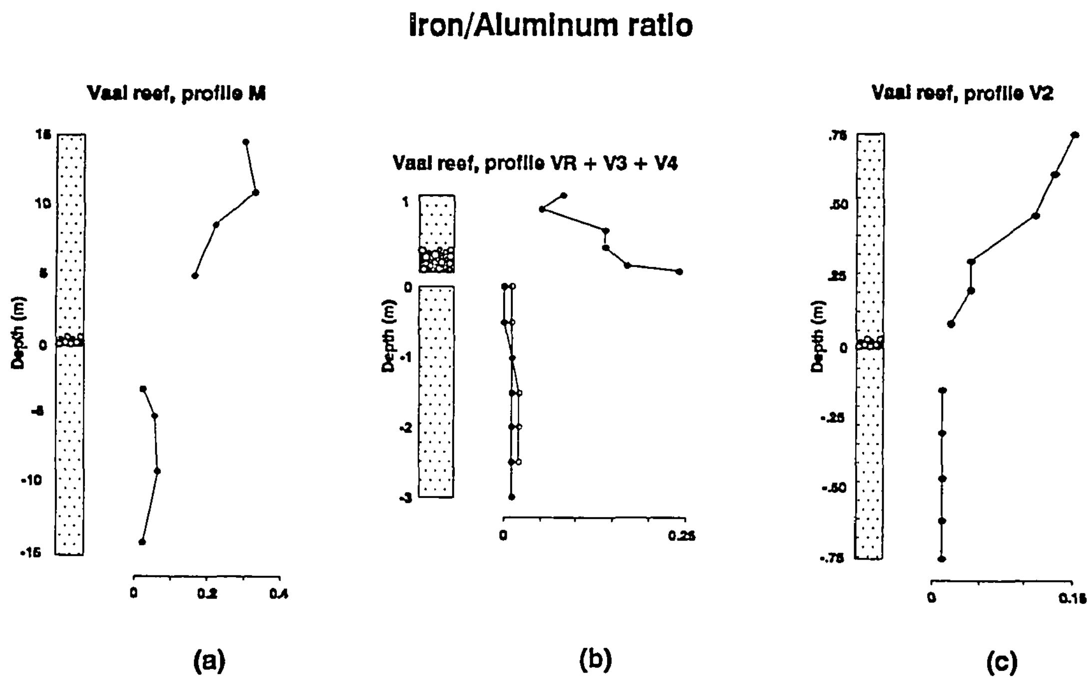

Figure 44. Fe/Al ratio across the Vaal reef from three locations in the Klerksdorp goldfield. Only non-pyrite iron enters into the ratio. The profiles are markedly asymmetric, with extreme iron loss in the footwall relative to the hanging wall. Loss of iron during weathering in the low oxygen Archean atmosphere would be expected (Holland, 1984).

Iron/Aluminum ratio

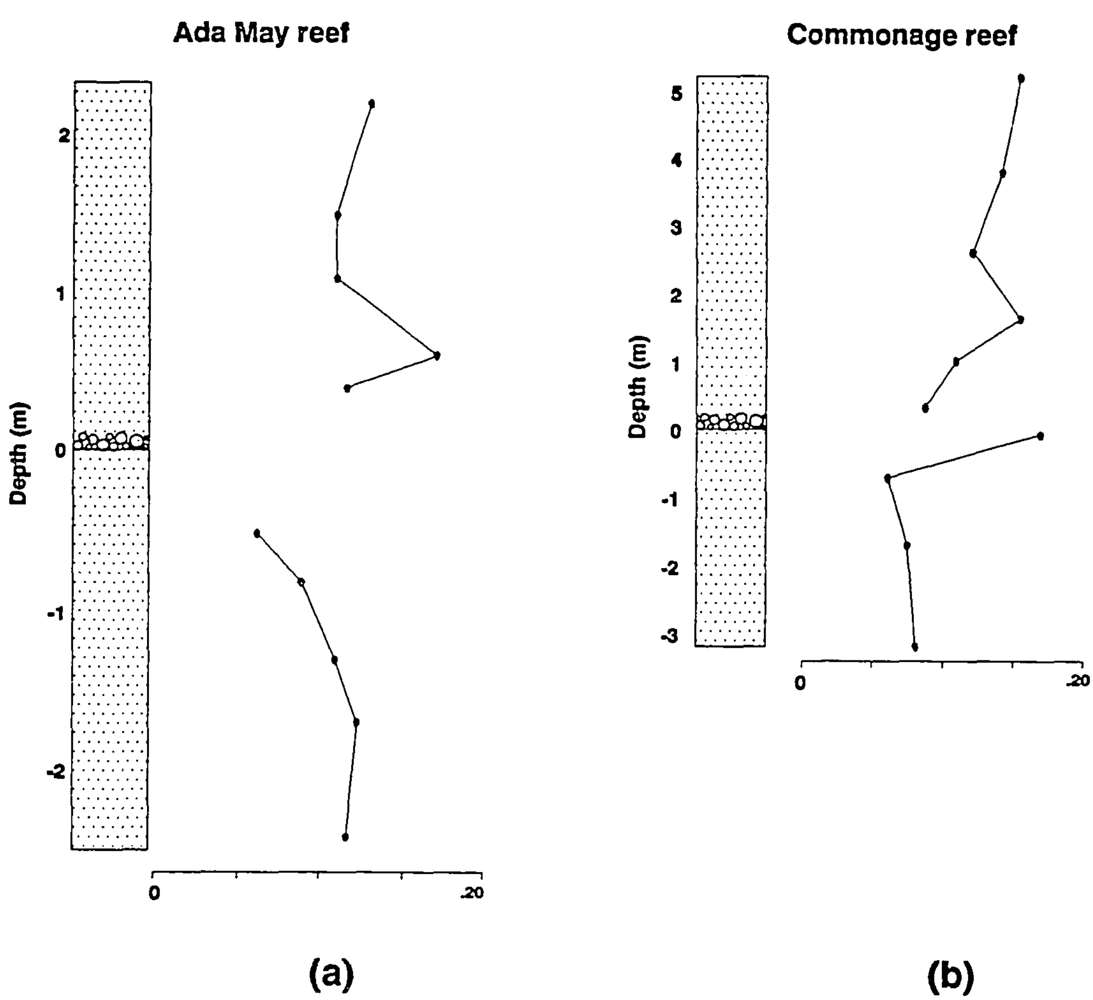

Figure 45. Fe/Al ratio across the Ada May and Commonage reefs in the Welkom goldfield. Essentially the same pattern of alteration recorded by the CIA index (figure 42) is observed here--Fe loss approximately 1 m below the the Ada May reef and no consistent trend beneath the Commonage reef.

Iron/Aluminum ratio

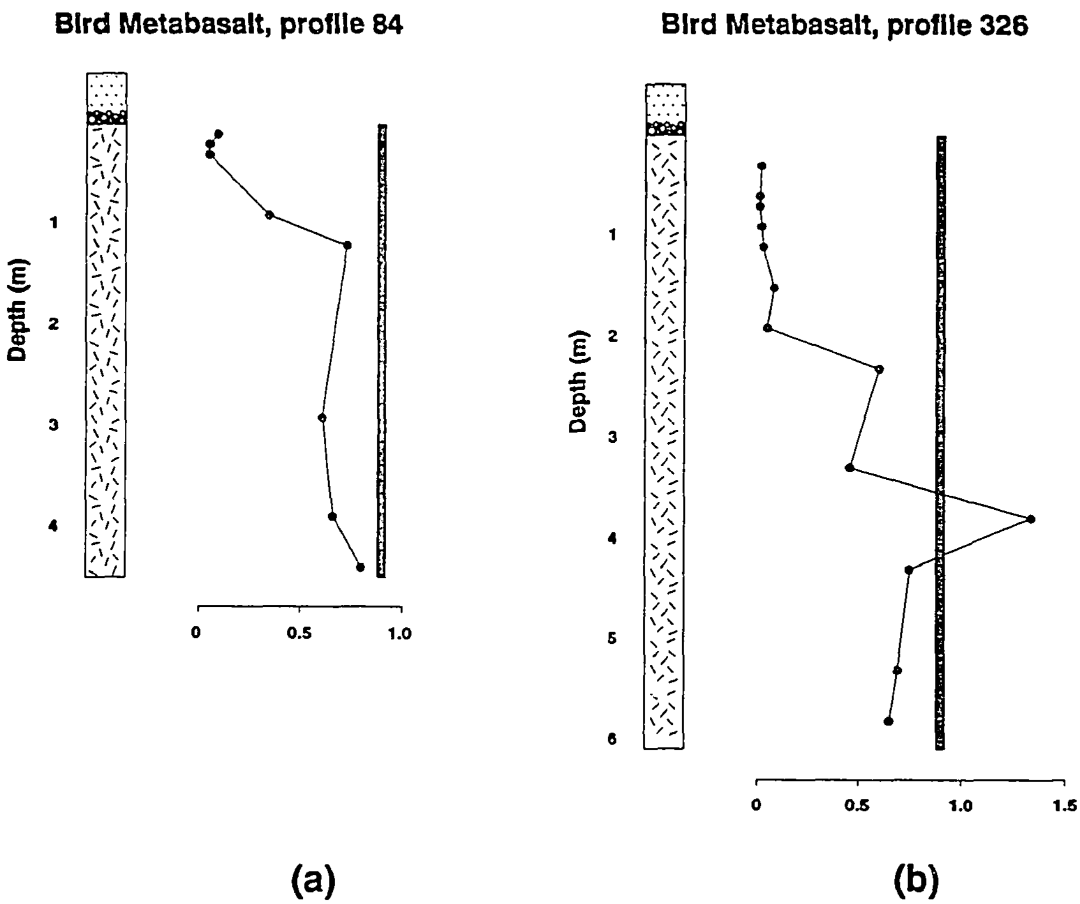

Figure 46. Fe/Al ratio in the Bird metabasalt from the Evander goldfield. The vertical stippled bar is the Fe/Al ratio of average, unaltered basalt. Fe loss in these profiles closely parallels alteration as measured by the CIA index (compare figure 43). In profile 84 the zone of Fe loss extends 1 m beneath the uncomformity, and in profile 326 Fe loss extends to 3.5 m depth. Average Fe loss from the most deeply weathered samples (the top 3 samples of profile 84 and the top 7 samples of profile 326) is 94 percent.

The significance of these major element trends (Fe loss, CIA increase, and the presence or absence of asymmetric profiles across each reef) will be discussed below.

Discussion

Tectonic, structural, and sedimentologic evidence suggests that the Witwatersrand is a foreland basin with its hinterland to the northwest (see chapter 2). In addition to the thick clastic packages that record subsidence (Heller et al., 1988), foreland basins such as the Witwatersrand are characterized by numerous angular unconformities that record isostatic relaxation and uplift in the basin. Basal conglomerates occur on many of these unconformities in the Witwatersrand, where gold, uraninite and other heavy minerals have been concentrated, presumably by the same sedimentologic processes that form placers today. It is beneath these reefs, on the subaerially exposed unconformity surface, that weathering is likely to have occurred.

However, weathered horizons may have been eroded from the unconformities as easily as they formed. Preservation would be expected only if little erosion occurred, or if erosion proceeded so slowly that weathering could keep pace. To assess the likelihood of preservation of a paleosol, it is therefore essential that the depositional/erosional history of the footwall-to-hanging wall sequence be well characterized. Then the geochemical evidence of weathering can be interpreted in the context of the sedimentologic history.

Vaal reef. It is in part because of the need for a thorough sedimentologic reconstruction that I chose the Vaal reef to study paleosols in the Witwatersrand basin. The Vaal reef is one of the major gold producers in the basin and is therefore well exposed underground and has been thoroughly studied from a sedimentologic perspective.

The angular unconformity beneath the Vaal reef extends over the entire Klerksdorp goldfield (Minter, 1976; Antrobus et al., 1986). A minimum of 160 feet of footwall has been removed along the basin margin (see figure 7 of Minter, 1976), with progressively less erosion towards the basin center. Weathering on this paleosurface probably took place in parallel with erosion and also during deposition of the Vaal reef. That weathering occurred in conjunction with erosion is supported by the very planar, low angle nature of the truncation surface. At Buffelsfontein, which is approximately 6 km from the study area, the gradient of the truncation surface is 1:360 (p. 165, Minter, 1976), indicating a very broad, expansive deflation surface that was eroding very slowly. That weathering may have occurred later, in concert with deposition of the reef, is suggested by the sedimentology of the Vaal reef itself. There are no deep scours into the footwall; rather, the mineralized sands were deposited in very broad and shallow meandering channels (width:depth ratio up to 1,000) between which are unmineralized topographic highs of one meter or less relief (Minter, 1976). Clay clasts, possibly indicating periods of subaerial exposure and consequent mud-cracking, are found in the reef. Also, carbon seams, most likely the preserved remains of algal mats, are found immediately beneath and within the reef (Minter, 1976), again suggesting at least very shallow water, and perhaps even periods of subaerial exposure, as on a tidal flat. The sedimentologic evidence thus indicates little erosion and probable subaerial exposure of the semi-consolidated, broad, flat footwall during Vaal reef sedimentation.

Following deposition of the Vaal reef, which is generally less than one meter thick, transgression led to burial of the reef beneath hanging wall sediments transported from the southwest by longshore currents. Associated with these transgressive sediments was a deepening of the water column (Minter, 1976), thus removing the sequence from the influence of further weathering.

In sum, the depositional record of the footwall and hanging wall of the Vaal reef provides favorable conditions for the formation and preservation of a paleosol, and the CIA profiles (figure 41) fully support this scenario by virtue of the strong footwall alteration they reveal. CIA values in the footwall (with the exception of sample M-27, which apparently lies deeper than the weathered horizon) average 91 (with a standard deviation of $\pm$ 4), whereas those of the hanging wall average 82 $\pm$ 1.5. For comparison, the average CIA value of 75 Central Rand quartzite samples, none of which are immediate footwall samples, is 79 $\pm$ 3 (table 1 of Sutton et al., 1990). The Vaal reef footwall, therefore, is highly altered relative to the average detritus in the upper part of the Witwatersrand basin, whereas the Vaal reef hanging wall is essentially unaltered.

The CIA profiles also suggest that the weathering profile beneath the Vaal reef is thicker than other Precambrian paleosols. Profiles V2 and VR (<1 m and 3 m deep, respectively) do not approach the base of the altered zone but profile M does, and returns to a hanging wall-like CIA value of 80 somewhere between 10 and 15 m depth, indicating at least a 10 m thick paleosol after compaction. Considering the unlithified, porous nature of the substrate at the time of weathering, it is not surprising that a deep profile developed.

In profiles V2 and VR (figures 41a and 41b), where samples are spaced closely enough to provide better resolution, there is a slight reduction in CIA values in the uppermost 30-40 cm of the footwall. This runs counter to the expected weathering trend of increasing alteration upwards, and may reflect local metamorphic equilibration between the reef/hanging wall and the footwall. If metamorphic equilibration is recorded, the fact that the fundamental footwall-to-hanging wall asymmetry is still preserved suggests that significant movement of the alkalis during metamorphism is limited to a scale of 1 meter or less. This is in strong contrast to the major element mobility proposed by Phillips (1988).

The strongly asymmetric Fe/Al profiles across the Vaal reef also support a footwall paleosol (figure 44). The average Fe/Al ratio of 22 footwall samples is 0.02 with a standard deviation of ± 0.01. In contrast, 16 hanging wall samples yield an average Fe/Al ratio of 0.13 ± 0.12, and the 75 Central Rand quartzite samples from Sutton et al. (1990) yield an average Fe/Al ratio of 0.22 ± 0.09. As with the CIA index, Fe/Al ratios indicate that the Vaal reef footwall samples are significantly altered relative to average Central Rand quartzite samples, whereas Vaal reef hanging wall samples are essentially unaltered.

The direction of footwall Fe alteration (loss of Fe) is significant. When Fe is released in a soil by acid attack of its host mineral(s), it can either be retained in the soil as insoluble ferric iron or removed from the soil as soluble ferrous iron, depending on the availability of oxygen (Holland, 1984). Soils younger than about 2 billion years retain iron (Holland et al., 1989), presumably reflecting the presence of significant amounts of free oxygen in the atmosphere. Soils older than 2,000 Ma, with a few exceptions, lose iron (Button and Tyler, 1981; Grandstaff et al., 1986; Gay and Grandstaff, 1980), an observation used to indicate lower levels of atmospheric oxygen (Holland et al., 1989). Thus, on the basis of their 2,900 Ma age alone, paleosols in the Witwatersrand basin would be expected to be iron-depleted. Also, detrital pyrite and uraninite in the overlying Vaal reef provide independent, internal evidence that weathering in the Witwatersrand basin proceeded under low oxygen conditions, and therefore that the observed iron trends are as expected for a Witwatersrand paleosol.

The depth of iron depletion beneath the Vaal reef is substantial. Profile M, which is 15 m deep, is iron-depleted through its entire depth.

<u>Ada May and Commonage reefs.</u> As discussed earlier, the depositional history of the Ada May and Commonage reefs is continuous--there is no significant unconformity beneath either reef (Minter et al., 1986). Lacking a major unconformity (and the prolonged subaerial exposure that would accompany the unconformity), there is little opportunity for weathering. However, the very presence of the reefs, with their suite of enriched heavy minerals implies that there was a period during which the light mineral fraction was winnowed away, allowing the placer minerals to be concentrated. During this period of non-accumulation, any decrease in the water level might expose the footwall subaerially and allow for some weathering. The sedimentologic evidence as it relates to paleosol development is therefore somewhat inconclusive. Although

weathering might have taken place during subaerial exposure of the Ada May and Commonage footwalls, the absence of significant unconformities argues against the development of deep, strongly altered profiles such as occur beneath the Vaal reef. The CIA and Fe/Al trends associated with the Commonage and Ada May reefs (figures 42 and 45) are consistent with this sedimentological interpretation. The Commonage profiles exhibit no significant footwall or hanging wall alteration trends. Beneath the Ada May reef evidence of footwall alteration consists of an upwards increase in the CIA and an upwards decrease in the Fe/Al ratio, as beneath the Vaal reef. However, the degree of alteration is much less than for the Vaal reef: the Vaal reef footwall has an average CIA of 91, the Ada May alteration achieves a maximum CIA of 71; Fe loss beneath the Vaal reef is almost complete, whereas less than 50% Fe loss occurs in the Ada May footwall. Also, the depth of alteration beneath the Ada May reef is only about 1 m (figures 42a and 45a), in contrast to the 10 m (minimum) of alteration beneath the Vaal reef.

The development of only slightly altered to unaltered horizons beneath these two reefs strongly supports the conclusion that sub-reef alteration trends are paleosols rather than later diagenetic or metamorphic alterations. If the footwall alterations were the product of diagenesis or metamorphism acting along the lithologic boundary between footwall and reef, then each reef should have an associated alteration. Instead, the correlation is between unconformities and alteration--where a major unconformity exists (beneath the Vaal reef) there is profound footwall alteration, and where no major unconformity exists (beneath the Ada May and Commonage reefs) there is little to no alteration.

<u>Bird metabasalt.</u> The lithologies along these two profiles--footwall basalt versus hanging wall conglomerate to sandstone--simplifies their sedimentologic reconstruction. Because there is no evidence of submarine deposition of the relatively thin Bird lava flows (most are several meters thick according to Palmer, 1986), and because they are overlain by a fluvial conglomerate rather than marine (or inland sea) sediments, the flows must have been exposed subaerially. Evidence of weathering during exposure is present in both the CIA and Fe/Al profiles (figures 43 and 46), which document a CIA increase and Fe/Al decrease beneath the unconformity.

With no hanging wall samples, it is not possible to document the symmetry or asymmetry of these profiles, nor would it be reasonable to do so, considering the very different footwall and hanging wall rock types. However, even without hanging wall data, I interpret these profiles as weathering horizons rather than the hydrothermally altered zones of Palmer et al. (1989) for several reasons. First is the similarity of alteration styles between the

Bird profiles and the Vaal/Ada May profiles: the upwards increase in CIA and decrease in Fe and Mg is observed in all of the profiles. Given these similar chemical alterations in similar stratigraphic settings (i.e., beneath unconformities), I conclude that a similar alteration mechanism was at work (weathering). Second, the thickness of the Bird altered horizon is consistent with a weathering interpretation--the Bird profiles are thinner than the Vaal reef paleosols, as would be expected considering the much lower permeability of basalt. Third, the zone of Ca enrichment from 1-4 m depth in profile 84 (table 6) is analogous to modern caliche-forming soils in which intermittent wetting and drying leads to near-surface leaching of Ca followed by its deeper precipitation. Finally, although Palmer (1986) and Palmer at al. (1989) argued against a paleosol interpretation in part because no characteristic soil structures are present, recall that the entire basin, paleosols included, has been metamorphosed (Phillips, 1987). Because soil structures and soil-forming processes in general are dominated by clay minerals, metamorphism would have destroyed the bulk of the physical evidence.

The chemistry of the Bird profiles can be compared to a known, unaltered basalt composition. By assuming that each Bird lava flow was chemically homogeneous the amount of weathering in the Bird profiles can be quantified. Because the lavas are clearly altered, I will use the composition of average basalt as reported in Manson (1967) in lieu of any actual Bird analyses to represent this (unaltered) parent rock. The deep Bird samples are close to this average basalt in composition, indicating that the approach is reasonable. With a known parent rock composition, it is possible to examine the behavior of the individual elements that make up the CIA index.

Comparison of measured compositions with my basalt "standard" reveals contrasting behavior between Ca and Na on the one hand, and K on the other. Whereas Ca and Na are lost in the weathered horizon (see table 6), K is enriched. The average K_2O content of an unaltered basalt is 1.1 wt.% (Manson, 1967), whereas the average of the 14 highly weathered samples from the two profiles (samples 112-115 in profile 84 and samples 120-129 in profile 326) is 7.0 wt.% K_2O. That this increase in K represents addition to the altered horizon, and not just a relative increase brought about by the loss of other elements, can be seen by examining Al_2O_3 in the same altered samples. Assuming aluminum immobility, the increase from 15.1 wt.% Al_2O_3 in the unaltered basalt to 29.4 wt.% in the altered basalt permits only an equivalent doubling of the K_2O content (to 2.2 wt.% rather than the observed 7.0 wt%). The addition of K to Precambrian paleosols is quite common (Grandstaff et al., 1986; Holland et al., 1989; G-Farrow and Mossman, 1988; Rainbird et al., 1990), and probably represents the equilibration of the paleosols' alkali-depleted aluminosilicate assemblage with K-bearing, continentally derived groundwaters (Nesbitt and Young, 1989), either during diagenesis or low grade metamorphism. MacFarlane and Holland (in prep) concluded on the basis of Rb/Sr ages that K addition postdated paleosol formation by an average of 500 million years for the 3 paleosols they examined, and was related to local or regional thermal disturbances.

In this study, the significance of post-paleosol K addition is that it depresses the CIA index. Alteration (removal of alkalis) by weathering in the Witwatersrand was therefore probably even more extreme than the present day CIA profiles indicate.

Similar quantitative calculations can be used to determine iron loss in the Bird profiles. An average, unaltered, basalt has 10.5 wt.% FeO (Manson, 1967). The most iron-depleted portions of the Bird profiles (samples 112-114 of profile 84 and samples 120-126 of profile 326) have, on average, 1.3 wt% FeO. Thus, again normalizing to aluminum, approximately 94% of the iron in the basalt was removed from the most deeply weathered portion of the profiles. This loss of iron is again consistent with a low oxygen atmosphere, and with the behavior of other iron-rich Precambrian paleosols. High iron parent rocks (i.e., basalts) are particularly susceptible to iron loss because the rock releases large amounts of iron during acid attack, consuming any small amount of free oxygen and allowing most of the iron to be removed in solution as Fe^{2+}. Low iron parent rocks, on the other hand, may retain iron because the release of iron is small enough to permit oxidation and retention even in a low oxygen atmosphere. Holland and others have quantified this relationship between high and low iron parent rocks and their respective iron-retentive capabilities by use of the "R-value", which is the ratio of the demand for oxygen to the demand for acid in weathering (see Holland, 1984, or Pinto and Holland, 1987, for further discussion of the R-value). A plot that relates iron loss or retention to R-value through geologic time (figure 47) indicates that the behavior of iron in soils has changed since the Archean. To calculate R for the Bird paleosols, I have averaged the three deepest, apparently unaltered samples (130-132 of profile 326) and calculated an R of 0.039, which is reasonable considering that R for Manson's (1967) average basalt is 0.035. With an R of 0.039, these Bird paleosols fall well within the expected range of iron behavior for an Archean soil (figure 47).

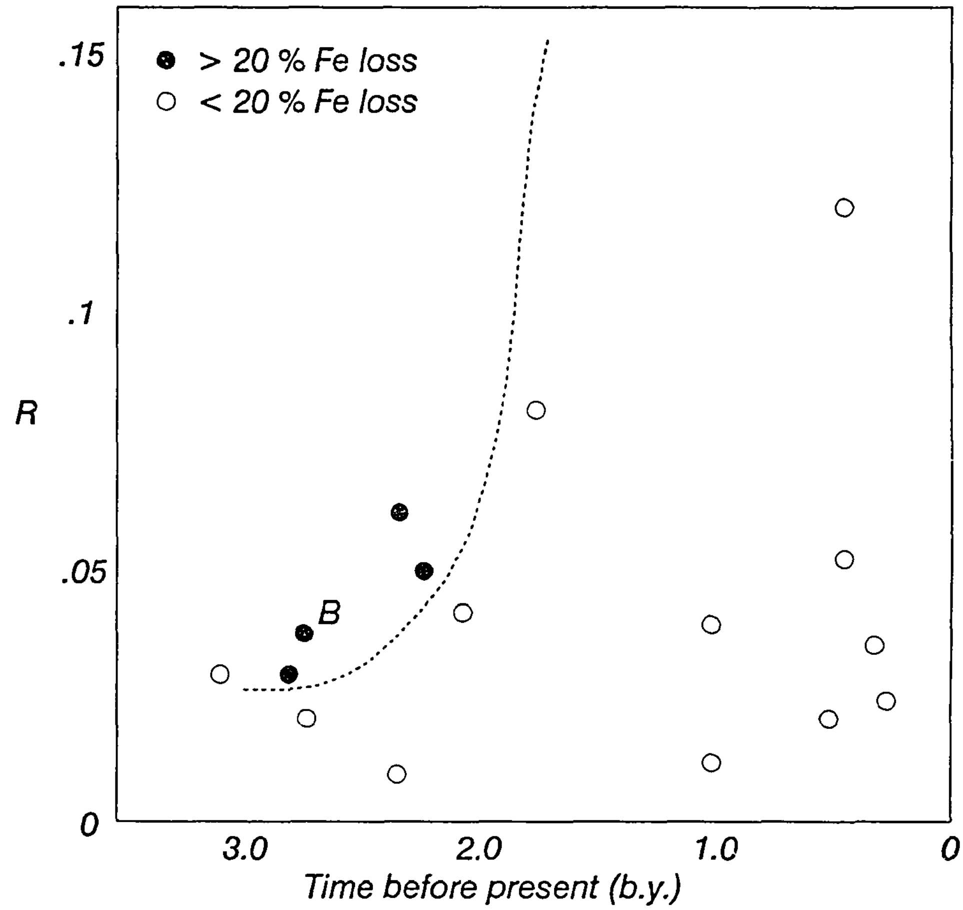

Figure 47. R-value and Fe loss through time, modified from Holland et al. (1989). R is the ratio of O_2 demand to CO_2 demand of the parent rock during weathering (see p. 238 of Holland, 1984). The dashed line separates paleosols that lose iron from those that retain iron. Prior to 2,000 Ma, parent rocks with high R-values lost iron during weathering; after 2,000 Ma and with an apparent rise in atmospheric oxygen, high iron parent rocks retained iron during weathering. The Bird metabasalt profiles plot at B.

Summary of evidence for paleosols

Highly altered, aluminous horizons beneath unconformities in the Witwatersrand basin are best interpreted as paleosols rather than as the products of lithologically controlled hydrothermal alteration (Palmer et al., 1989). Evidence that supports a weathering origin and, at the same time, discounts a hydrothermal origin for these altered horizons is as follows:

1.) The alteration profiles are stratigraphically asymmetric, with only footwall sediments developing exceptionally aluminous compositions. This is to be expected in a weathering alteration, but difficult to explain hydrothermally.

2.) Alteration correlates positively with the presence of a significant unconformity surface--below the Vaal reef paleosurface and in the upper part of the Bird metabasalts, both of which were subaerially exposed, thick, highly altered profiles are present; below the Ada May and Commonage paleosurfaces, which are not significant unconformities, and therefore probably underwent minimal subaerial exposure, alteration is slight to non-existent. If alteration were the result of hydrothermal exploitation of reefs, then reefs in general, regardless of subaerial exposure, should demonstrate approximately equal alteration.

3.) The chemistry of alteration is consistent with a weathering origin. Alkalis are removed (except K_2O, as noted above), as they are in modern soil profiles (Kronberg et al., 1979; Nesbitt et al., 1980; Nesbitt and Young, 1989). Iron, which is retained in modern soils but leached from many Archean soils, was leached from the 2.8-2.9 billion year old Witwatersrand soils.

The presence and ultimate preservation of these altered horizons is difficult to reconcile with the hydrothermal model of Phillips and Myers (1989), which demands that metamorphic fluids be concentrated along the more permeable reefs, where they sulfidize iron oxides, precipitate gold, and alter aluminosilicates. The metasomatism that is postulated, particularly when concentrated along the conglomerates, would have almost certainly erased, or at least significantly modified, the strong, asymmetric, chemical gradients in the immediate footwall. Also, the hydrothermal model calls for an iron-oxide/hydroxide residuum on the paleosurface which would later induce sulfide and gold precipitation. As seen here, and as reported from other Archean paleosols, iron is lost, not retained, in the prevailing low oxygen atmosphere of the Archean.

Chapter 7. Conclusion

Although I have separately discussed the tectonic, metamorphic, petrographic, and geochemical histories of the Witwatersrand basin quartzites, these four different perspectives produce a remarkably consistent model of basin evolution. Of central importance is the tectonic model of the upper portion of the West Rand Group and all of the Central Rand Group as a foreland basin. Integral to any foreland basin are the numerous unconformities brought about by syndepositional deformation and migration of the basin, both of which occur in response to hinterland tectonism.

In the Witwatersrand basin major unconformities coincide with the stratigraphic positions of the auriferous conglomerates, or reefs. Prolonged subaerial exposure on the unconformities is indicated by the erosion of underlying units, by the accumulation of major detrital gold and uranium deposits, and by analogy with younger foreland basins. A further consequence of subaerial exposure is the major petrographic and geochemical alteration of most of the Central Rand Group quartzites, as described in Chapters 4 and 5. Each major unconformity permitted CO_2-charged meteoric water to enter the groundwater system, where large amounts of Na, Ca, Fe, and Mg were removed, particularly near the tops of formations. Petrographically, this meteoric leaching is apparent in the distribution of feldspar, which is preserved in the Central Rand quartzites only near formation bottoms and in unusually impermeable horizons.

The most intense sub-unconformity alteration occurs at the very top of individual formations, immmediately beneath the unconformities. The paleosols that are preserved here, where CO_2-enriched meteoric water infiltrated the sediments, are characterized by an almost total loss of Ca, Na, Fe, and Mg. The loss of Fe is particularly interesting because it suggests soil formation in a low oxygen atmosphere.

The role of syndepositional tectonism is also critical to an understanding of the Witwatersrand basin's metamorphism. The omnipresent pyrophyllite plus chloritoid metamorphic assemblage suggests a broadly isothermal maximum temperature profile of 300-400°C, but thermal modeling does not permit such a uniform maximum temperature over the 7.5 km thick basin. A more reasonable interpretation recognizes that virtually all Witwatersrand samples have been recovered from the dipping strata along the basin margin. Because the deformation that tilted and exposed these strata was syn-depositional, along the basin margin the entire Witwatersrand Supergroup was probably exposed to isobaric, isothermal conditions during simple burial metamorphism.

The results of this study support the modified placer model of mineralization. The major chemical and petrographic alterations to the Witwatersrand quartzites are pre-metamorphic, not syn-metamorphic as suggested by Phillips (1988), Palmer et al. (1989), and Phillips and Myers (1989).

Lacking evidence of syn-metamorphic alteration in the quartzites, it is unlikely that a reasonable model for gold mineralization during metamorphism can be developed. The Witwatersrand basin appears to have evolved chemically to its present state well in advance of metamorphism.

References cited

Allen, P.A., Homewood, P., and Williams, G.D., 1986, Foreland basins: an introduction, in, Allen, P.A., and Homewood, P., eds., Foreland Basins, p.3-12

Antrobus, E.S.A., Brink, W.C.J., Brink, M.C., Caulkin, J., Hutchinson, R.I., Thomas, D.E., VanGraan, J.A., and Viljoen, J.J., 1986, The Klerksdorp goldfield, in, Anhauesser, C.R., and Maske.S., eds., Mineral Deposits of Southern Africa, p.549-598.

Antrobus, E.S.A., and Whiteside, H.C.M., 1964, The Geology of certain mines in the East Rand, in, Haughton, S.H., ed, The geology of some ore deposits in Southern Africa, Vol.1, Geol.Soc. S. Afr., p.125-160.

Aradon, P., Cabrera, L., Colombo, F., Marzo, M., and Riba, O., 1986, Syntectonic intraformational unconformities in alluvial fan deposits, eastern Ebro basin margins (NE Spain), in, Allen, P.A., and Homewood, P., eds., Foreland Basins, p.259-272.

Armstrong, R.A., Compston, W., Retief, E.A., Williams, I.S., and Welke, H.J., 1990, Single zircon ion microprobe studies bearing on the age and evolution of the Witwatersrand triad: Precambrian Res., submitted.

Ashworth, J.R., and Evirgen, M.M., 1984, Mineral chemistry of regional chloritoid assemblages in the chlorite zone, Lycian nappes, south-west Turkey: Mineral. mag., v.48, p.159-165.

Baker, E.B., 1988, Quantitative cathodoluminescence of quartz: M.S. thesis, Univ. of Cincinnati, U.S.A., 101 p.

Barton, E.S., Compston, W., Williams, I.S., Bristow, J.W., Hallabauer, D.K., and Smith, C.B., 1989, Provenance ages for the Witwatersrand Supergroup and the Ventersdorp Contact reef: constraints from ion microprobe U-Pb ages of detrital zircons: Econ. Geol., v.84, p.2012-2019.

Barton, J.M., Hunter, D.R., Jackson, M.P.A., and Wilson, A.C., 1980, Rb-Sr age and source of the Bimodal Suite of the Ancient Gneiss complex, Swaziland: Nature, v.283, p.756-758.

Bickle, M., J., and Eriksson, K.A., 1982, Evolution and Subsidence of early Precambrian sedimentary basins: Phil. Trans. R. Soc. London, v.305, p.225-247.

Bisschoff, A.A., 1982, Thermal metamorphism in the Vredefort dome: Trans. Geol. Soc. S. Afr., v.85, p.43-57.

Buck, S.G., and Minter, W.E.L., 1985, Placer formation by fluvial degradation of an alluvial fan sequence: the Proterozoic Carbon Leader placer, Wiotwatersranc Supergroup, South Africa: Jour. Geol. Soc. London, v.142, p.757-764.

Burke, K., and Kidd, W.S.F., 1978, Were Archean continental geothermal gradients much steeper than those of today?: Nature, v.272, p.240-241.

Burke, K., Kidd, W.S.F., and Kusky, T., 1985, Is the Ventersdorp rift system of southern Africa related to a continental collision between the Kaapvaal and Zimbabwe cratons at 2.64 Ga ago?: Tectonophysics, v.115, p.1-24.

Burke, K., Kidd, W.S.F., and Kusky, T., 1986, Archean foreland basin tectonics in the Witwatersand, South Africa: Tectonics, v.5, p.439-456.

Button, A., 1986, The Transvaal sub-basin of the Transvaal sequence, in, Anhaeusser, C.R., and Maske, S., eds., Mineral deposits of southern Africa, p.549-598.

Button, A.B., and Tyler, N., 1981, The character and economic significance of Precambrian paleoweathering and erosion surfaces in southern Africa: Econ. Geol. 75th Ann. volume, p.686-709.

Cahen, L., Snelling, N.J., Delhal, J., and Vail, J.R., 1984, The geochronology and evolution of Africa, 512 p.

Cameron, K.L., and Blatt, H., 1971, Durabilities of sand size schist and "volcanic" rock fragments during fluvial transport, Elk Creek, Black Hills, South Dakota: Jour. Sed. Pet., v.41, p.565-576.

Covey, M., 1986, The evolution of foreland basins to steady state: evidence from the Western Taiwan foreland basin, in, Allen, P.A., and Homewood, P., eds., Foreland basins, p.77-90.

Crow, C., and Condie, K.C., 1987, Geochemistry and origin of late Archean volcanic rocks from the Rhenosterhoek Formation, Dominion Group., South Africa: Precambrian Res., v.37, p.217-229.

Cross, T.A., 1986, Tectonic controls of foreland basin subsidence and Laramide style deformation, western United States, in, Allen, P.A., and Homewood, P., eds., Foreland basins, p.15-40.

Crow, C., and Condie, K., C., 1988, Geochemistry and origin of late Archean volcanics from the Ventersdorp Supergroup, South Africa: Precambrian Research, v.42, p.19-37.

Cruickshank, R.D., and Ghent, E.D., 1978, Chloritoid-bearing pelitic rocks of the Horsethief Creek Group, southeastern British Columbia: Contrib. Min. Pet., v.65, p.333-339.

Dickinson, W.R., 1985, Interpreting provenance relations from detrital modes of sandstones, in, Zuffa, G.G., ed., Provenance of Arenites, p.333-361.

Dickinson, W.R., and Suczek, C.A., 1979, Plate tectonics and sandstone composition: Am. Assoc. Pet. Geol. Bull., v.63, p.2164-2182.

Dorobek, S., 1989, Migration of orogenic fluide through the Suluro-Devonian Helderberg Group during late Paleozoic deformation: constraints on fluid sources and implications for thermal histories of sedimentary basins: Tectonophysics, v.159, p.25-45.

Drever, J.I., 1982, The Geochemistry of Natural Waters: Prentice-Hall, New Jersey, 388 p.

Els, B.G., and Beukes, N.J., 1987, Sedimentology of the Middlevei Placer, Doornfontein gold mine, Witwatersrand Supergroup: S.Afr.Jour.Geol., v.90, p.72-85.

England, R.N., 1972, Lamellar intergrowths of pyrophyllite and muscovite and the assemblage kyanite-pyrophyllite-quartz in quartzites from the Petermann ranges Northern Territory: Bur. Min. Res. of Australia Bulletin, v. 125, p.67-73.

Feather, C.E., and Koen, G.M., 1975, The minerology of the Witwatersrand reefs: Minerals Sci. Engineering, v.7, p.189-224.

Ferry, J.M., 1984, A biotite isograd in South-Central Maine, USA: mineral reactions, fluid transfer, and heat transfer: Jour. of Petrology, v. 25, p.871-893.

Franceschelli, M., Leoni, L., Memmi, I., and Puxeddu, M., 1986, Regional distribution of Al-silicates and metamorphic zonation in the low-grade Verrucano metasediments from the Northern Appenines, Italy: Jour. Meta. Geology, v.4, p.309-321.

Franzinelli, E., and Potter, P.E., 1983, Petrology, chemistry, and texture of modern river sands, Amazon river system: Jour. Geology, v.91, p.23-39.

Frey, M., 1987, The reaction-isograd kaolinite + quartz = pyrophyllite + H_2O, Helvetic Alps, Switzerland: Schweiz. Mineral. Petrogr., Mitt. 67, p.1-11.

Frey, M., Saunders, J., and Schwander, H., 1988, The mineralogy and metamorphic geology of low-grade metasediments, Northern Range, Trinidad: Jour. Geol., Soc. London, v.145 p.563-575.

Fuller, A.O., 1958, A contribution to the petrology of the Witwatersrand system: Trans. Geol. Soc. S. Afr., v.61, p.19-45.

G-Farrow, C.F., and Mossman, D.J., 1988, Geology of Precambrian paleosols at the base of the Huronian Supergroup, Elliot Lake, Ontario, Canada: Precambrian Research, v.42, p.107-139.

Garrels, R.M., and Mackenzie, F.T., 1971, Evolution of sedimentary rocks: W.W. Norton and Co., New York, 397 p.

Gay, A.L., and Grandstaff, D.E., 1980, Chemistry and mineralogy of Precambrian paleosols at Elliot Lake, Ontario, Canada: Precambrian Research, v.12, p.349-373.

Graham, S.A., and 14 others, 1986, Provenance modelling as a technique for analysing source terrane evolution and controls on foreland sedimentation, in, Allen P.A., and Homewood P., eds., Foreland Basins, p.425-436.

Graham, S.A., Ingersoll, R.V., and Dickinson, W.R., 1976, Common provenance for lithic grains in carboniferous sandstone from the Ouachita mountains and Black Warrior basin: Jour. Sed. Pet., v.46, p.620-632.

Grandstaff, D.E., Edelman, M.J., Foster, R.W., Zbinden, E., and Kimberly, M.M., 1986, Chemistry and mineralogy of Precambrian paleosols at the base of the Dominion and Pongola Groups (Transvaal, South Africa): Precambrian Research, v.32, p.97-131.

Gupta, A. das, and Paudyal, G.N., 1988, Estimating aquifer recharge and parameters from water level observations: Jour. of Hydrology, v.99, p.103-116.

Halferdahl, L.B., 1961, Chloritoid: its composition, x-ray and optical properties, stability and occurrence: Journal of Petrology, v.2, p.40-135.

Hallbauer, D.K., and Barton, J.M., 1987, The fossil gold placers of the Witwatersrand: Gold Bulletin, v.20, p.68-79.

Hallbauer, D.K., and Utter, T., 1977, Geochemical and morphological characteristics of gold particles from recent river deposits and the fossil placers of the Witwatersrand: Mineral. Deposita, v.12, p.293-306.

Hallbauer, D.K., and VanWarmelo, K.T., 1974, Fossilized plants in thucholite from Precambrian rocks in the Witwatersrand, South Africa: Precambrian Research, v.1, p.199-212.

Hallbauer, D.K., and von Gehlen, K., 1983. The Witwatersrand pyrites and metamorphism: Mineralogical Magazine, v.47, p.473-479.

Hallbauer, D.K., and Kable, E.J.D., 1982, Fluid inclusion and trace element content of quartz and pyrite pebbles from the Witwatersrand conglomerates: their significance with respect to the genesis of primary deposits, in, Amstutz, G.C., ed., Ore genesis - the state of the art, p.742-752.

Hamilton, P.J., Evensen, N.M., O'nions, R.K., Smith H.S., and Erlank, A.J., 1979, Sm-Nd dating of Onverwacht group volcanics, Southern Africa: Nature, v.279, p.298-300.

Hart, M.H., 1978, The evolution of the atmosphere of the Earth: Icarus, v.33, p.23-39.

Hart, R.J., Nicolaysen, L.O., and Gale, N.H., 1981, Radioelement concentrations in the deep profile through Precambrian basement of the Vredefort structure: Journal Geophys. Res., v.86. p.10639-10652.

Haugerud, R.A., 1986, 1DT--an interactive, screen-oriented microcomputer program for simulation of 1-dimensional geothermal histories: U.S.G.S. Open-file report 86-511, 19 p.

Heller, P., Angevine, C.L., Winslow, N.S., and Paola, C., 1988, Two-phase stratigraphic model of foreland-basin sequences: Geology, v.16, p.501-504.

Hirst, J.P.P., and Nichols, G.J., 1986, Thrust tectonic controls on Miocene alluvial distribution patterns, southern Pyrenees, in, Allen, P.A., and Homewood, P., eds., Foreland Basins, p.247-258.

Hoisch, T.O., 1987, Heat transport by fluids during Late Cretaceous regional metamorphism in the Big Maria mountains, southeastern California: G.S.A. Bull., v.98, p.549-553.

Holland, H.D., 1984, The Chemical Evolution of the Atmosphere and Oceans: Princeton University Press, Princeton, New Jersey, 582 p.

Holland, H.D., and Beukes, N.J., 1990, A paleoweathering profile from Griqualand West, South Africa: Evidence for a dramatic rise in atmospheric oxygen between 2.2 and 1.9 BYBP: Amer. Jour. Sci., v.290-A, p.1-34.

Holland, H.D., Feakes, C.R., and Zbinden, E.A., 1989, The Flin Flon paleosol and the composition of the atmosphere 1.8 BYBP: American Journal of Science, v.289, p.362-389.

Hooper, P.R., 1988, The Columbia River Basalt, in, Macdougall, J.D., ed., Continental Flood Basalts, p.1-33.

Johnson, N.M., Jordan, T.E., Johnsson, P.A., and Naeser, C.W., 1986, Magnetic polar stratigraphy, age and tectonic setting of fluvial sediments in an eastern Andean foreland basin, San Juan province, Argentina, in, Allen, P.A., and Homewood, P., eds., Foreland Basins, p.63-76.

Johnsson, M.J., and Stallard, R.F., 1989, Physiographic controls on the composition of sediments derived from volcanic and sedimentary terrains on Barro Colorado Island, Panama: Jour. Sed. Pet., v.59, p.768-781.

Jowett, E.C., 1986, Genesis of Kupferschiefer Cu-Ag deposits by convective flow of Rotliegende brines during Triassic rifting: Econ. Geol., v.81, p.1823-1838.

Kaufman, S., 1982, Crustal faults in North America: a report of the COCORP project, in, Hsu, K.J., eds., Mountain building processes, p.243-246.

Klemd, R., and Hallbauer, D.K., 1987, Hydrothermally altered peraluminous Archean granites as a provenance model for Witwatersrand sediments: Mineral. Deposita, v.22, p.227-235.

Koppel, V.H., and Saager, R., 1974, Lead isotope evidence on the detrital origin of Witwatersrand pyrites and its bearing on the provenance of the Witwatersrand gold: Econ. Geol., v.69, p.318-331.

Kronberg, B.I., Fyfe, W.S., Leonardos, Jr., O.H., and Santos, A.M., 1979, The chemistry of some Brazilian soils: element mobility during intense weathering: Chem. Geol., v.24, p.211-229.

Land, L.S., Milliken, K.L., and McBride, E.F., 1987, Diagenetic evolution of Cenozoic sandstones, Gulf of Mexico sedimentary basin: Sed. Geol., v.50, p.195-225.

Light, M.P.R., 1982, The Limpopo mobile belt: A result of continental collision: Tectonics, v.1, p.325-342.

Lundegard, P.D., Land, L.S., and Galloway, W.E., 1984, Problem of secondary porosity: Frio Formation (Oligocene), Texas Gulf Coast: Geology, v.12, p.399-402.

Mack, G.H., 1984, Exceptions to the relationship between plate tectonics and sandstone composition: Jour. Sed. Pet., v.54, p.212-220.

MacLean, P.J., and Fleet, M.E., 1989, Detrital pyrite in the Witwatersrand gold fields of South Africa: Evidence from truncated growth banding: Econ. Geol., v.84, p.2008-2011.

Mahoney, J.J., 1988, The Deccan Traps, in, Macdougall, J.D., ed., Continental Flood Basalts, p.151-194.

Majorowicz, J.A., Jones, F.W., Lam, H.L., and Jessop, A.M., 1984, The variability of heat flow both regional and with depth in southern Alberta, Canada: effect of groundwater flow?: Tectonophysics, v.106, p.1-29.

Manson, V., 1967, Geochemistry of basaltic rocks: Major elements, in Hess, H., and Poldervaart, A., eds., Basalts, p.215-269.

Massari, F., Grandesso, P., Stefani, C., and Jobstraibizer, P.G., 1986, A small polyhistory foreland basin evolving in a context of oblique convergence: the Venetian basin (Chattian to Recent, Southern Alps, Italy), in, Allen, P.A., and Homewood, P., eds., Foreland Basins, p.141-168.

Maynard, J.B., 1984, Composition of plagioclase feldspar in modern deep-sea dands: relationship to tectonic setting: Sedimentology, v.31, p.493-501.

Maynard, J.B., Ritger, S.D., and Sutton, S.J., 1991, Chemistry of sands from the modern Indus River and the Archean Witwatersrand Basin: Implications for the composition of the the Archean atmosphere: Geology, v.19, P.265-268.

McKenzie, D., 1978, Some remarks on the development of sedimentary basins: Earth and Planet. Sci. Lett., v.40, p.25-32.

McKenzie, D., Nisbet, E., and Sclater, J.G., 1980, Sedimentary basin development in the Archean: Earth and Planet. Sci. Lett., v.48, p.35-41.

Meyer, M., Oberthur, T., Robb, L.J., Saager, R., and Stupp. H.D., 1985, Ni, Co, and Au contents of pyrites from Archean granite-grenstone terranes and early Proterozoic sedimentary deposits in Southern Africa: Univ. of the Witwatersrand Econ. Geol. Res. Unit Info. Circ. No. 176, 11 p.

Miall, A.D., 1978, Tectonic setting and syndepositional deformation of molasse and other nonmarine-paralic sedimentary basins: Can. J. Earth Sci., v.15, p.1613-1632.

Miall, A.D., 1984, Principles of Sedimentary Basin Analysis: Springer-Verlag, New York, 490 p.

Minter, W.E.L., 1976, Detrital gold, uranium, and pyrite concentrations related to sedimentology in the Precambrian Vaal reef placer, Witwatersrand, South Africa: Econ. Geol., v.71, p.157-176.

Minter, W.E.L., 1979, Examples that illustrate sedimentological aspects of the Proterozoic placer model on the Kaapvaal craton, Witwatersrand, South Africa: in, Genesis of Uranium and gold-bearing Precambrian quartz-pebble conglomerates, U.S.G.S. Prof. Paper 1161 A-BB, p.E1-E5.

Minter, W.E.L., 1988, Comment on "Problems with the placer model for Witwatersrand gold": Geology, v.16, p.1153-1154.

Minter, W.E.L., Hill, W.C.N., Kidger, R.J., and Snowden, P.A., 1986, The Welkom goldfield, in Anhaeusser, C.R., and Maske, S., eds., Mineral Deposits of Southern Africa, p.497-539.

Nesbitt, H.W., Markovics, G., and Price, R.C., 1980, Chemical processes affecting alkalis and alkaline earths during continental weathering: Geochimica et Cosmochimica Acta, v.44, p.1659-1666.

Nesbitt, H.W. and Young, G.M., 1982, Early Proterozoic climates and plate motions inferred from major element chemistry of lutites: Nature, v.299, p.715-717.

Nesbitt, H.W., and Young, G.M., 1989, Formation and diagensis of weathering profiles: Jour. Geology, v.97, p.129-147.

Ness, G., Levi, S., and Couch, R., 1980, Marine magnetic anomaly timescales for the Cenozoic and Late Cretaceous: a precis, critique, and synthesis: Rev. Geophys. Space Phys., v.18, p.753-770.

Nicolaysen, L.O., Hart, R.J., and Gale, N.H., 1981, The Vredefort radioelement profile extended to supracrustal strata at Carletonville, with implications for continental heat flow: Journal Geophys. Res., v.86, p.10653-10661.

Nisbet, E.G., 1984, The continental and oceanic crust and lithosphere in the Archean: Isostatic, thermal, and tectonic models: Can. J. Earth Sci., v.21, p.1426-1441,

Owen, M.R., and Carozzi, A.V., 1986, Southern provenance of Upper Jackfork Sandstone, Southern Ouachita mountains: cathodoluminescence petrology: Geol. Soc. Am. Bull., v.97, p.110-115.

Owen, T., Cess, R.D., and Ramanathan, V., 1979, Enhanced CO_2 greenhouse to compensate for reduced solar luminosity on early Earth: Nature, v.277, p.640-642.

Palmer, J.A., 1986, Palaeoweathering in the Witwatersrand and Ventersdorp supergroups: M.S. Thesis, University of the Witwatersrand, 185 p.

Palmer, J.A., Phillips, G.N., and McCarthy, T.S., 1989, Paleosols and their relevance to Precambrian atmospheric composition: Jour. Geology, v.97, p.77-92.

Phillips, G.N., 1987, Metamorphism of the Witwatersrand gold fields: Conditions during peak metamorphism: Jour. Met. Geol., v.5, p.307-322.

Phillips, G.N., 1988, Widespread fluid infiltration during metamorphism of the Witwatersrand goldfields: generation of chloritoid and pyrophyllite: Jour. Met. Geol., v.6, p.311-332.

Phillips, G.N., and Myers, R.E., 1989, The Witwatersrand gold fields: Part II. An origin for Witwatersrand gold during metamorphism and associated alteration: Econ. Geol., Mon. 6, p.598-608.

Phillips, G.N., Myers, R.E., and Palmer, J.A., 1987, Problems with the placer model for Witwatersrand gold: Geology, v.15, p.1027-1030.

Pinto, J.P., and Holland, H.D., 1988, Paleosols and the evolution of the atmosphere, Part II, in Reinhardt, J., and Sigleo, W.R., eds., Paleosols and weathering through geologic time: Geol. Soc. Sp. Paper 216, p.21-34.

Potts, P.J., 1987, A handbook of silicate rock analysis, Chapman and Hall, New York, 622 p.

Pretorius, D.A., 1975, The depositional environment of the Witwatersrand goldfields: A chronological review of the speculations and observations: Min. Sci. Eng., v.7, p.23-47.

Pretorius, D.A., 1976, The nature of the Witwatersrand gold-uranium deposits, in, Wolf, K.H., ed., Handbook of Strata-bound and Stratiform ore deposits, v.7, p.29-88.

Pretorius, D.A., 1981, The Witwatersrand Supergroup, in, Hunter, D.R., ed., Precambrian of the southern hemisphere, p.511-519.

Rainbird, R.H., Nesbitt, H.W., and Donaldson, J.A., 1990, Formation and diagensis of a Sub-Huronian saprolith: comparison with a modern weathering profile: Jour. Geology, v.98, p.801-822.

Reid, A.M., Roex, A.P.le, and Minter, W.E.L., 1988, Composition of gold grains in the Vaal placer, Klerksdorp, South Africa: Mineral. Deposita, v.23, p.211-217.

Reimer, T.O., 1986, Alumina-rich rocks from the early Precambrian of the Kaapvaal craton as indicators of paleosols and as products of other decompositional reactions: Precambrian Research, v.32, p.155-179.

Reimer, T.O., 1987, The Late Archean Dominion conglomerates (South Africa): new aspects of their derivation and their relationship with those of the Witwatersrand: Neves Jahrbuch Miner. Abh., v.158, p.13-46.

Reimer, T.O., and Mossman, D.J., 1990, The Witwatersrand Controversy revisited: Econ. Geol., v.85, p.337-343.

Ricci Lucchi, F., 1986, The oligocene to recent foreland basins of the northern Apennines, in, Allen, P.A., and Homewood p., eds., Foreland Basins, p.105-140.

Robb, L.J., and Meyer, F.M., 1990, The nature of the Witwatersrand hinterland: conjectures on the source area problem: Econ. Geol., v.85, p.511-536.

Robb, L.J., Davis, D.W., and Kamo, S.L., 1990, U-Pb ages on single detrital zircon grains from the Witwatersrand basin, South Africa: constraints on the age of sedimentation and on the evolution of granites adjacent to the basin: Jour, Geology, v.98, p.311-328.

Saager, R., 1976, Geochemical aspects of the origin of detrital pyrite in Witwatersrand conglomerates: Univ. of the Witwatersrand Econ. Geol. Res. Unit Info. Circ. No. 105, 20 p.

SACS, 1980, South African committee for stratigraphy. Stratigraphy of South Africa. Part I. Lithostratigraphy of the Republic of South Africa, South West Africa/Namibia, and the Republics of Bophuthatswana, Transkei, and Venda: Geol. Surv. South Africa Handbook, 8.

Savage, K.M., Decesero, P., and Potter, P.E., 1988, Mineralogic maturity of modern sand along a high-energy tropical coast: Baxiada de Jacarepequa, Rio de Janeiro, Brazil: Jour. South American Earth Sciences, v.1, p.317-328.

Schmidt, V., and McDonald, D.A., 1979, The role of secondary porosity in the course of sandstone diagenesis, in, Scholle, P.A., and Schluger, P.R., eds., Aspects of Diagenesis, SEPM Sp. Publ. No. 26, p.175-207.

Schopf, J.W., 1975, Precambrian paleobiology: Problems and perspectives: Ann. Rev. Earth Planet. Sci., v.3, p.213-249.

Schreyer, W., and Bisschoff, A.A., 1982, Kyanite as a metamorphic mineral in Witwatersrand sediments at Johannesburg and Krugersdorp, South Africa: Trans. Geol. Soc. S. Afr., v.85, p.211-214.

Schwab, F.L., 1976, Modern and ancient sedimentary basins: comparative accumulation rates: Geology, v.4, p.723-727.

Sharma, P.V., 1986, Geophysical methods in geology, Elsevier, New York, 442 p.

Shepherd, T.J., 1977, Fluid inclusion study of the Witwatersrand gold-uranium ores: Phil. Trans. Roy. Soc. London, v.A286, p.549-565.

Siebert, R.M., Moncure, G.K., and Lahann, R.W., 1984, A theory of framework grain dissolution in sandstones, in, McDonald, D.A., and Surdam, R.C., eds., Clastic Diagenesis, AAPG Mem.37, p.163-175.

Smith, L., and Chapman, D.S., 1983, On the thermal effects of groundwater flow 1. Regional scale systems: Journal Geophys. Res., v.88, p.593-608.

Smith, N.D., 1989, Comment on "Problems with the placer model for Witwatersrand gold": Geology, v.17, p.91-92.

Sprunt, E.S., 1981, Causes of quartz cathodoluminescence colors: Scanning Electron Microscopy, v.1, p.525-535.

Stannistreet, I.G., McCarthy, T.S., Charlesworth, E.G., Myers, R.E., and Armstrong, R.A., 1986, Pre-Transvaal wrench tectonics along the northern margin of the Witwatersrand basin, South Africa: Tectonophysics, v.131, p.53-74.

Surdam, R.C., Boese, S.W., Crossey, L.J., 1984, The chemistry of secondary porosity, in, Clastic Diagenesis, AAPG Mem.37, p.127-149.

Sutton, S.J., Ritger, S.D., and Maynard, J.B., 1990, Stratigraphic control of chemistry and mineralogy in metamorphosed Witwatersrand quartzites: Jour. Geol., v.98, p.329-341.

Tankard, A.J., Jackson, M.P.A., Eriksson, K.A., Hobday, D.K., Hunter, D.R., and Minter, W.E.L., 1982, Crustal evolution of southern Africa, 523 p.

Tardy, Y., N'Kounkou, R., and Probst, J., 1989, The global water cycle and continental erosion during Phanerozoic time (570my): Am. Jour. Sci., v.289, p.455-483.

Thomas, J.M., Carlton, S.M., and Hines, L.B., 1989, Ground-water hydrology and simulated effects of development in Smith Creek valley, a hydrologically closed basin in Lander County Nevada: U.S.G.S. Prof. paper no. 1409-E.

Veizer, J. 1986, The evolving exogenic cycle, in, Gregor, C.B., Garrels, R.M., Mackenzie, F.T., and Maynard, J.B., eds., Chemical cycles in the evolution of the earth, p.175-220.

Viljoen, R.P., Saager, R., and Viljoen, M.J., 1970, Some thoughts on the origin and processes responsible for the concentration of gold in the early Precambrian of southern-Africa: Mineral. Deposita, v.5, p.164-180.

Von Gehlen, K., 1983, Silver and mercury in single gold grains from the Witwatersrand and Barberton, South Africa: Mineral. Deposita, v.18, p.529-534.

Vos, R.G., 1975, An alluvial plain and lacustrine model for the Precambrian Witwatersrand deposits of South Africa: Jour. Sed. Pet., v.45, p.480-493.

Walker, J.C.G., 1977, Evolution of the atmosphere: Macmillan, New York, 318 p.

Watchorn, M.B., 1981, Sedimentological controls on stratabound placer mineralization in the lower Witwatersrand West Rand Group, South Africa: Univ. of the Witwatersrand Econ. Geol. Res. Unit Info. Circ. No.153, 4 pp.

Wheelock, G.M., 1987, The sedimentology and mineralization of the Archean Elsburg No. 5 reef on Vaal Reefs West gold mine, Transvaal South Africa: M.S. thesis, Univ of Cincinnati, 104 p.

Williams, H., and McBirney, A.R., 1979, Volcanology, Freeman, Cooper and company, 397 p.

Williamson, A.K., Prudic, D.E., and Swain, L.A., 1989, Ground-water flow in the Central Valley, California: U.S.G.S. Prof. paper no. 1401-D.

Windley, B.F., 1977, The evolving continents: John Wiley and Sons, New York, 385 p.

Winter, H. de la R., 1976, A lithostratigraphic classification of the Ventersdorp succession: Trans. Geol. Soc. South Africa, v.79, p.115-121.

Winter, H.R., 1987. A cratonic foreland model for Witwatersrand Basin development in a continental back-arc, plate-tectonic setting: S. Afr. J. Geol., v.90, p.409-427.

Wood, W.W., and Petraitis, M.J., 1984, Origin and distribution of carbon dioxide in the unsaturated zone of the southern High Plains of Texas: Water Res. Research, v.20, p.1193-1208.

Wyllie, P.J., 1980, The origin of kimberlite: Journal of Geophys. Res., v.85, p.6902-6910.

Zinkernagel, V., 1978, Cathodoluminescence of quartz and its application to sandstone petrology: Contrib. to sedimentology, v.8, 69 p.

Appendix 1. Sample locations

A. Sample locations for DL-301 to DL-410 (sample suite of chapters 4 and 5). The depths refer to recovery depth (meters below surface), not to stratigraphic depths as reported in chapters 4 and 5. See map at end of appendix for core locations.

Sample no.	Core	Depth	Formation
DL-301	MMB-1	2073.73	Elsburg
DL-302	MMB-1	2086.80	Elsburg
DL-303	MMB-1	2096.00	Elsburg
DL-304	MMB-1	2109.97	Elsburg
DL-305	MMB-1	2129.97	Elsburg
DL-306	MMB-1	2147.74	Elsburg
DL-307	MMB-1	2166.81	Elsburg
DL-308	MMB-1	2169.64	Elsburg
DL-309	MMB-1	2193.48	Elsburg
DL-310	MMB-1	2197.96	Elsburg
DL-311	MMB-1	2231.15	Elsburg
DL-312	MMB-1	2247.25	Elsburg
DL-313	MMB-1	2260.79	Elsburg
DL-314	MMB-1	2289.67	Elsburg
DL-315	MMB-1	2305.87	Elsburg
DL-316	MMB-1	2320.07	Elsburg
DL-317	MMB-1	2336.63	Klerksdorp
DL-318	MMB-1	2353.19	Klerksdorp
DL-319	MMB-1	2373.62	Klerksdorp
DL-320	MMB-1	2394.18	Klerksdorp
DL-321	MMB-1	2406.51	Klerksdorp
DL-322	MMB-1	2418.25	Klerksdorp
DL-323	MMB-1	2449.67	Klerksdorp
DL-324	MMB-1	2474.17	Klerksdorp
DL-325	MMB-1	2491.91	Klerksdorp
DL-326	MMB-1	2533.15	Klerksdorp
DL-327	MMB-1	2559.04	Klerksdorp
DL-328	MMB-1	2587.62	Klerksdorp
DL-329	MZA-4	2943.75	Klerksdorp
DL-330	MZA-4	2953.46	Klerksdorp
DL-331	MZA-4	2967.58	Klerksdorp
DL-332	MZA-4	2984.00	Klerksdorp
DL-333	MZA-4	3009.82	Klerksdorp
DL-334	MZA-4	3041.89	Gold Estates
DL-335	MZA-4	3065.55	Gold Estates
DL-336	CY-1	3126.65	Gold Estates
DL-337	CY-1	3133.14	Gold Estates
DL-338	CY-1	3159.58	Gold Estates

Appendix 1 - continued

Sample no.	Core	Depth	Formation
DL-339	CY-1	3173.89	Strathmore
DL-340	CY-1	3202.65	Strathmore
DL-341	CY-1	3212.98	Strathmore
DL-342	CY-1	3230.82	Strathmore
DL-343	CY-1	3247.96	Strathmore
DL-344	CY-1	3265.92	Strathmore
DL-345	CY-1	3280.73	Strathmore
DL-346	CY-1 (defl.)	2413.62	Strathmore
DL-347	CY-1 (defl.)	2462.35	Strathmore
DL-348	CY-1 (defl.)	2483.00	Strathmore
DL-349	CY-1 (defl.)	2490.05	Strathmore
DL-350	CY-1 (defl.)	2504.39	Strathmore
DL-351	CY-1 (defl.)	2521.92	Strathmore
DL-352	CY-1 (defl.)	2559.74	Strathmore
DL-353	KR-1	441.35	Stilfontein
DL-354	KR-1	455.98	Stilfontein
DL-355	KR-1	475.49	Stilfontein
DL-356	KR-1	503.10	Stilfontein
DL-357	KR-1	511.76	Stilfontein
DL-358	KR-1	552.30	Stilfontein
DL-359	KR-1	582.04	Stilfontein
DL-360	KR-1	604.42	Stilfontein
DL-361	KR-1	618.13	Stilfontein
DL-362	KR-1	640.99	Stilfontein
DL-363	KR-1	654.56	Stilfontein
DL-364	KR-1	677.27	Stilfontein
DL-365	KR-1	713.23	Commonage
DL-366	KR-1	776.32	Commonage
DL-367	KR-1	813.60	Commonage
DL-368	KR-1	862.53	Commonage
DL-369	KR-1	940.61	Commonage
DL-370	KR-1	979.93	Commonage
DL-371	KR-1	1013.16	Commonage
DL-372	KR-1	1058.49	Commonage
DL-373	KR-1	1132.17	Commonage
DL-374	KR-1	1193.90	Commonage
DL-375	KR-1	1247.55	Commonage
DL-376	KR-1	1261.57	Commonage
DL-377	G-13	1778.81	Roodepoort
DL-378	G-13	1795.27	Roodepoort
DL-379	G-13	1805.64	Roodepoort
DL-380	G-13	1848.61	Roodepoort
DL-381	G-13	1862.63	Roodepoort
DL-382	G-13	1904.70	Roodepoort
DL-383	G-13	1974.49	Roodepoort

Appendix 1 - continued

Sample no.	Core	Depth	Formation
DL-384	G-13	1989.12	Roodepoort
DL-385	G-13	2004.06	Roodepoort
DL-386	G-13	2036.98	Roodepoort
DL-387	G-13	2093.06	Roodepoort
DL-388	G-13	2208.58	Roodepoort
DL-389	G-13	2277.47	Roodepoort
DL-390	G-13	2359.46	Roodepoort
DL-391	G-13	2476.50	Babrosco
DL-392	G-13	2604.21	Babrosco
DL-393	G-13	2706.93	Rieutkuil
DL-394	G-13	2777.34	Rieutkuil
DL-395	R-1	2336.90	Palmietfontein
DL-396	R-1	2486.56	Palmietfontein
DL-397	R-1	2554.53	Palmietfontein
DL-398	R-1	2626.46	Palmietfontein
DL-399	R-1	2766.97	Palmietfontein
DL-400	R-1	2821.53	Welgegund
DL-401	R-1	2887.98	Welgegund
DL-402	R-1	3018.13	Welgegund
DL-403	R-1	3185.46	Welgegund
DL-404	MGR-3	2333.40	Bonanza
DL-405	MGR-3	2379.80	Bonanza
DL-406	VHD-1	2766.67	Rooipoort
DL-407	VHD-1	2894.69	Rooipoort
DL-408	VHD-1	3048.61	Rooipoort
DL-409	DRH-13	298.00	Goedgevonden
DL-410	DRH-13	309.00	Goedgevonden

B. Sample locations for paleosol profiles (chapter 6)

Profile M: From core MZA-4 (see map at end of appendix)

Sample	Depth (m)
M-20	3260.5
M-21	3264.1
M-22	3266.5
M-23	3270.1
reef	3275.0
M-24	3278.1
M-25	3280.0
M-26	3284.1
M-27	3288.9

Appendix 1 - continued

Profile V2: From mine exposure at Vaal Reefs East, #9 shaft

Sample	Depth (m)
V-2-1	0.75
V-2-2	0.61
V-2-3	0.46
V-2-4	0.30
V-2-5	0.20
V-2-6	0.10
reef	0.00
V-2-9	-0.15
V-2-10	-0.30
V-2-11	-0.46
V-2-12	-0.61
V-2-13	-0.75

Profile VR: From mine exposure at Southvaal, #8 shaft

Sample	Depth (m)
VR-1	1.10
VR-2	0.90
VR-3	0.60
VR-4r	0.35
VR-6r	0.09
VR-7r	0.03
reef	0.00

Profile V3: From mine exposure at Vaal Reefs West, #4 shaft

Sample	Depth (m)
reef	0.00
V-3-7	-0.05
V-3-6	-0.50
V-3-5	-1.00
V-3-4	-1.50
V-3-3	-2.00
V-3-2	-2.50
V-3-1	-3.00

Appendix 1 - continued

Profile V4: From mine exposure at Vaal Reefs West, #4 shaft

Sample	Depth (m)
reef	0.00
V-4-1	-0.05
V-4-2	-0.50
V-4-3	-1.00
V-4-4	-1.50
V-4-5	-2.00
V-4-6	-2.50

Profile WAM:From core NG-1, deflection TOW-6, AAPS, Welkom

Sample	Depth (m)
WAM-1	2910.10
WAM-2	2911.10
WAM-3	2911.70
WAM-4	2912.30
WAM-5	2912.70
reef	2913.24
WAM-6	2913.90
WAM-7	2914.40
WAM-8	2915.00
WAM-9	2915.60
WAM-10	2916.63

Profile WC: From core NG-1, deflection TOW-14, AAPS, Welkom

Sample	Depth (m)
WC-1	2695.30
WC-2	2698.10
WC-3	2700.50
WC-4	2702.50
WC-5	2703.60
WC-6	2705.10
reef	2705.75
WC-7	2705.85
WC-8	2707.00
WC-9	2709.00
WC-10	2712.00

Core location map